Progress in Materials Science 147 (2025) 101357

Contents lists available at ScienceDirect

Progress in Materials Science

journal homepage: www.elsevier.com/locate/pmatsci

Effects of build orientation and inclined features on physical, microstructural and mechanical properties of powder bed fusion additively manufactured metallic parts

Ivan Aiza [a], Chiara Baldi [b], Federico Matías de la Vega [b], Sara Sebastiani [b], Niccolò Enrico Veronese [b], Mohammad Yousefi [a], Mohammad Hossein Mosallanejad [a], Erfan Maleki [b,1], Mario Guagliano [b], Luca Iuliano [a], Abdollah Saboori [a,*], Sara Bagherifard [b,*]

[a] Integrated Additive Manufacturing Center (IAM), Department of Management and Production Engineering, Politecnico di Torino, Turin, Italy
[b] Department of Mechanical Engineering, Politecnico di Milano, Milan, Italy

ARTICLE INFO

Keywords:
Additive manufacturing
Build orientation
Design for additive manufacturing
EB-PBF
L-PBF
Metal

ABSTRACT

In Additive Manufacturing (AM), parts are normally fabricated along the direction perpendicular to the build plate. However, the main axis of the part may differ from this direction, leading to the concept of "build orientation" that is an essential aspect in Design for AM (DfAM). Build orientation defines the required support structures, that in turn affects build time, material waste, and part's surface and mechanical properties. The present paper reviews the literature, focusing on the most utilized Powder Bed Fusion (PBF) techniques in metal AM. The findings are categorized based on properties affected by build orientation. First, manufacturability, geometrical accuracy, surface roughness, and porosity are reviewed. Then microstructural analysis, mechanical properties such as hardness, tensile strength, fatigue strength and fracture toughness are explored, followed by wear and corrosion properties. Consistent attention is given to studies describing the effects of build orientation on efficiency and applicability of post-processing techniques. Critical discussion of results highlights build orientation as a major factor to be considered in design and evaluation of PBF. In addition, prospects for the field are outlined, including the necessity of creating DfAM guidelines regarding build orientation, for which the current work is intended to serve as a starting point.

Abbreviations: AM, Additive Manufacturing; CE, Chemical Etching; DfAM, Design for Additive Manufacturing; DMLS, Direct Metal Laser Sintering; DED, Directed Energy Deposition; EBSD, Electron Back Scatter Diffraction; EBM, Electron Beam Melting; EB-PBF, Electron Beam-Powder Bed Fusion; FEM, Finite Element Method; HT, Heat Treatment; HFMI, High-Frequency Mechanical Impact; HIP, Hot Isostatic Pressing; LoF, Lack-of-fusion; LSP, Laser Shock Peening; L-PBF, Laser-Powder Bed Fusion; μCT, Micro Computed Tomography; Nd: YAG, Neodinium Ytterbium Aluminium Garnet; PSD, Particle Size Distribution; PL, Polishing; PBF, Powder Bed Fusion; SB, Sand Blasting; SLM, Selective Laser Melting; SP, Shot Peening; SS, Stainless steel; SR, Stress Relieving; TPMS, Triply Periodic Minimal Surface; UTS, Ultimate Tensile Strength; YS, Yield Strength.

* Corresponding author.
E-mail addresses: abdollah.saboori@polito.it (A. Saboori), sara.bagherifard@polimi.it (S. Bagherifard).
[1] Current affiliation: National Center for Additive Manufacturing Excellence (NCAME), Auburn University, Auburn, AL, United States.

https://doi.org/10.1016/j.pmatsci.2024.101357
Received 5 December 2023; Received in revised form 26 July 2024; Accepted 23 August 2024
Available online 25 August 2024

1. Introduction

Metal additive manufacturing (metal AM) is an emerging technology that is gaining significant attention in multiple sectors including automotive [1], aerospace [2], and biomedical [3,4](Fig. 1). This interest originates from the unique advantages that AM can offer compared to the traditional manufacturing techniques. AM processes typically start with a virtual three-dimensional (3D) model of the part to be produced, which is then virtually sliced and manufactured layer-by-layer [5–7]. These technologies enable the production of complex-shaped components that were not feasible with conventional manufacturing methods. Other advantages of AM include high cost-efficiency, easy customization, reduced material waste, reduced lead time, the processability of high resistance metallic materials, and flexibility of the design and process, compared to traditional manufacturing techniques [8–10].

ISO/ASTM 52900:2015 [11] international standard has categorized AM technologies into 7 categories of Binder Jetting (BJ), Directed Energy Deposition (DED), Material Extrusion, Material Jetting, Powder Bed Fusion (PBF), Sheet Lamination, and Vat Photopolymerization. In the context of metal AM, the major classes are PBF, described as an "AM process in which thermal energy selectively fuses regions of a powder bed", DED, defined as the "AM process in which focused thermal energy is used to fuse materials by melting as they are deposited" and BJ defined as the "AM process that involves selectively depositing a liquid bonding agent to join powder materials", followed by sintering. PBF and DED technologies resort to the melting of metallic materials, with the main difference being in the application of a powder bed with respect to a contemporary deposition and melting of the material. The present work focuses on PBF technologies, particularly Laser-PBF (L-PBF) and Electron Beam-PBF (EB-PBF). These processes are based on using a laser/electron beam as the thermal energy source to selectively melt the powder bed following the Computer-Aided Design (CAD) model of the object. In addition to the standard terminologies introduced in ISO/ASTM 52911-1:2019 standard [12], several other terms have been interchangeably used in the literature; for instance, L-PBF has been also referred to as Selective Laser Melting (SLM) [13] while other terms like Electron Beam Melting (EBM) [14] and Electron Beam Selective Melting (EBSM) [15] can be found for EB-PBF.

Despite the unique advantages of metal AM, several intrinsic challenges are still open in this field limiting their wider application, as shown in Fig. 2. Besides internal defects and porosity [16], size restriction, production time and cost of the machinery that are current obstacles to the rapid growth of metal AM [17], another major challenge to be tackled is the limited production quality in terms of dimensional accuracy and surface quality [18–20]. As-built parts typically have a rough surface finish, implying the need for post-processing. The extent of surface irregularity and morphological features depends on feedstock characteristics, the AM technology, and the process parameters. Moreover, support structures may be required during manufacturing, and their removal typically reduces the surface quality [21,22]. These aspects make the overall process less sustainable [23,24].

Build orientation, also referred to as part orientation, build angle, and inclination angle, is a crucial step of the AM build preparation. It represents the orientation of the part to be produced with respect to the 'build direction', which is the normal direction to the build plate, along which the virtual model is sliced and manufactured layer-by-layer. As a rule of thumb, it is recommended to optimize the part orientation to minimize the use of support structures and the stair-stepping effect [28,29], as shown in Fig. 3. Moreover, during part fabrication using AM technologies, like L-PBF and DED that are inherently thermal-based processes, the effect of build orientation is reflected also in the fact that powder has different thermal properties compared to the melted material [26,30]. Part orientation influences the extent of overlap between consecutive layers, hence affecting the portion of the layer that is supported by the melted material or powder. This can affect the part quality and properties [31], for instance, leading to dimensional variations and an increase

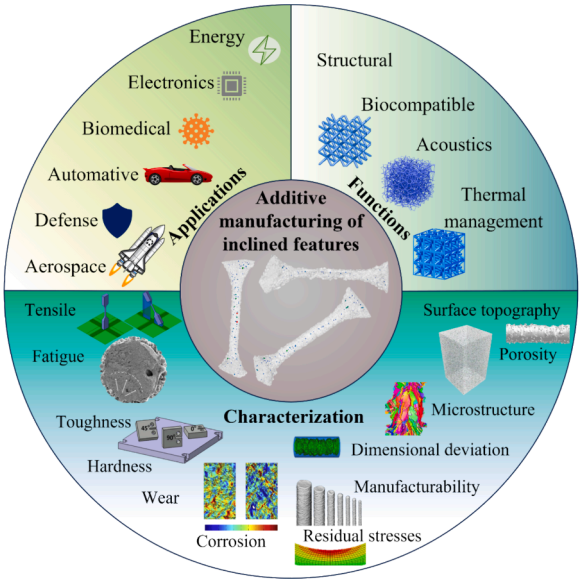

Fig. 1. A schematic illustration of metal AM applications, functions, characterizations, and testing, along with a depiction of inclined features.

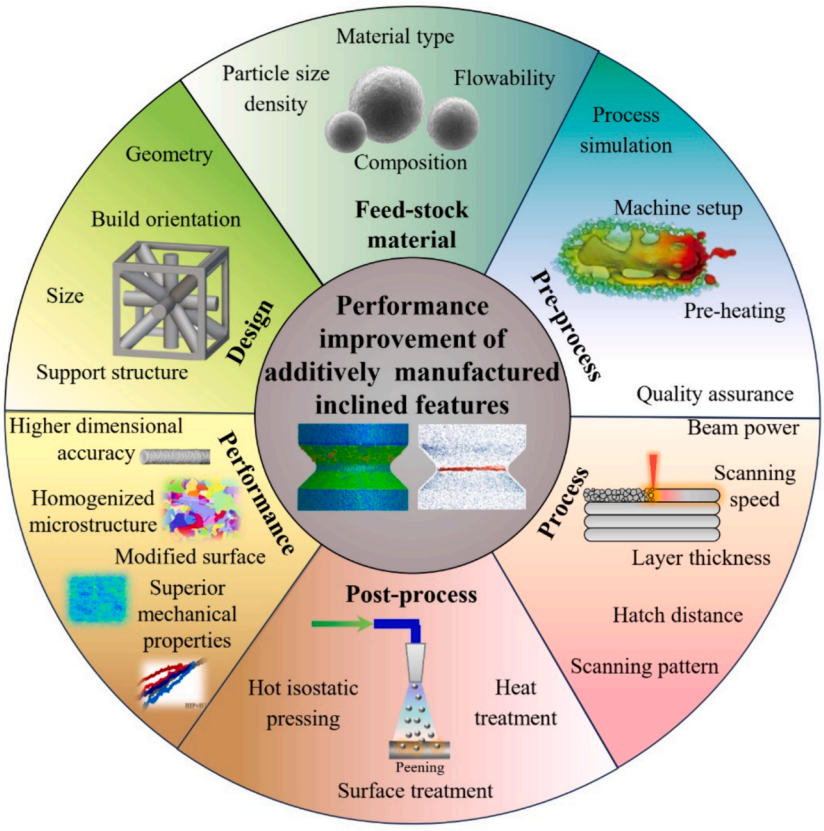

Fig. 2. Different routes to be leveraged for performance improvement of inclined features.

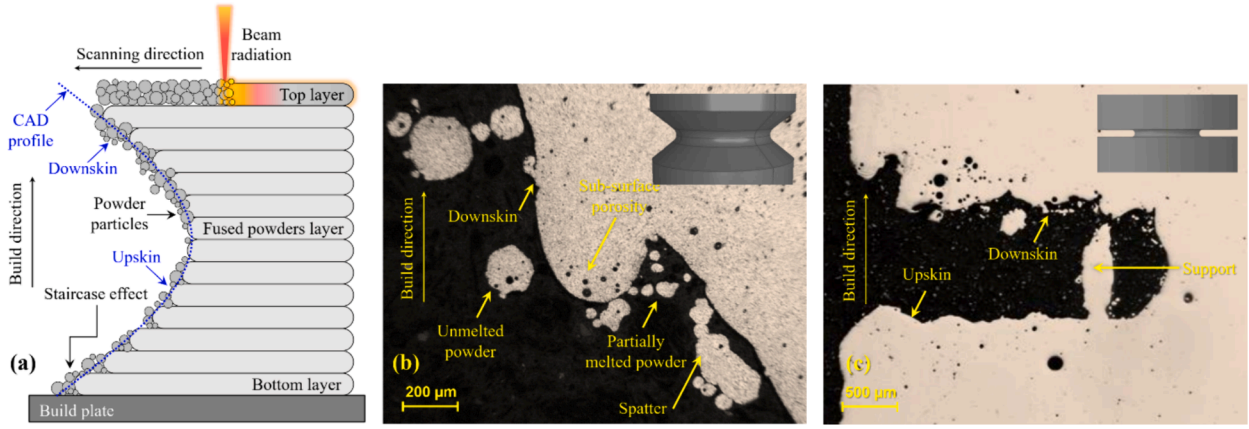

Fig. 3. Representative illustration of some of the most common defects caused by building orientation and presence of inclined features; adopted from [20,24–27] with modifications.

in surface roughness by adherence of partially melted and un-melted powder particles to the built periphery (Fig. 3).

This implies the importance of exploring the effects of build orientation on the properties of metallic AM parts to understand the fundamental relationships and find correlations, which would allow for process control and reproducibility. This theme has recently attracted the attention of many researchers. Experimental and sometimes numerical approaches have been used to study the potential effect of build orientation on the surface and mechanical properties of metal AM parts [32,33] mostly considering L-PBF and EB-PBF techniques. Regarding the materials, the most studied ones are Titanium alloys (mainly Ti6Al4V) [34], Aluminium alloys (mainly AlSi10Mg) [35], Stainless Steel (mainly 316L) [36], and Nickel alloys (mainly Inconel 718) [37]. As shown in Fig. 1, Apart from physical, microstructural, and mechanical properties, some studies focused also on the limits of manufacturability and geometrical

accuracy [38,39]. Regarding geometries in bulk parts, standard, either tensile or fatigue test specimens that directly analyse the mechanical performance of as-built parts are typically used. A vast portion of the available studies investigates the effect of build orientation on lattice structures, either strut-based or Triply Periodic Minimal Surface (TPMS) designs, where the build orientation is particularly critical due to the complex geometry of the structure. The majority of these studies explore single struts as the basic element of the lattice affecting its performance depending on their individual orientation, thus leading to potential anisotropy within the structure [40].

Despite the efforts that have been undertaken to study this aspect, there is a lack of a systematic analysis of orientation effects, and no precise design/evaluation guidelines are available. The studies resort to different technologies, materials, geometries, and sizes, thus making a direct comparison very challenging. The size of the component can affect multiple properties. For instance, small parts are influenced by a miniaturization effect, as given the higher surface-to-volume ratio, their mechanical performance is more sensitive to surface effects [41]. Most importantly, each metal AM technology involves several process parameters, which can influence the morphology, geometrical accuracy, surface quality, as well as microstructural and mechanical properties [42,43]. The interplay between the build orientation, process parameters and other factors cannot be ignored although it highly complicates the task of drawing general conclusions from single studies.

Hence, the present work aims to collect and review the literature on this critical topic, providing a comprehensive overview of the effects of the build orientation on the properties of metal parts produced through PBF technologies. The review is organized in the following sections, according to the main properties studied in the literature, to identify what has already been investigated and which topics could benefit further research. Manufacturability is reviewed initially, followed by geometrical accuracy, surface roughness, porosity and microstructure. Thereafter, mechanical properties such as hardness, static strength, fatigue strength and fracture toughness are explored, and the available results on wear and corrosion resistance are discussed. Then, the relationship between the build orientation and post-treatments is evaluated. Finally, the last section critically reviews the overall results, the existing challenges, and future perspectives in this area. This work aims to offer a guideline for build orientation effects in PBF and serve as a reliable source for future research in producing metallic components.

2. Effects of build orientation on manufacturability

Metal AM technologies attempt to accurately imitate the geometry described in the digital file into a physical object through layer wise manufacturing in accordance with the Design for AM (DfAM) guidelines [44]. Manufacturability is considered one of the most important aspects in producing complex shape components, and it depends on several factors, such as material properties, technology, process parameters, slicing technique, topology, and part orientation [45]. The term “manufacturability” describes how simple, effective, and generally feasible it is to produce a given design using a certain manufacturing process. It takes into account factors like: i) Material suitability: can the selected method process the selected material in an efficient manner? ii) Geometric complexity: does the part’s geometry work with the constraints of the manufacturing process (such as surface roughness and minimum feature size)? iii) Process constraints: are there any innate constraints in place that could make it more difficult to produce the intended object (such as residual stresses in AM methods)? iv) Economy of scale: is the cost of production realistic when taking into account labour, material, and machine time? and v) Production rate: in order to reach production targets, how rapidly can the part be manufactured?

As shown in Fig. 3, in layer-by-layer fabrication of inclined features, it is essential to use suitable support structures to ensure the correct construction of the desired geometry on the build plate. These support structures provide stability and prevent deformation during the manufacturing process, allowing for the accurate creation of complex shapes and inclined features. Properly designed supports also facilitate the removal of the final part from the build plate without damaging the intended geometry. Plus, it is recommended to optimize part orientation to minimize the number of overhanging features in the component [46,47]. Since overhangs are not always avoidable, support structures have been introduced to provide physical support, avoid heat accumulation in thin edges, facilitate the removal of the part from the build plate and thus provide broader design freedom [48–50]. The presence of support structures also generates several drawbacks such as increasing the use of material and the manufacturing time, as well as the need for additional post-processing steps for their removal [51]. Besides increasing the manufacturing process cost, support removal can reduce the surface quality of the component. Hence, DfAM guidelines suggest minimizing the use of support structures. Build orientation is a crucial factor in determining the manufacturability of a component in different AM technologies [28].

The requirements of L-PBF and EB-PBF regarding supports design are affected by the differences between the AM technologies [52]. In L-PBF, the machine applies a layer of loose powder, the laser selectively melts the current layer, then another powder layer is applied, and the selective melting process continues [53,54]. In each layer, the rest of the powder remains loose and free to move on the bed, with no connection between the metallic particles. At the end of the print, the part is easily removed from the building chamber and the remaining powder can be sieved and reutilized [55]. Since the loose powder does not provide any support to the subsequent layers, additional structures are required to provide mechanical support to the overhangs [56]. In the EB-PBF, on the other hand, an intermediate pre-heating step is performed before each layer melting, i.e., the electron beam is de-focused and scanned on the whole build plate, to sinter the powder [57,58]. A second sintering is then performed on the region where the component is built. At the end of the manufacturing process, the component and the sintered powder are extracted from the build chamber and blasted to obtain the clean object [59]. Sintered powder provides support for the subsequent layers, thus support structures are not necessary for the overhangs, although still used for heat dissipation [60]. Even if parts with any orientation are possible through EB-PBF, a highly inclined surface can result in poor surface quality. At any rate, EB-PBF parts generally exhibit relatively higher surface roughness [61,62] compared to L-PBF. This can be linked to their larger particle sizes and usually wider melt pools, necessitating a post-processing step [63].

Although build orientation may not be a major factor influencing manufacturability in EB-PBF, it may become an issue for thin components like lattice structures. Cansizoglu et al. [64] performed a process capability study, manufacturing Ti6Al4V single struts through EB-PBF. They found that manufacturability is affected by strut diameter, strut orientation and layer thickness, since these

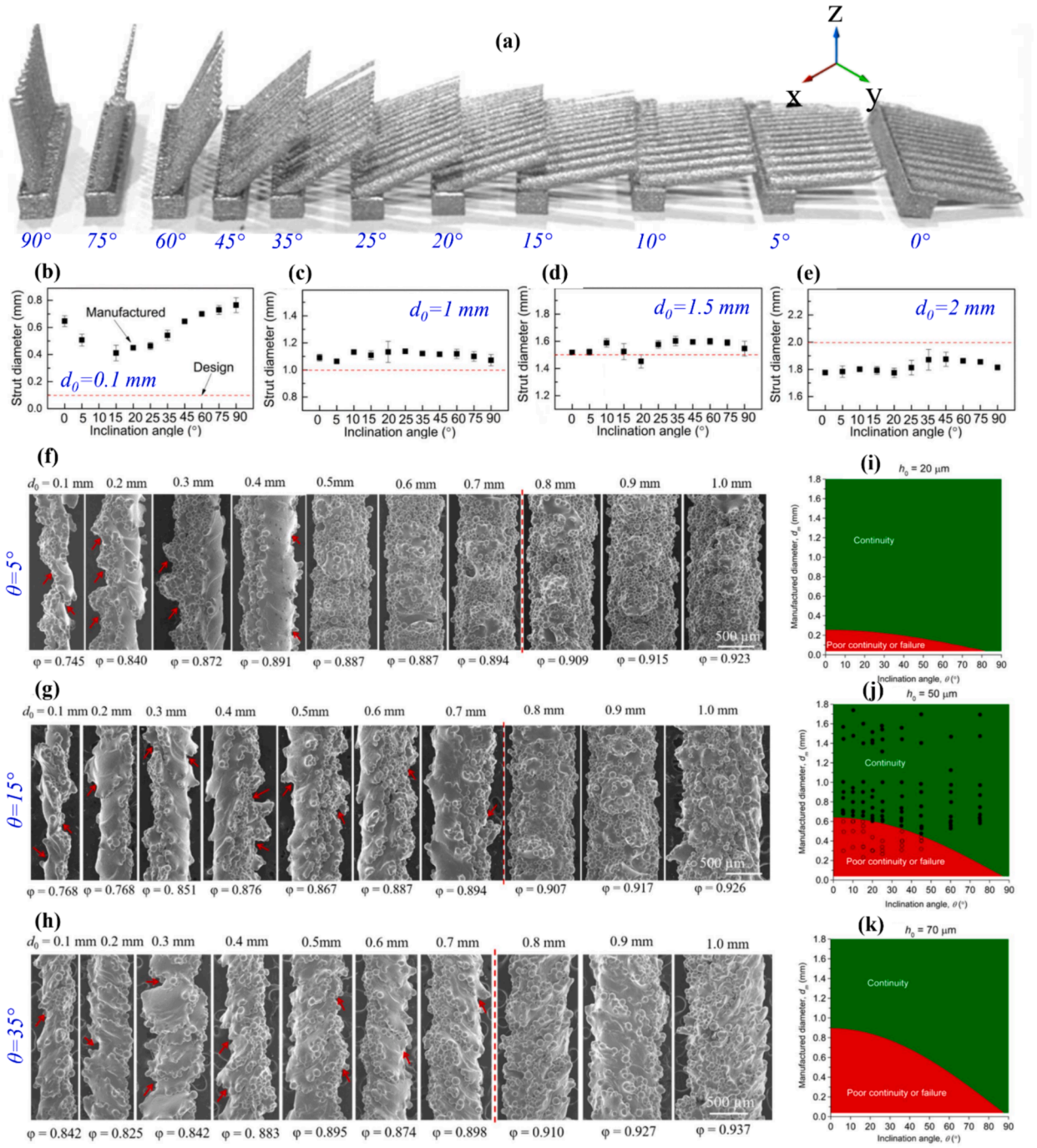

Fig. 4. (a) The analysed EB-PBF Ti6Al4V specimens, highlighting build orientations of 90°, 75°, 60°, 45°, 35°, 25°, 20°, 15°, 10°, 5° and 0° and design diameters of 0.05, 0.1, 0.2, 0.3, 0.4, 0.5, 0.6, 0.7, 0.8, 0.9, 1, 1.5, 2, 2.5 and 3 mm. (b) Manufactured diameters versus inclination angle with respect to different design diameters, d_0, of (b) 0.1, (c) 1, (d) 1.5 and (e) 2 mm [65]. Correspondence between minimum threshold parameter and strut morphology for Ti-6Al-4V struts manufactured by EB-PBF at different build orientations of (f) 5, (g) 15, and (h) 35° for different strut diameters. The threshold value of 0.9, ensuring good strut continuity, is indicated by the red dotted line [66]. Additive continuity maps (for EB-PBF Ti6Al4V specimens) depending on strut orientation and strut diameter for different layer thicknesses, h_0, of (i) 20, (j) 50, and (k) 70 μm with ideal $\rho_{PBD} = 0.6\rho_{TD}$ [66]. (For interpretation of the references to color in this figure legend, the reader is referred to the web version of this article.)

parameters determine the overlap between the subsequent layers. It was concluded that to achieve good strut integrity, struts with diameter > 0.7 mm and inclination angle $> 20^\circ$ should be designed. Zhang et al. [65] made Ti6Al4V strut specimens through EB-PBF with design diameters ranging from 0.05 to 3.0 mm, at 11 different building orientations of 90°, 75°, 60°, 45°, 35°, 25°, 20°, 15°, 10°, 5° and 0° (Fig. 4a) to study their manufacturability. The results indicated that the combination of strut diameter and inclination angle is crucial to ensure geometrical accuracy. Fig. 4b-e reveals the comparison of the manufactured diameters versus inclination angle with respect to different design diameters 0.1, 1, 1.5, and 2 mm, respectively. The results indicated that as-built struts with a diameter < 0.3

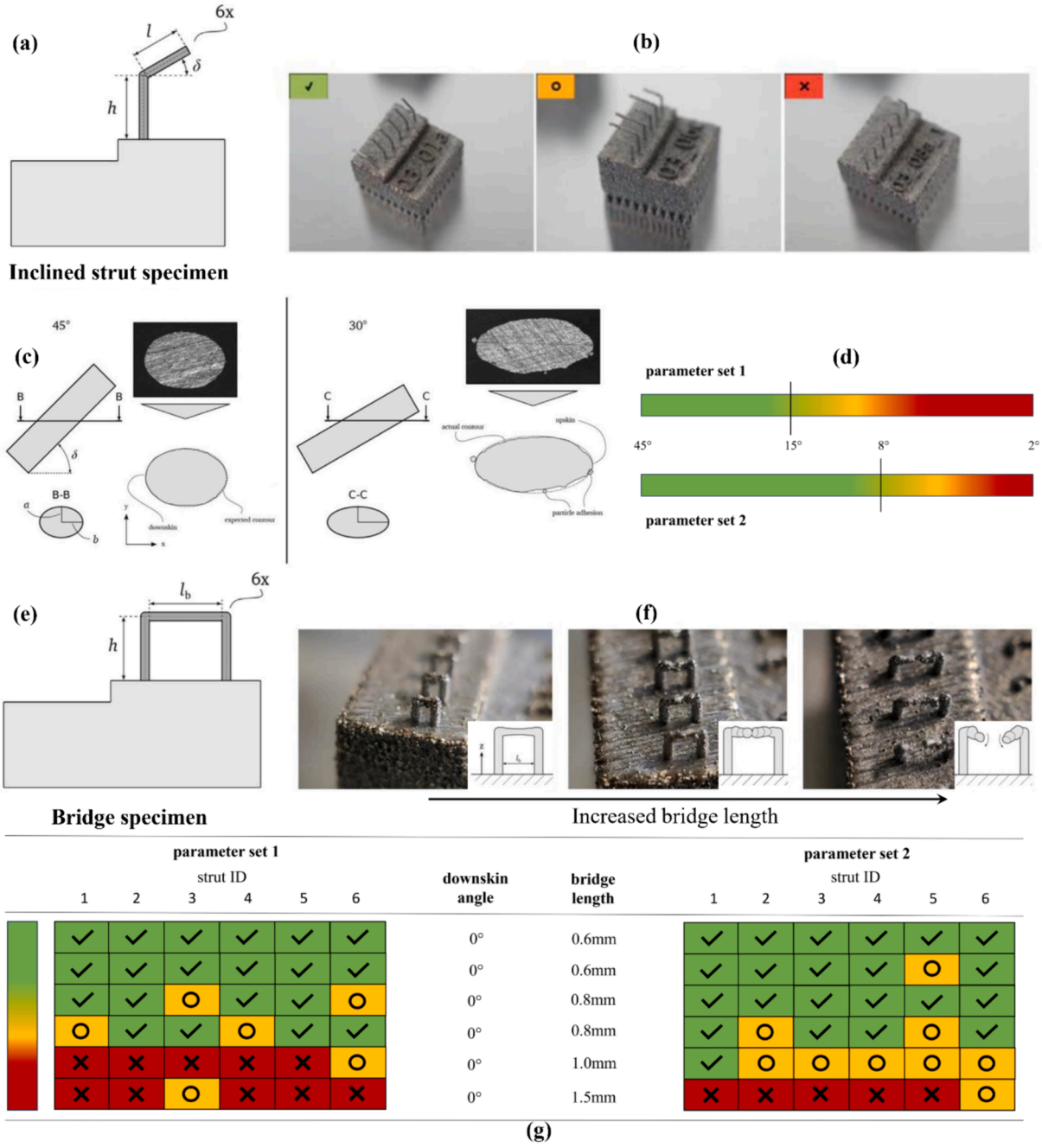

Fig. 5. (a) Geometry of the designed inclined strut and (b) L-PBF printed AlSi10Mg inclined specimens with build orientation ranging between 45° and 2°. (c) Comparison of strut manufacturing quality for 45° and 30° inclination angles. (d) 15° and 8° were identified as the limit angles for a successful print of inclined strut specimen. (e) Geometry of the designed bridge specimen and (f) visualizations of successful and failed prints for horizontal (bridge) AlSi10Mg specimens with different lengths. (g) Summary of successful or failed printability of bridge specimens considering two sets of parameters with different bridge lengths [38].

mm produced by orientation $< 25^{\circ}$ exhibited a cuboidal shape instead of the as-designed cylindrical form. For larger diameters > 0.3 mm, this discrepancy was observed for build orientation build orientation is an essential parameter $n < 10^{\circ}$; thus, the results suggested to avoid build orientations less than 10°. In a more recent study, Zhang et al. [66] highlighted the lack of a design guideline for strut continuity in EB-PBF lattice structures. Leveraging on their previous results, they tried to fill this gap, formulating a minimum threshold as a guideline for the design and manufacturing of such structures with robust continuity. In addition to strut diameter and strut inclination angle, the layer thickness and the density of the powder bed are also relevant parameters included in the formulation of the threshold. The results of the first study by Zhang et al. [65] were used to assess the value of the threshold to ensure good strut continuity, which was found to be 0.9, as visually noticeable in Fig. 4f-h, depicting the correspondence between minimum threshold parameter and the strut morphology for Ti6Al4 V struts manufactured by EB-PBF at different build orientations of 5, 15 and 35°, respectively. According to these results, the density of the powder bed (ρ_{PBD}) was suggested to be > 60 % of the theoretical density (ρ_{TD}), with the authors recommending the use of thin layers of powder [66]. The synergistic effect of these parameters is visually represented in "additive continuity maps" reported in Fig. 4i-k for different layer thicknesses of 20, 50, and 70 μm, respectively. Particularly, the results for a layer thickness of 50 μm are superimposed in this figure. The maps show how build orientation, in interplay with other factors, influences manufacturability, highlighting that extremely inclined struts are more challenging to manufacture.

On the other hand, build orientation holds a crucial role in the manufacturability of parts through L-PBF technology, imposing the necessity of developing mechanical support for overhanging features. This notion is strongly assessed in the knowledge of the process and reported in international standards. Particularly, the ISO standard [12] for the design of L-PBF parts prescribes the use of support structures under a critical angle ranging from 45 to 30°. Studies are typically oriented to enable the extension of such thresholds, producing complex parts with higher inclination without the need of support structures [67,68].

Meyer et al. [38] investigated the manufacturability of AlSi10Mg struts fabricated by L-PBF. They printed specimens with building orientations ranging from 45° to 2°, using two sets of parameters. Parameter set 2 comprises higher laser power and more than doubled energy density compared to Parameter set 1, while using almost 60 % lower scan speed. Fig. 5a and e illustrate the designed inclined strut and bridge specimens, respectively. The specimens were qualitatively assessed through visual evaluation and categorized as succeeded, partial, or failed print, as shown in Fig. 5b and f. The findings of the study revealed that as the inclination angle decreases, the exposed cross-section gradually transforms into a more elliptical shape. Eventually, it reaches a configuration where two parallel scanning lines closely resemble a rectangular pattern (Fig. 5c), where the relationship between the melt pool geometry and the hatch distance between those two lines becomes decisive for the strut printability. As presented in Fig. 5d, the results exhibit a limit angle of 8° and 15°. The results suggested that the higher energy density used in Set 2 (4.2 vs 2.0 J/mm^2) could provide a more stable molten pool. Considering bridge specimens, horizontal bridges (0°) were manufactured with different lengths. The print succeeded with a maximum length of 0.8 mm and 1 mm, respectively, with parameter set 1 and parameter set 2; however, poor section qualities were reported, as shown in Fig. 5g. In another work, Leary et al. [69] investigated the manufacturability of AlSi10Mg strut specimens built through L-PBF technology, as part of a wider study on lattice structures. Based on the findings, it was impossible to manufacture horizontal struts of any diameter. However, 35.3° specimens were feasible despite variations in geometrical fidelity caused by particles adhering to the down-skin area.

In conclusion, considering different build orientations and inclined features in AM, which significantly affect the manufacturability of parts, specific strategies should be implemented to optimize manufacturability. First, already at the design stage selecting an orientation that minimizes overhangs and reduces the need for support structures is essential. This approach not only enhances the efficiency of the manufacturing process but also reduces material waste, production and post-production time. Additionally, using advanced schemes to design and implement support structures that are easy to remove and provide adequate stability is crucial. These support structures must be robust enough to hold the part in place during the build process, yet easily detachable to avoid damaging the final product. Moreover, adjusting process parameters such as layer thickness, scanning speed, gas flow and cooling rates can significantly enhance feature resolution and part strength. Fine-tuning these parameters ensures that the fabricated parts meet the desired specifications. Employing design optimization techniques, such as topology optimization, helps create structurally efficient parts that require minimal support. This optimization leads to lighter, more cost-effective parts that do not compromise on strength or functionality. Utilizing simulation tools to predict and mitigate potential issues related to thermal stresses and material behavior during the build process is another vital solution. These simulations can foresee and address problems before they arise, ensuring a smoother manufacturing process and higher quality parts. Finally, implementing post-processing steps such as heat treatment, machining, or surface finishing is essential to achieve the desired part quality and tolerance. These steps refine the parts, enhancing their aesthetic and functional properties to meet the requirements. By integrating these solutions, the manufacturability of complex parts with inclined features can be significantly improved in AM. This comprehensive approach not only addresses the challenges inherent in producing intricate geometries but also ensures that the final products are of the highest quality, meeting both design and performance requirements. It should be noted that the manufacturability of inclined features or complex geometries for PBF technologies varies significantly between L-PBF and EB-PBF. For EB-PBF, the primary concern is the geometrical accuracy of the produced specimens, as this technology allows for manufacturing without the need for additional mechanical support structures. Conversely, for L-PBF, the focus is on minimizing the need for support structures. Both technologies face specific challenges when dealing with thin structures, such as lattice designs.

3. Effects of build orientation on dimensional accuracy

Apart from the manufacturability, part orientation can also significantly affect the geometrical accuracy. This can cause major

issues regarding the certification of AM products, especially for high-precision applications like in aerospace and biomedical sectors. Various studies have investigated the effect of DfAM and build orientation selection on geometrical accuracy in bulk and lattice specimens. Besides altering the size of the geometrical features with respect to the ideal as-designed dimensions, the build orientation can have a more diffused effect on the geometrical accuracy by influencing the overall shape of the structure, causing deviation and

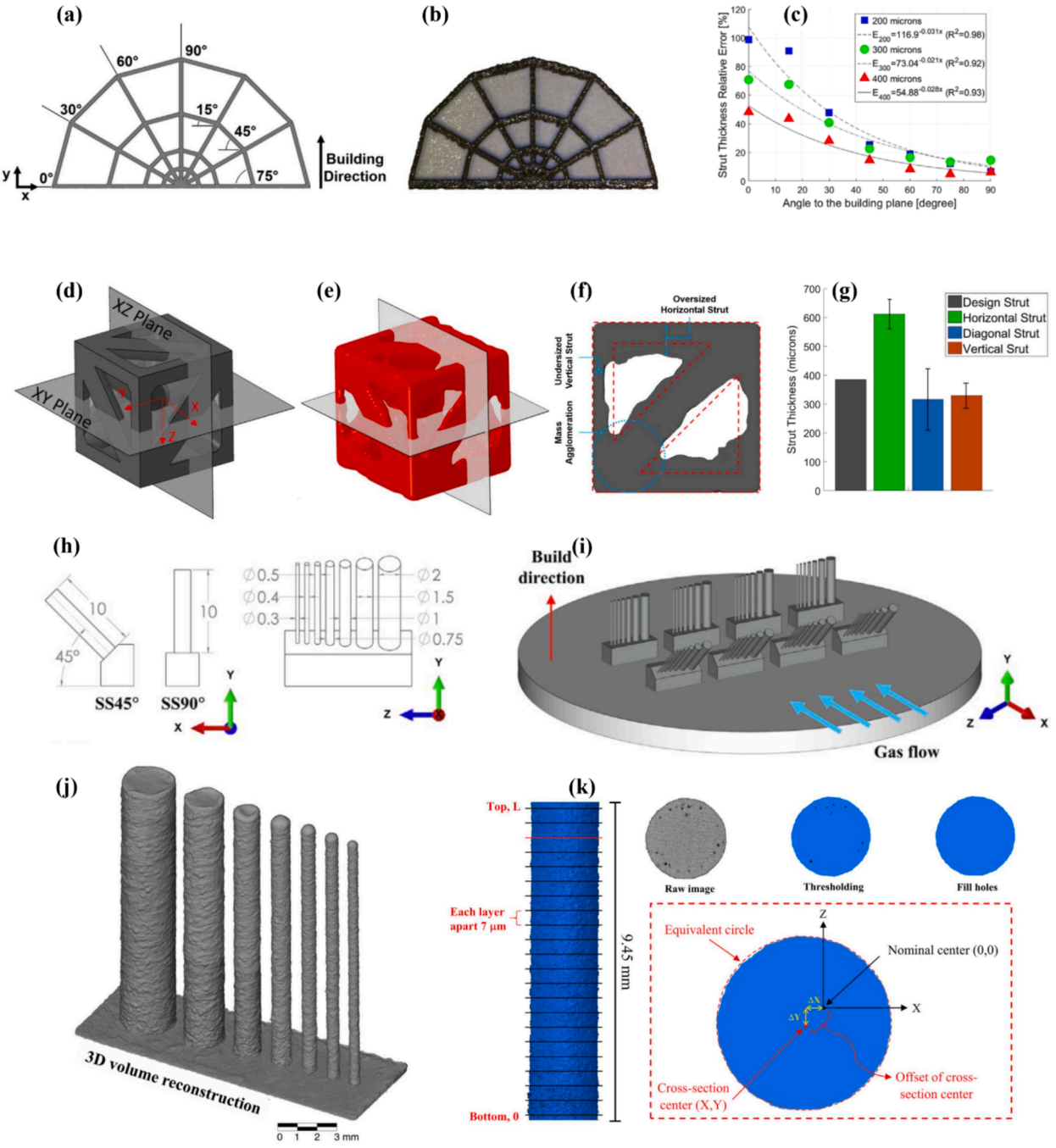

Fig. 6. (a) CAD design and (b) the fabricated Ti6Al4V spider web specimen through L-PBF. (c) Variation in strut thickness in the spider web specimen as a function of build angle [75]. Representative tetrahedron-based cell (obtained by µCT scanning) in (d) designed and (e) fabricated configuration. (f) Front view of fabricated lattice specimen geometry reconstructed from µCT with respect to the geometry of the designed cell shown in red. (g) Comparison of the thickness of the designed strut with the fabricated horizontal, vertical, and diagonal struts in the tetrahedron-based cell lattice geometry. (h) Dimensions and (i) build platform of single struts with vertical and 45° orientation [39]. (j) Reconstruction of 3D objects obtained from the µCT scanning for single struts with different diameters. (k) Extraction of data for the variation of the strut diameter [39]. (For interpretation of the references to color in this figure legend, the reader is referred to the web version of this article.)

other discrepancies. The methods for measuring the dimensional accuracy of AM parts include several advanced techniques. Coordinate measuring machines (CMMs) provide high precision measurements by probing the surface of the part with a tactile sensor, allowing for accurate dimensional verification against the design specifications [70]. Laser scanning captures the part's surface geometry by projecting laser beams onto the surface and measuring the reflected light, creating a detailed point cloud that represents the part's external shape. This method is particularly useful for complex geometries and large parts. Micro Computed Tomography (μCT) scanning offers detailed internal and external measurements by taking multiple X-ray images from different angles and reconstructing a 3D model of the part [71]. This non-destructive technique allows for the inspection of internal features and detection of any hidden defects or inconsistencies. Optical microscopy can be used for high-resolution surface measurements, providing detailed insights into the surface finish and microstructural features of the part. This method is especially useful for examining small and intricate details that might not be captured by other techniques. Traditional mechanical gauges and calipers are employed for simpler, less precise measurements [72]. These tools are easy to use and provide quick, on-the-spot measurements, making them suitable for initial checks and less critical dimensions. Each method varies in terms of accuracy, complexity, and suitability depending on the specific requirements and features of the AM parts. The choice of the measurement method often depends on factors such as the part's size, geometry, required precision, and the specific characteristics that need to be inspected. By selecting the appropriate measurement technique, manufacturers can ensure that AM parts meet the desired quality standards and functional requirements.

The following sections briefly describe the different aspects related to geometrical accuracy studied in the literature.

3.1. Strut size, thickness, and diameter

Numerous studies have focused on the correlation between build orientation and geometrical accuracy, investigating the variations in the strut size or thickness of specific features in the structure with respect to the as-designed geometry [73–81]. Murchio et al. [73] manufactured Ti6Al4V single struts with junctions along the gauge length through the L-PBF process in 4 different orientations with respect to the build plate: 0° (horizontal), 15°, 45°, and 90°(vertical). The strut-thickness analysis indicated that the average thickness of the struts with 90° angles was lower than the nominal one, while the thickness was increased compared to the expected values for the other angles. In general, 45° struts showed the best results in terms of the deviation from their average thickness, but among all, 90° ones were the most accurate with respect to the nominal thickness.

In another study, Liu et al. [74] manufactured AlSi10Mg prismatic cellular specimens via L-PBF process with two different unit cells of regular octet and rhombicuboctahedron design. Analysing the size of struts produced in horizontal (h), vertical (v), and diagonal (d) directions revealed that the horizontal struts were 24.5 % thicker than their theoretical value. Contrary to the oversized horizontally built struts, the vertical and diagonal ones were under size. Bagheri et al. [75] manufactured a planar spider-web geometry in Ti6Al4V made by L-PBF with struts at different inclinations ranging from 0 to 90° at 15° step (see Fig. 6a and b). Also, this study confirmed the significant variation of strut thickness as a function of build angle, reporting the horizontal direction to show the highest discrepancy and the vertical one the lowest (see Fig. 6c). They also investigated the effects of building orientation on strut size and thickness on lattice geometry considering tetrahedron-based cell design [75]. Fig. 6d and e represent the designed and fabricated lattice cell (obtained by μCT scanning), respectively. Fig. 6f illustrates the front view of fabricated lattice specimen reconstructed from μCT. The as-designed geometry (hidden red lines) is overlaid on the reconstructed images of the unit cell, demonstrating a significant geometry mismatch. In particular, the over-melting of the horizontal struts, the stair-case effect of the diagonal struts, under-sized vertical struts, and parasitic mass accumulation at the joints can be clearly perceived. Comparison of the thickness of the designed strut with fabricated horizontal, vertical, and diagonal struts is depicted in Fig. 6g. The results reveal that the fabricated horizontal strut had the highest thickness deviation, about two times higher compared to the designed size.

In another study, the diameter of AlSi10Mg struts produced by L-PBF was fixed at 1 mm, and the build orientation was varied from 10 to 45° with a 5° step. Higher absolute error in strut size was reported for the lower angle struts [35]. This observation was attributed to the higher tendency of partially melted/unmelted particles to the down-skin at lower angles, creating higher surface roughness, larger interlayer offset, and thus a larger molten pool.

Lu et al. [76] analysed the effects of different building orientations on triply periodic minimal surface (TPMS) specimens made of Ti6Al4V by L-PBF. Twelve specimens were produced along the part height (21 mm) and 12 others along the width (15 mm). The series produced along height exhibited 3.3 % wider width and 3 % shorter height compared to the original design dimensions. On the other hand, the specimens produced along width had 4.1 % narrower width and 2 % longer height with respect to the original design. Different types of TPMS designs (i.e., Primitive (P), Diamond (D), and Gyroid (G)) with different shell thicknesses and cell orientations ([1 0 0], [1 1 0] and [1 1 1] along loading direction) (see Fig. 6d) were investigated regarding geometrical accuracy in another study [77]. The results indicated deviation from the designed thickness in all the studied cases; in particular, the highest variance was reported for the P100 and P111 directions, while the Diamond unit cell designs showed the lowest sensibility to the building orientation. Regarding the Gyroid geometry, G110 and G111 showed high geometrical accuracy, whereas higher dimensional variation was reported in the case of the G100 specimen.

The geometrical accuracy of EB-PBF made Ti6Al4V octet-truss unit cells, including struts oriented along vertical (90°), diagonal (45°), and horizontal (0°) directions, was investigated by Suard et al. [78]. The results confirmed the previous observations revealing undersized features for vertical and diagonal (45°) struts compared to the nominal dimensions. The authors defined a geometrical equivalent diameter, which is the diameter of an ideal cylinder having the same length as the strut and a cross-section area equal to the inscribed surface area. The measured equivalent diameter for the specimens was reported to be significantly smaller compared to the nominal values. The deviation was higher for horizontal struts due to the over-melting and elongation of the cross-section along the build direction. The same group reported a similar trend for L-PBF Inconel 718 specimens [79], highlighting reduced diameter for

vertical struts compared to the inclined (35.3°) ones. The *iso*-volumic equivalent diameter, defined as the diameter of a cylinder with perfectly circular section with the same volume and height as the strut, showed a 7 % deviation with respect to the nominal value. However, interestingly, the mechanical equivalent diameter, which corresponds to the diameter of the ideal cylinder having the same stiffness as the as-built one, calculated using a fast Fourier transform (FFT), did not show a notable mismatch.

Following the same approach for dimensional comparison, Weißmann et al. [80] manufactured Ti6Al4V struts through both L-PBF and EB-PBF, considering two inclinations of vertical and 45°. The highest deviation was reported for the vertical EB-PBF specimens in this case. The L-PBF specimens demonstrated a higher dimensional accuracy compared to the EB-PBF series. Using diameter deviations

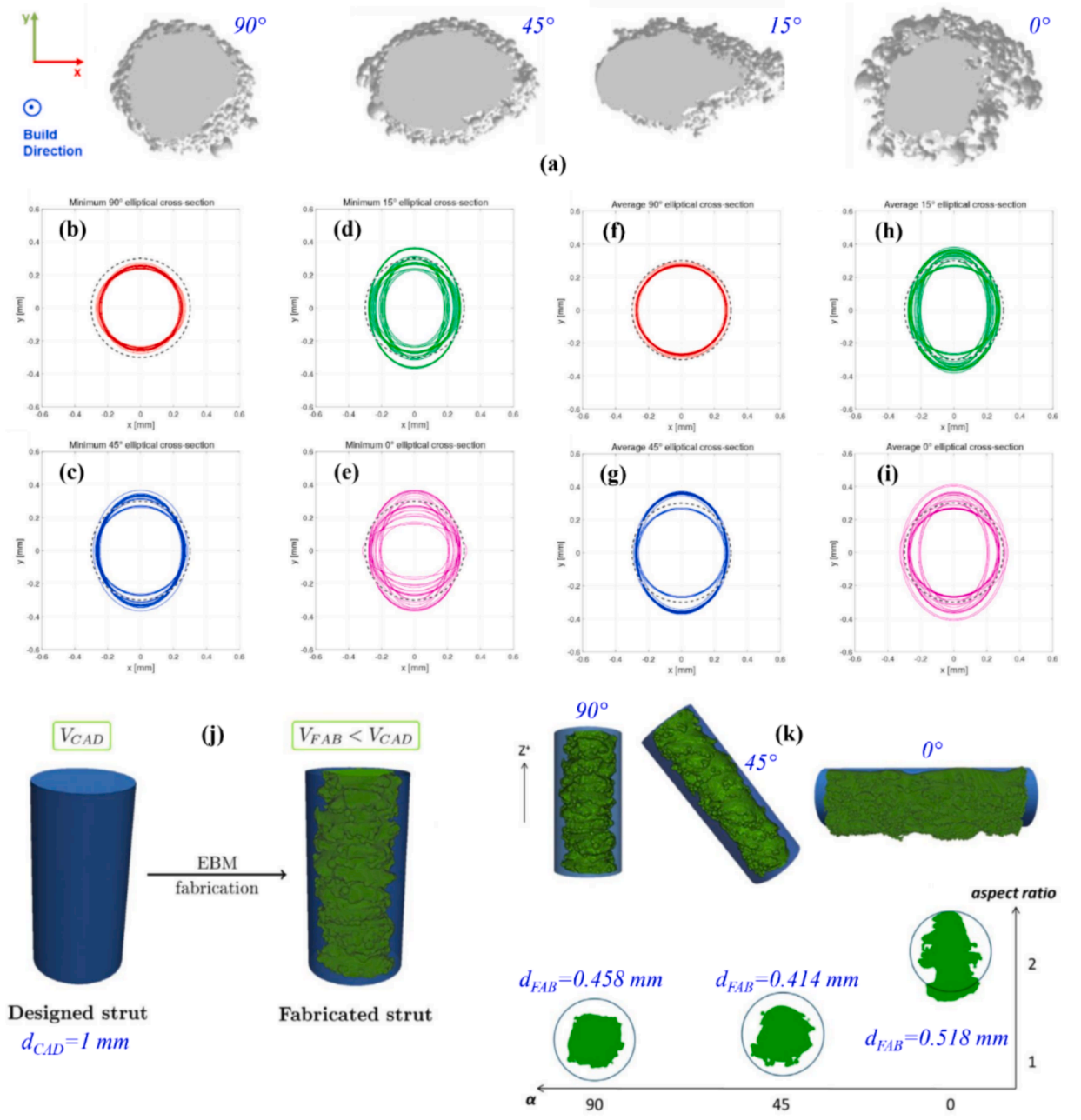

Fig. 7. (a) Cross-sections for different build orientations of 90°, 45°, 15° and 0° for Ti6Al4V thin struts produced via L-PBF. Minimum cross-section size measured by stereo optical images for the struts with build orientation of (b) 90°, (c) 45°, (d) 15° and (e) 0°. Average cross-section size for the struts with build orientation of (f) 90°, (g) 45°, (h) 15° and (i) 0° where the dashed black circle in all the plots represents the designed cross-section [41]. The 90° inclination struts presented a cross-section smaller than the designed one, but with a small standard deviation. The 0° inclined struts exhibited a lower geometrical accuracy with higher deviations from the nominal cross-section. (j) Comparing the designed and EB-PBF fabricated struts (k) Cross-section of vertical (i), 45° (ii), and horizontal (iii) single struts [78].

as the indicator for geometrical accuracy. Pérez-Sánchez et al. [81] measured smaller mean inner and outer diameters of vertical struts in EB-PBF Ti6Al4V specimens compared to those for 45° struts. However, the authors did not find significant differences between the actual and equivalent diameters. Sombatmai et al. [39] studied the variations of internal and external defects in EB-PBF Ti6Al4V single struts of different diameters and orientations (vertical and 45°), as shown in Fig. 6h and i, by analysing the reconstruction of 3D objects obtained from μCT scans (Fig. 6j and k). The results showed a maximum diameter deviation of approximately 15 %. Larger sizes were generally observed on the 45° struts as opposed to the 90° ones, which is consistent with the previous studies. The results were attributed to the fact that down-skin areas were supported by powder, which has lower thermal conductivity than the bulk material and thus provides lower heat dissipation, commonly resulting in a larger melt pool.

3.2. Strut shape and curvature

Apart from dimensions, the overall shape of the specimens and their features can also be significantly controlled by build orientation. Evaluating the eccentricity and form variations with respect to the nominal CAD model performed on Ti6Al4V thin struts produced via L-PBF showed that vertical specimens tended to be more circular, while lower printing angles resulted in a more elliptical drop-like cross-section (increased eccentricity) elongated in the y-direction. This is shown in Fig. 7a, which depicts *xy* cross sections for different build orientations of 90°, 45°, 15° and 0° [41]. In addition, vertical specimens were characterized with reduced cross-section, while the ones with 45° inclination exhibited higher shape deviation. Overall, the horizontal struts showed the lowest accuracy with a high standard deviation compared to the nominal shape, as presented in Fig. 7b-e for a minimum size of elliptical cross-sections and in Fig. 7f-i, which depict the average size of elliptical cross-sections in terms of different build orientations of 90°, 45°, 15° and 0°. A similar trend was confirmed in another study in L-PBF Ti6Al4V struts with junctions along the gauge length [73] considering four different orientations of 0°, 15°, 45°, and 90°, with respect to the build plate. The lowest minimum cross-sectional area was measured

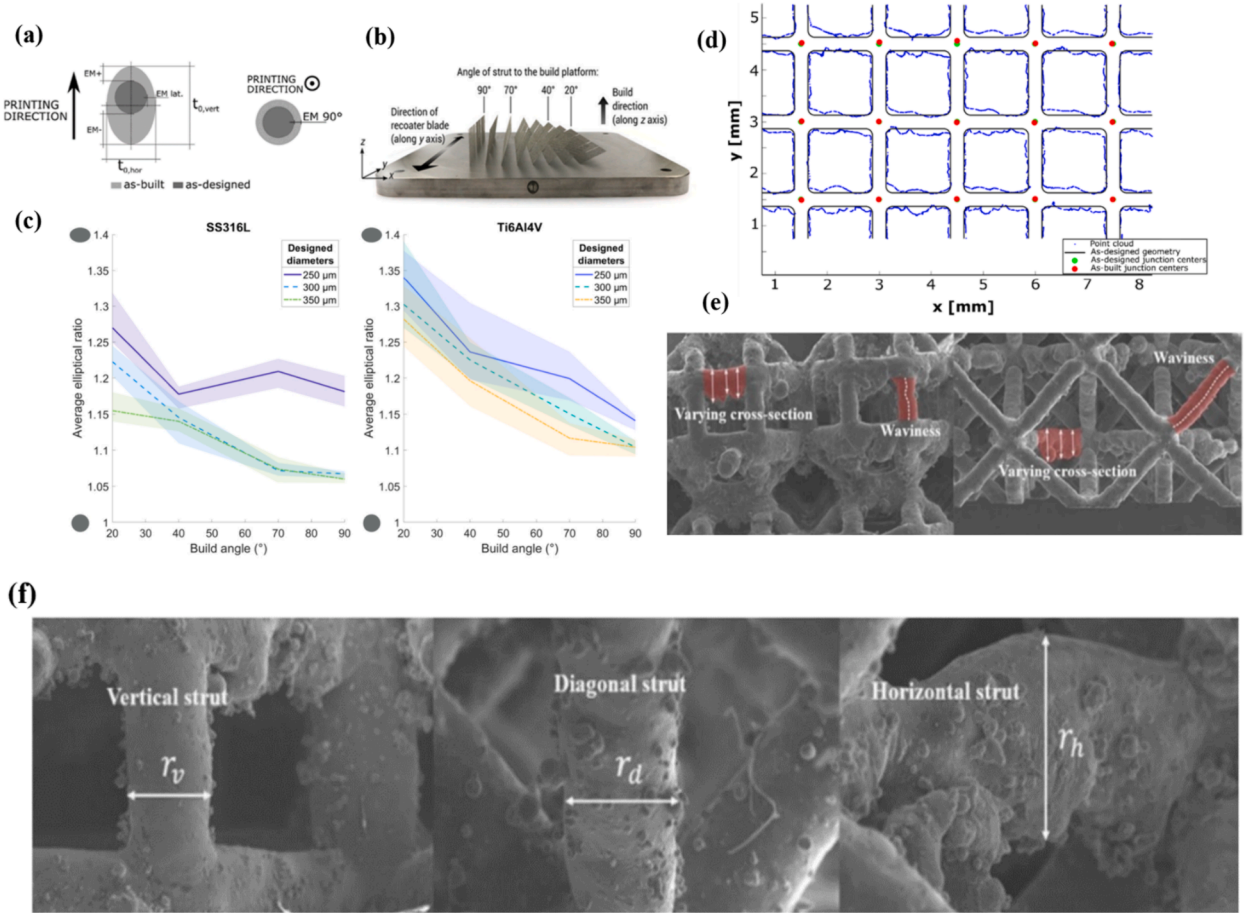

Fig. 8. (a) Comparison of as-built vs. as-designed cross-section for horizontal (left) and vertical (right) specimens along the build direction [83], (b) specimen design with different orientations, and (c) comparison of their average elliptical ratio for different build angles for both SS316L and Ti6Al4V [84]. (d) Curvature map of the horizontal and 45° struts, appearing as horizontal and vertical, respectively in the 2D picture, [86], (e) comparison of curvature and varying cross-section for horizontal struts (left) and diagonal struts (right) [74], and (f) comparison between thickness of vertical, diagonal and horizontal struts [74].

in the vertical struts, while the 0° specimens exhibited the highest cross-sectional area. The highest standard deviation for the minimum and average cross-section were reported in 15° and 0° specimens, whereas those printed at 90° and 45° displayed lower cross-section size variation along the gauge length. Similar results are reported by Suard et al. [78] where EB-LPB Ti–6Al–4V lattice structures with octet-truss unit cells of different orientations (90°, 45° and 0°) were investigated. It was reported that the diameter of the fabricated struts in all cases was lower than the designed one with $d_{cad} = 1$ mm (Fig. 7j); diameters of 0.458, 0.414, and 0.518 mm were obtained for fabricated struts with build orientation of 90°, 45° and 0°, respectively. Although for vertical and oblique struts, the cross-sections were rather equiaxed, with lower angles, until 0°, the cross-sections were clearly stretched towards the building direction as illustrated in Fig. 7k. Similar trends are also reported for L-PBF specimens evidencing rather equiaxed cross-section for vertical and 45° struts, while that of the horizontal ones was elongated in the build direction again due to the over-melting on down-skin that originated from the lower thermal conductivity of the loose powder [82,83].

Suard et al. [58] conducted a study to evaluate the shape deviation of L-PBF Inconel 718 struts from a perfect cylinder. The study showed that when the build direction was inclined, the cross-section tended to be elliptical, elongated in the build direction, rather than circular (Fig. 8a). Additionally, the mean shape deviation slightly increased, for example, from 0.05 for vertical struts to 0.10 for 35.3° inclined struts. This shape deviation was quantified in L-PBF Ti6Al4V and SS316L single-struts with 3 different diameters and 4 orientations of 20°, 40°, 70°, and 90° [84]. The results indicated that the elliptical ratio, that is, the ratio between the major axis length and the minor axis length of the ellipse fitted on the cross-section of the specimens, ranged from 1.06, in the case of 90° struts, to 1.34 for 20° of building orientation (Fig. 8b and c). The elliptical ratio in the vertical strut approached 1, which indicates a circular shape. The study confirmed that the struts were less circular when highly inclined due to increased overhang. Interestingly, the results also indicated that the titanium struts showed a lower geometrical accuracy compared to SS316L ones.

TPMS structures were also analysed for their geometrical shape sensitivity to build orientation. Yan et al. [85] considered TPMS Ti6Al-4V cellular structures of different types (Schoen gyroid, Schwarz diamond, Schwarz W, Neovius' surface) manufactured via L-PBF. The as-built cell types with a fixed volume fraction of 15 % and cell size of 5 mm were rotated on the Y-axis from 0° reference normal plane to 20°, 40°, 60°, 80°, 100°, 120°, 140°, 160°, and 180°. The worst orientation for each design corresponds to the angle with the largest overhang area and a range of 40–50° strut inclination with respect to the horizontal base plane. Basically, this orientation theoretically should be the most difficult to build in metal AM, especially for large cell sizes. However, all the TPMS typologies with different build orientations were successfully manufactured with an overall satisfactory geometrical accuracy. The designed and built architectures coincided with a standard deviation of approximately 0.12 mm.

In the TPMS structures, the inclination angle of the circular strut continuously varies along the spherical pore. As a result, the cross-section area grows gradually between two subsequent layers. In this way, the next layer is well supported by the previously solidified one. This implies that the TPMS lattice structures have a self-supported unique characteristic in a wider range of cell sizes, volume fractions, and cell orientations, making them suitable for the L-PBF process. However, it was reported that when the cell orientation with respect to the horizontal build plane was less than a certain angle, typically 45°, the cell wall quickly deformed, leading to build failure [85]. This agrees with the previous results on the lack of geometrical accuracy and shape control of horizontal and small-inclination angle struts.

Another dimensional deviation that affects the shape of struts is the waviness or the curvature, mostly induced due to the layer-by-layer nature of the AM process. This parameter is described as the mean deviation of the strut axis along its length [79]. Curvature in the struts can lead to significant geometric inaccuracies, which may compromise the structural integrity and performance of the manufactured part. This deviation occurs when the strut axis, ideally straight, bends or curves due to various factors such as thermal stresses, material shrinkage, or improper support during the build process. Addressing and minimizing these deviations are crucial for ensuring the reliability and precision of AM parts, especially in applications where dimensional accuracy is critical. Suard et al. [79] reported that inclined struts with an angle of 35.3° were characterized by a higher curvature (19 μm) compared to the vertical ones (12 μm). Dallago et al. [86] reported the highest curvature for the horizontal struts with a broader distribution compared to 45° struts (Fig. 8d). Liu et al. [53] confirmed that horizontal struts were wavier than the diagonal struts and had irregular cross-sections with greater strut thickness variation. It was concluded that in comparison with all the directions, horizontal struts had more significant geometrical defects. Thus, it was again confirmed that the horizontal struts exhibit the worst geometrical accuracy with respect to the other build directions (Fig. 8e and f).

4. Effects of build orientation on physical parameters

Apart from geometrical accuracy, other physical characteristics of the AM parts like surface topography and porosity can be also significantly affected by build orientation and, consequently, influence static and fatigue strength [84,87,88]. For this reason, notable effort has been put into investigating the correlation between build orientation and surface topography as well as porosity, as discussed in the following sections.

4.1. Surface roughness and topography

Characterizing the as-built surface topography and identifying topographical features for PBF processed materials is both crucial and challenging. This characterization is essential because the surface topography significantly influences the mechanical properties, performance, and functionality of the final parts. The intricate nature of PBF processes often results in complex and inhomogeneous surface textures, including partially melted powder particles, surface roughness, and layer lines, which must be accurately assessed to ensure quality and consistency. Several studies in the literature have comprehensively investigated the characterization of as-built

surface topography [89–92]. Additionally, researchers have employed statistical and computational methods to analyze surface roughness parameters, quantify topographical features, and understand their impact on the overall mechanical performance [93,94] of the part under various loading conditions. Through these investigations, the studies aim to develop standardized methods for surface characterization, optimize process parameters, and enhance the surface quality of PBF materials. Average roughness of the parts has been reported to generally decrease with higher build angles, that is, the vertical builds exhibit the minimum surface roughness. However, it is important to verify whether this is a valid observation among various AM technologies and if it is the same for both the up-skin/low-skin surfaces [41,80,95,96].

Weißmann et al. [80] compared this aspect for L-PBF and EB-PBF technologies using Ti6Al4V specimens with a custom shape composed of two cylindrical and parallel plates (top and base areas) connected through four perpendicular struts. In L-PBF specimens, both R_a and R_z were lower in vertical struts than those inclined by 45°, while surface analysis indicated an opposite trend in the EB-PBF series. In L-PBF, due to the energy flow, the powder particles adhere to the underside causing deviations from the designed geometry; this phenomenon leads to higher roughness in 45° struts compared to the vertical ones. In EB-PBF, on the other hand, the same phenomenon leads to reduced surface roughness since it cases filling of some surface unevenness. Interestingly, L-PBF specimens were reported to have an equivalent diameter closer to the design value compared to the EB-PBF ones. Nguyen H. et al. [97] also reported smoother surfaces obtained for L-PBF Ti6Al4V alloy specimens compared to EB-PBF ones. This was attributed to the higher thermal radiation associated to the electron beam in EB-PBF that promoted the adhesion of partially melted powders to the outer surface of the specimens.

Dealing with surface quality of AM parts with different fabrication conditions, Hoving [98] investigated the effects of several build orientations including 0°, 15°, 30°, 45°, 60°, 75°, 90°, 105°, 120° and 135° on the surface topography of L-PBF maraging steel grade 300 (18Ni300) (see Fig. 9a). Fig. 9b shows roughness oscillating between 0° and 90° with nearly constant value, while increasing swiftly at build angles higher than 90°. This trend can be due to the fact at angles higher than 90°, the surface shifts from up-skin to down-skin. The results also indicate that parts with 60° and 75° build orientations had the lowest surface roughness. Considering build orientation of 0°-90° the surface roughness values of about 10–15 μm were obtained in terms of R_a; however, higher surface roughness of about 20, 28 and 73 μm were achieved for the orientations of 105°, 120° and 135°, respectively. It should be noted that a similar trend was observed for R_z as well. In addition, influences of build orientation on the surface topography of the parts are illustrated in Fig. 9c and d considering the cross-sectional and top view demonstrating very poor surface quality for the parts fabricated with build orientation of more than 90°. Furthermore, up-skin surfaces were commonly reported to have lower surface roughness compared to down-skin ones [35,41,69,98,99].

Zhang et al. [35] investigated L-PBF AlSi10Mg specimens and found similar surface roughness in the up-skin area for all specimens tilted between 10°-45° inclinations, while the down-skin surface roughness decreased with increasing the tilt angle (getting closer to the vertical direction) due to the lower density of agglomerated powders adhered to the surface. Investigated the effect of strut size on surface roughness both for up and down-skin indicated that increasing the strut size results in slightly rougher up-skin surface, with no impact on the down-skin quality. Murchio et al. [41] analysed the roughness difference between the up-skin and down-skin surfaces more in-depth at different inclinations of 90°, 45°, 15° and 0° for Ti6Al4V printed with L-PBF as depicted in Fig. 9e. Fig. 9f represents the surface roughness values over the considered strut build orientations. Strut with build orientation of 90° exhibited the lowest surface roughness with about 17 μm in terms of R_a, followed by parts produced with build orientation of 45°, 15° and 0° having R_a values of about 23, 34 and 73 μm, respectively. Overall, surface topography was affected by the orientation of the building, with a non-linear trend from higher to lower angles. Fig. 9g shows how inclination increased surface roughness, with up-skin surface being always smoother than down-skin. Fig. 9h and i reveal the surface topography of the up-skin and down-skin faces at different build orientations, respectively. Higher surface anomalies were identified along the down-skin surface with respect to the up-skin part of the specimen. This mismatch was again further enhanced with the strut inclination with respect to the vertical fabricated struts [41].

Similar results were obtained for L-PBF Inconel 625 cylindrical struts built with orientations of 90°, 80°, 70°, 60°, 50°, 40° and 30°, as depicted in Fig. 9j [100]. This study analysed the arithmetic mean primary profile (P_a) that is an equivalent of the surface roughness but using cylindrical coordinates instead of cartesian ones. This factor was considered as the specimens were cylindrical; P_a is plotted as a function of build orientation in Fig. 9k and l. The results indicated the insensitivity of up-skin roughness (denoted as US in Fig. 9l) with respect to the build orientation, also considering the staircase effect. Instead, when this effect was eliminated, the US roughness slightly increased as a function of build orientation. In this study, another parameter called the re-entrant features ratio (q) was defined as the ratio between the sum of the areas with a negative radius component of the normal vector and the sum of all areas. As represented in Fig. 9m and n, the re-entrant features ratio strictly depends on the build direction and the roughness. It increases with inclination at the down-skin, while decreasing on the up-skin surfaces. The results indicated a linear correlation between roughness and q, indicating no re-entrant features at surfaces with low roughness [100].

In another study, Suard et al. [78] surveyed the circumferential variation of roughness on EB-PBF Ti6Al4V cylindrical specimens at different orientations. In vertical single-struts, no significant surface roughness variations were noted circumferentially, whereas, on inclined or horizontal struts, the down-skin roughness was higher due to over-melting and the higher density of partially melted adhered particles. This difference in roughness, particularly for low angles, has to be considered since it changes the mechanical strength of the specimens, as will be described in the next sections.

Another interesting but less studied aspect is the differences between the surface roughness of inner and outer surfaces. Maculotti G. et al. [101] analysed EB-PBF Ti6Al4V with a shape composed of plates at different inclinations. The results were compared both for different orientations (30–50–70–90°) and the inner and outer surfaces per each inclination. The outcome highlighted the lower surface quality of the outer surfaces compared to the inner ones for each build orientation.

In summary, the orientation of the build has been identified as a significant factor influencing the surface roughness of specimens.

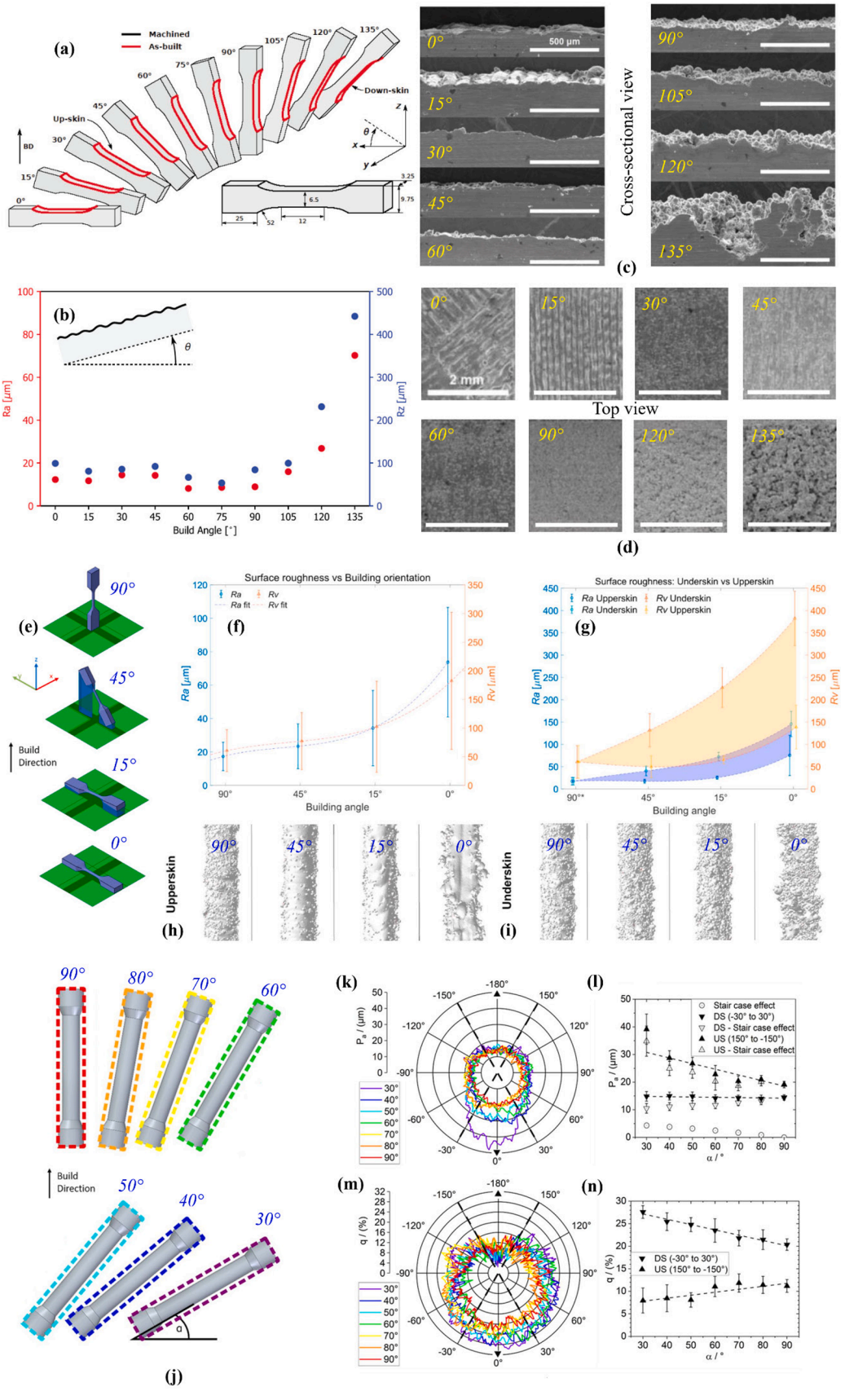

(caption on next page)

Fig. 9. (a) Specimen orientations of 0°, 15°, 30°, 45°, 60°, 75°, 90°, 105°, 120° and 135° and the specimen dimensions for the L-PBF 18Ni300 (BD indicates the build direction). (b) Surface roughness (R_a and R_z) as a function of build orientation for L-PBF 18Ni300. Surface topography of parts fabricated with different build orientations in (c) cross-sectional and (d) top view demonstrating the inferior surface quality of parts fabricated with build orientation more than 90° [98]. (e) Build orientations of 90°, 45°, 15° and 0° for L-PBF Ti6Al4V specimens. (f) Surface roughness in terms of R_a and R_v over the considered strut build orientations demonstrating that fabricated strut with build orientation of 90° had the lowest surface roughness, followed by those produced at 45°, 15°, and 0°, respectively. (g) Surface topography variations at different inclinations for up and down-skin were obtained with L-PBF for Ti6Al4V struts. Surface topography of the (h) up-skin and (i) down-skin faces at different build orientations showing more surface anomalies on the down-skin faces [41]. (j) L-PBF Inconel 625 cylindrical struts built with orientations of 90°, 80°, 70°, 60°, 50°, 40° and 30°. (k) Variation of roughness index (P_a) as a function of alpha (build orientation) and (l) correlation between build orientation and the roughness index. (m) Variation of re-entrant features ratio (q) as a function of build orientation and (n) correlation between build orientation and re-entrant features ratio (q) in L-BPF Inconel 625 struts [73].

In L-PBF, it has been observed that roughness tends to increase with the inclination angle, with down-skin surfaces exhibiting higher roughness and more defects compared to up-skin surfaces. Conversely, an opposite trend has been reported in EB-PBF, where higher inclination angles result in lower roughness. Furthermore, studies have demonstrated that feature sizes, particularly the strut size in lattice structures, have an impact on roughness. These studies have shown that feature size correlates with an increase in up-skin roughness while yielding no significant effect on the quality of down-skin surfaces.

4.2. Porosity

Several studies have indicated that build orientation can significantly influence the porosity content of the AM parts [35,65,100,102]. An uncontrolled increase in porosity content would result in lower part density and, therefore, lower load-bearing capacity [103]. Moreover, in the case of cellular structures, the un-desired porosity within the struts affects the overall density of the structure [104]. Internal pores in the as-built AM parts can originate from several sources, such as process parameters, part orientation, and powder properties [105,106]. Regarding the contribution of the process parameters, in metal AM, the first step in material processing is to identify the optimized parameters that lead to fully dense parts [107]. Studies have shown that through process parameter optimization for PBF technologies, it would be possible to produce components with a very low internal defect content (<1 %) [65,66,79].

Fritsch et al. [100] studied the effects of build orientation on porosity and surface quality in L-PBF Inconel 625 specimens with build orientations ranging between 30° and 90° with a 10° step. While the number of pores on the up-skin did not show a clear trend, the results in Fig. 10a and Fig. 10b indicated a decrease in the number of down-skin pores and the stability of up-skin pores' number when the build orientation varied from 30° to 90° with respect to the build plate. This analysis suggested a lower global number of pores in vertical specimens. The decreasing trend was attributed to the reduction in the density of small pores, while pores of larger dimensions showed no significant decrease in their number (see Fig. 10c). Moreover, the results highlighted a higher number of pores close to the down-skin surface compared to the up-skin for all orientations. For instance, Fig. 10d represents the locations of pores along the height of the strut with a build orientation of 30°, where the pores are color-coded based on their size: small (≤30 μm, green) and large (>30 μm, red) pores. Multiple experimental studies have reported higher porosity in the down-skin zone of inclined parts [35,66,102,104]. For instance, Fig. 10e represents the results obtained for L-PBF Ti6Al4V specimens fabricated with build orientations of 35.5°, 45°, 60°, and 90°, indicating higher porosity in the down-skin zone for all the considered build orientations, while in vertical specimens the porosity distribution is homogeneous across the whole surface. Detailed micrographs of porosities in the considered scan areas on up-skin (area A) and down-skin (area B) are represented in Fig. 10f [104]. These results are confirmed by another study performed by Delroisse et al. [102] on L-PBF AlSi10Mg specimens; they observed that the porosity of vertical struts was comparable to that of the up-skin of inclined parts (0.4–0.1 %), while it was more than one order higher in the down-skin (4 %). This trend is typically attributed to the complex thermal history of the built part, i.e., at low building angles, the interlayer offset is larger, so a larger portion of the part is supported by powder, which has a lower thermal conductivity [35]. Hence, the down-skin side of inclined parts stays at higher temperatures for a longer time due to the lower cooling rate. This causes an excessive pre-heating, leading to a larger [39] and more severe [35] molten pool characterized by instabilities and the formation of gas pores [102]. In fact, according to Delroisse et al. [102], the observed porosity was mainly composed of hydrogen pores since the solubility and diffusion of hydrogen in the cavities increased with the temperature.

Beyond the overall porosity, some researchers examined the relationship between build orientation and other porosity characteristics in more detail. However, the literature results are not always consistent. Suard et al. [79] reported that build orientation in L-PBF Inconel 718 specimens did not affect the mean diameter and the sphericity of pores. Moreover, as shown in Fig. 10g and Fig. 10h (for fabricated specimens with 90° and 35.3° build orientations), pore distribution along the width and length of the part was not affected by build orientation and was described as uniform. The authors considered two single struts of 1 mm diameter with different build orientations to estimate the porosity distributions in BCCZ lattice structures.

Although the link between build orientation, thermal history, and porosity is highly relevant, its interplay with other process parameters should be further investigated. One example of such analysis is reported by Zhang et al. [35] who studied the relative density of L-PBF AlSi10Mg specimens changing both the scanning speed and the build orientation. As shown in Fig. 10i lower scanning speed induced more pores (lower relative density (%)) for highly inclined (<20°) parts. On the contrary, at lower inclinations (>20°), the influence of scanning speed was negligible due to the wider interlayer offset region. Fig. 10j reveals the obtained results of porosity analyses considering same scanning speed of 2200 mm/s with different build orientations of 10°, 15°, 20°, 25°, 30° and 40°

demonstrating similar sphericity of pores as well. In contrast to these results, other studies found that pores can be more irregular (sphericity < 0.5) and elongated at low angles [41,65] reporting different distributions for superficial pores [41] with small pores increasing at lower angles [100].

Regarding porosity, instead, several studies report an opposite trend, i.e., a decrease in porosity at low build orientation angles [39,41,79,103,108]. For instance, Fig. 10*k* depicts the results obtained by Murchio et al. [41] on L-PBF Ti6Al4V specimens, showing that porosity decreased from vertically to horizontally built specimens. The results indicated mean porosities of 0.19, 0.09, 0.08, and 0.05 % for different build orientations of 90°, 45°, 15°, and 0°, respectively. These results were confirmed by Sombatmai et al. [39] for the same technology and material. Similar results were also reported for L-PBF AlSi10Mg fabricated with different build orientations of 0°-90°, as shown in Fig. 10l [109]. Mean porosities of 0.01, 0.06, and 0.08 % were obtained for bulk cubic specimens with build orientations of 0°, 45° and 90°, respectively. In addition, Fig. 10m depicts the normalized pore density and equivalent pore diameter (dp). Higher pore density was observed in 45° and 90° specimens, peaking at 1.2 mm^{-3} (45°) and 1.6 mm^{-3} (90°) for pore diameters of 60 μm ≤ dp < 70 μm. This trend in L-PBF is further confirmed also for 316L stainless steel [103]. These results revealed that specimens manufactured with a build orientation of 45° had a higher relative density with respect to the vertical ones; relative densities of about 99.71, 99.83, 99.91 and 99.96 % were reported for fabricated specimens with 90°, 75°, 60°, and 45°, respectively. Interestingly, the thermal history of the parts was used to justify this trend [39,79]. The occurrence of larger molten pools and heat accumulation on the down-skin of inclined specimens can prevent a deficient overlapping between the melted tracks, which can promote higher porosity. Thus, it can be noticed that different studies identify the same phenomenon as the cause of opposite trends. While other studies, such as Hossain et al. [84] studying L-PBF Ti6Al4V and 316L stainless steel specimens, found no clear correlation between porosity and build orientation. These discrepancies highlight the need for further systematic research to identify the nature and magnitude of such influence.

Consequently, the influence of build orientation on porosity remains a subject of ongoing debate, with diverse and, at times, contradictory findings reported in the literature. Notably, the degree of porosity appears to be significantly impacted by material selection, indicating a pronounced material-specific effect in specific scenarios. Some studies have documented elevated porosity in inclined specimens, while others have suggested that vertical specimens display the highest porosity levels. The complicated thermal history of the materials plays an important role in driving these divergent trends. Furthermore, achieving uniform heat distribution can be challenging on inclined surfaces, particularly those with complex geometries such as notched configurations. The latter, in turn, leads to the formation of areas with high and low energy levels, resulting in varying degrees of porosity.

5. Effects of build orientation on microstructural properties

Microstructure, as a fundamental characteristic, depends on multiple aspects. Particularly, thermal history is a key factor affecting the microstructure of metallic AM parts. In PBF technologies, parameters like energy source, scan speed, hatch distance, layer thickness, and build orientation are recognized to affect the microstructure of the produced part [110–113]. Due to the high scanning rate, the formation of very small melting pools, with high solidification and cooling rates and thus high thermal gradients, is typical in PBF. Therefore, these materials are commonly characterized with very refined cellular-like microstructures [114]. Due to the high cooling rates, the processing of certain types of alloys (steel or Ti) can lead to the formation of metastable phases (martensite) that are usually hard and brittle [115]. Consequently, it is necessary to perform posterior heat treatments to obtain a more suitable microstructure for in-service conditions [116]. Generally, the high thermal gradients promote epitaxial growth (columnar grains) and the generation of a crystallographic texture with preferential directions. This contributes to the anisotropic behaviour of AM parts [117,118].

Thermal gradients in PBF technologies, which have such a relevant influence on microstructure, are highly influenced by build orientation [119]. In fact, build orientation determines the amplitude of the overlapping region (a portion of the new layer supported by previously melted material), while the rest is supported by powder that has lower thermal conductivity compared to the melted material [30]. Moreover, part orientations different from vertical determine the presence of up-skin/down-skin regions in the part, which, as explained in previous sections, experience different thermal histories during the process. Thereafter, it is crucial to study the effect of build orientation on the microstructure of metal as-built parts.

Dong et al. [33] manufactured AlSi10Mg specimens through L-PBF to investigate the effect of build orientation on microstructure, geometrical accuracy, and mechanical properties. They compared the microstructure at different orientations of 35.5°, 45°, 60°, and 90° and reported a cellular-dendritic microstructure that was finer on the up-skin and coarser on the down-skin as shown in areas A and B for build orientation of 35.5° in Fig. 11a. The difference becomes more evident in more inclined struts by SEM observations, as shown in area B for all the four orientations on the down-skin zone in Fig. 11a. The coarsest grains could be noticed in the more inclined specimen with a build orientation of 35.5°. Moreover, 35.5° and 45° specimens showed coarser and elongated grains (columnar grains) with respect to 60° and vertical struts, which had fine equiaxed grains. Finally, the average grain size decreased going towards the vertical direction: from 3 μm in the 35.5° specimens to 2 μm at 45°, to 1.5 μm at 60°, and 1 μm in the vertical ones. The authors also investigated the thermal history of the inclined specimens through Finite Element Method (FEM) simulation and found a constant cooling rate on the up-skin, which increased by 51.5 % on the down-skin between 35.5° and vertical specimens. The FEM results confirmed the hypothesis that inclined specimens have a coarser microstructure, particularly on down-skin, due to the lower cooling rate allowing for grain growth.

These results were confirmed also by studying microstructural heterogeneity in L-PBF AlSi10Mg lattice specimens with a body-centred cubic (BCC) unit cell including vertical and 35.5° inclined struts [102]. The results indicated 2.5 to 3 times finer microstructure on the up-skin of 35.5° struts compared to their down-skin, justified by the thermal history of the part. Being partially

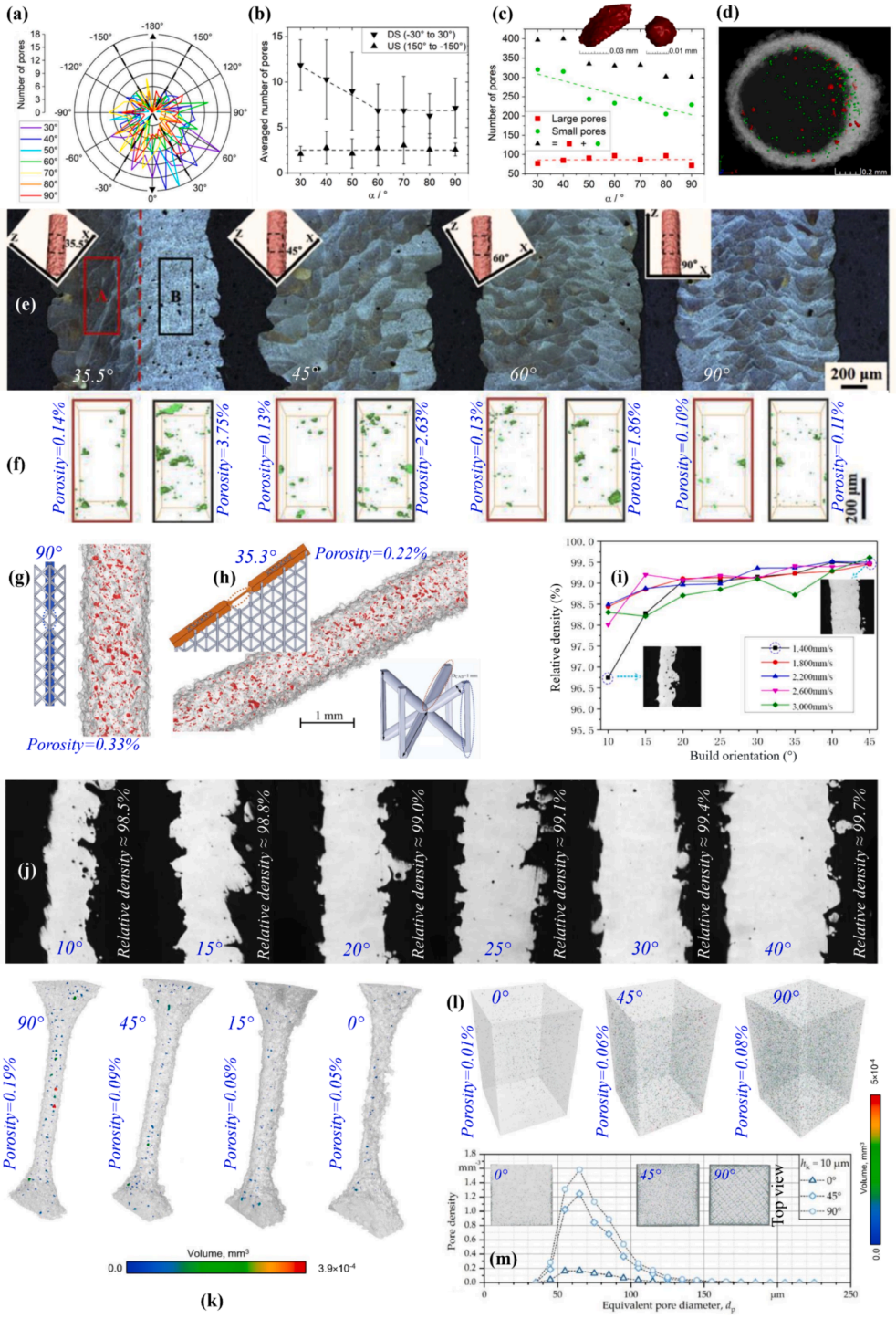

Fig. 10. The porosity analysis results for L-PBF Inconel 625 specimens with build orientations ranging between 30° and 90° with a 10° step in terms of (a) the number of pores estimated at each build orientations and (b) variation in the number of pores on the up-skin (US)/down-skin (DS) of the strut with respect to the build orientation. (c) Distribution of small (green) and large (red) pores on the strut cross-section as a function of build orientation. (d) Locations of pores along the height of the strut having a build orientation of 30° with the solid material being presented with a transparency of 90 % (black, in the centre) and the pores color-coded based on the size of small (≤30 µm, green) and large (>30 µm, red) pores [100]. (e) Distribution of pores between up-skin and down-skin zones in L-PBF Ti6Al4V struts made different inclinations of 35.5°, 45°, 60° and 90°. (f) Detailed micrographs of porosities in the considered scan areas on up-skin (area A) and down-skin (Area B) in the strut built with orientations of 35.5°-90° [104]. Uniform distribution of pores along the strut length and width for L-PBF Inconel 718 specimens fabricated with build orientations of (g) 90° and (h) 35.3° [79]. (i) The influence of scanning speed on the density of the L-PBF AlSi10Mg strut for different build orientations of 10°,

15°, 20°, 25°, 30°, 35°, 40° and 45°. (j) The results of porosity analysis considering the same scanning speed of 2200 mm/s with different build orientations of 10°, 15°, 20°, 25°, 30° and 40° [35]. (f) CT images of porosity distribution within the L-PBF Ti6Al4V struts built at different orientations (90°, 45°, 15°, 0°) in a volumetric scale [41]. (l) Porosity analysis for L-PBF AlSi10Mg fabricated with different build orientations of 0°-90°. (m) Comparison of defect density in different build orientations of 0°, 45° and 90° [109]. (For interpretation of the references to color in this figure legend, the reader is referred to the web version of this article.)

supported by powder, which acts as an insulator, the down-skin part of the strut stays at a higher temperature for a longer time, growing coarser grains. On the other hand, the up-skin portion is in a condition comparable to that of a vertically built strut since it is supported by melted material. The cooling rate is thus higher, leading to finer grains.

Nezhadfar et al. [91] reported that the typical grain structure produced in a metal AM process was made of columnar grains, with equiaxed grains particularly surrounding the molten pool. They studied the dependency of microstructure on horizontal and vertical build directions for five different Al alloys, all made using L-PBF with vertical and horizontal build orientations. Fig. 11b-e presents the Inverse Pole Figure (IPF) maps obtained by Electron Back Scatter Diffraction (EBSD) for specimens fabricated at 90° and 0° for different Al alloys of AlSi10Mg, Scalmalloy, QuesTek Al, and AlF357, respectively.

Isaac et al. [120] also surveyed the effects of different build orientations of 0°, 45° and 90° on the microstructure of L-PBF AlSi10Mg as depicted in Fig. 11f. The mean grain sizes of 8.9, 8.1, and 9 μm were reported for the parts with 0°, 45° and 90° build orientations, respectively, which exhibited very low differences. The results indicated that the microstructure mainly consisted of elongated columnar grains with refined fine grains around the melt-pool boundaries for all build orientations. These columnar grains, in which the grains appeared elongated along the build direction, can be observed surrounded by finer grains. This microstructure configuration is due to the repeated rapid melting and subsequent rapid cooling associated with the L-PBF process. Several studies in the literature report that build orientation can affect the growth of columnar grains, as the grains tend to grow aligned to build orientation [121,122]. This is because the heat flow is aligned with the build direction due to a higher thermal gradient, inducing a preferred grain orientation [123]. Ghorbanpour et al. [124] confirmed the grain elongation along the build direction in L-PBF Inconel 718 specimens made both horizontally and vertically, as shown in Fig. 11g. In addition, the obtained Grain Orientation Spread (GOS) maps (see Fig. 11h) revealed higher values for the horizontal specimens with a mean GOS of 0.88° compared to vertically built specimen having a mean GOS of 0.72°. The GOS plots indicate intragranular distortions and residual stress in the material, where higher GOS values imply higher misorientations and residual stress [125].

In another study, Leicht et al. [126] investigated the effects of different geometrical features and build orientations (90°, 45°, and 30°) on the microstructure of L-PBF 316L ribs. Fig. 11i illustrates the IPF maps of the fabricated ribs with different thicknesses and orientations. The results reveal that although the inclined specimens (45° and 30°) show random texture orientations, the ⟨0 0 1⟩ orientation (i.e., along the build direction), is dominant but with lower texture intensity with respect to the straight ones (90°). Large, elongated grains along the build direction can be observed in the fabricated ribs with 45° and 30° build angles. Also, similar to the straight ribs built at 90°, small grains are found along the surfaces of the inclined ribs. These finer grains can be observed on both up-skin and down-skin faces. It was concluded that these small grains are likely formed by the unmelted and partially melted powder, attached to both faces in varying amounts. However, most of them were incorporated at the down-skin. Reducing the build orientation from 45° to 30° resulted in more partially melted powders being fused at the down-skin. Moreover, those small grains do not seem to be growing towards the centre of the fabricated rib, as seen for the straight ribs as well. Instead, the small grains appear to be slightly elongated along the part surface. The variation in grain direction indicates a varying temperature gradient. The temperature gradient is determined by the thermal conductivity of both the powder bed and the part. Hence, the heat dissipation will change by variation of the build orientation and therefore affect the grain growth direction. In addition, it should be mentioned that the rib fabricated with 30° build orientation (Fig. 11i) was thinner compared to the specimens with a 45° build angle, highlighting again the geometrical accuracy limitation for manufacturing parts with inclination.

Dealing with columnar grain growth along the build direction, there are some contrasting results in the literature. For instance, Wauthle et al. [104] studied the microstructure of L-PBF Ti6Al4V lattice structures with various build orientations and reported that the grains could be elongated either along the build direction or along the strut orientation. Also, Murchio et al. [41] analysed the microstructure of L-PBF Ti6Al4V dog-bone specimens with 4 different orientations: 0, 15, 45, 90° (vertical). They found no significant differences in the microstructure of the 4 groups of specimens.

The investigated papers clearly confirm the significant influence of build orientation in PBF methods on the microstructure of the produced part. Thermal gradients resulting from different build orientations and their deviation from the preferred growth direction affect the formation of cellular/dendritic, columnar/equiaxed microstructures and grain sizes, depending on the composition. Different build orientations change the required sets of layers being scanned during the PBF procedure, which in turn affects the part thermal history. The results indicate that in inclined specimens, coarser and elongated columnar grains are observed on the down-skin, while finer equiaxed grains are seen on the up-skin. This difference in grain structure is attributed to varying cooling rates, with the down-skin experiencing lower cooling rates, resulting in coarser grains. Studies on different aluminium alloys confirm the dependency of microstructure on build orientation, with finer microstructures observed in specimens fabricated at vertical orientations. These findings highlight the importance of considering build orientation in metal AM to achieve the desired microstructural properties.

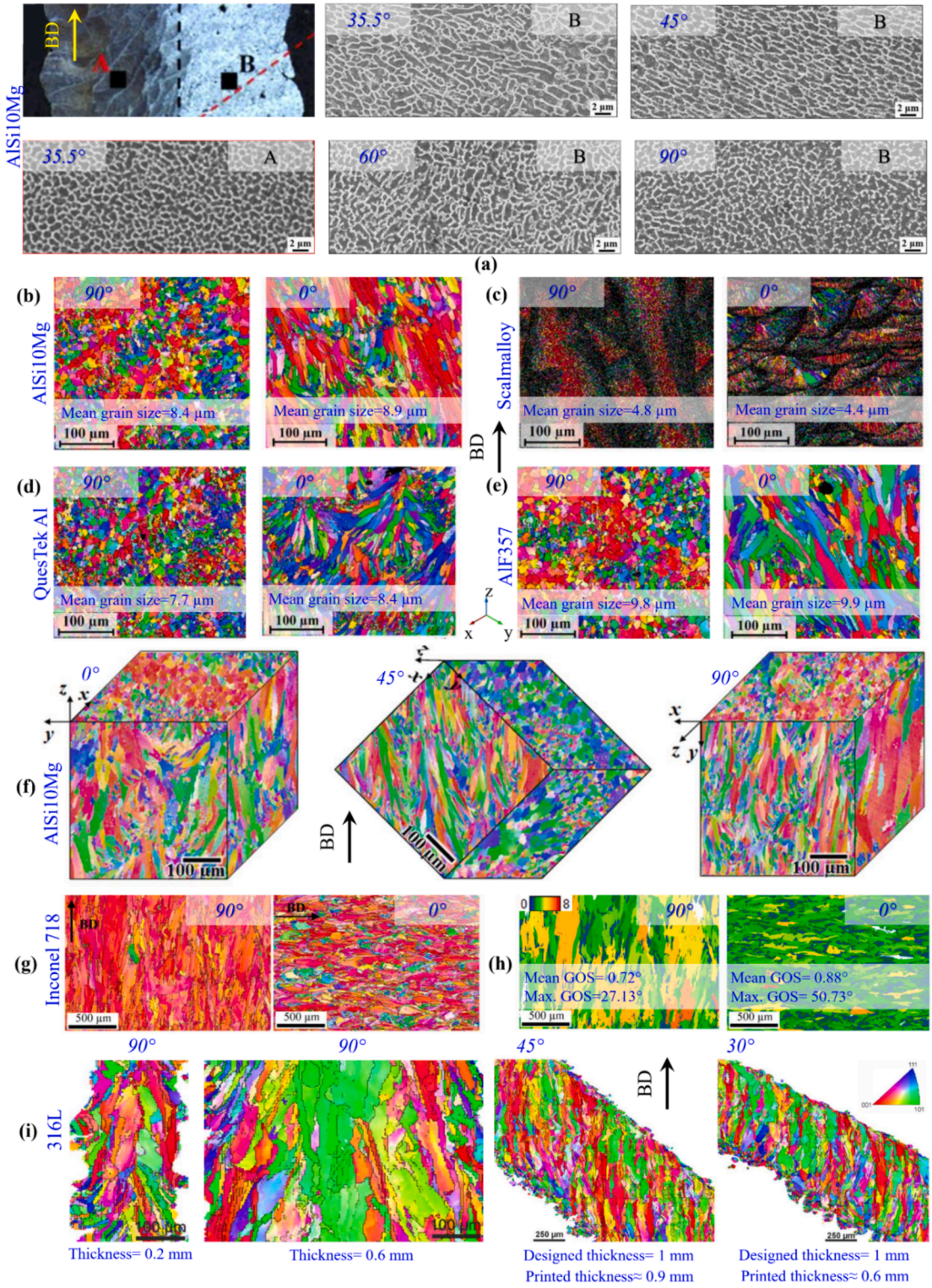

(caption on next page)

Fig. 11. (a) Microstructural analysis in L-PBF AlSi10Mg specimens with different orientations of 35.5°, 45°, 60°, 90° exhibiting cellular-dendritic microstructure on the up-skin and coarser on the down-skin shown in area A and B [33]. IPF maps of different Al alloys including (b) AlSi10Mg, (c) Scalmalloy, (d) QuesTek Al and (e) AlF357 all manufactured by L-PBF with vertical and horizontal build orientations. (f) Effects of build orientations of 0°, 45° and 90° on microstructure of L-PBF AlSi10Mg using IPF maps in three different xy, yz and yz planes [120]. (g) Grain elongation along the build direction in L-PBF Inconel 718 specimens fabricated with 90° and 0° build orientations and (h) the corresponding GOS maps indicating residual stresses and intragranular distortions [124]. (i) Effects of different geometrical features and build orientations of 90°, 45°, and 30° on the microstructure of L-PBF 316L ribs considering IPF maps [126].

6. Effects of build orientation on mechanical and chemical properties

6.1. Hardness

Hardness is one of the most widely analysed mechanical properties in AM, as it can be used as a valid index to evaluate the mechanical performance. In the case of struts, no microhardness dependency on build orientation has been reported [35,41,127]. However, a height dependency (i.e., distance from the build plate) was observed indicating lower microhardness in the top layer compared to the bottom ones. This is due to high cooling rates in the areas closer to the substrate, resulting in a finer microstructure. The average microhardness (HRC) values measured on the bottom and top layers of L-PBF Ti6Al4V specimens fabricated in three perpendicular orientations were respectively 33.55–31.65, 32.77–24.01 and 37.67–30.10 [127]. Palanisamy et al. [128] found slightly lower Vickers hardness in 45° Ti6Al4V struts compared to vertical ones, both for EB-PBF and L-PBF specimens. This observation was attributed to the microstructural difference, as in the vertical struts, alpha grains grew along the build direction in a more uniform pattern compared to the inclined struts.

6.2. Static strength

Static strength in AM materials, defined as the capacity to withstand fixed forces without breaking or yielding, can also be affected by build orientation. To evaluate this feature, various static and quasi-static tensile or compressive tests have been performed on different structures and building orientations ranging between 0° to 90° [39,103,104,122]. The results obtained from tensile and compressive tests are discussed separately in this section. Table 1 provides the summary of the studies performed on the performance of AM metallic materials under tensile testing.

Additionally, Pehlivan et al. [131] utilized L-PBF to fabricate a single strut made of CP-Ti Grade 2. The struts were produced in both vertical and horizontal orientations, with cross-sectional areas ranging from 0.07 mm^2 to 2.3 mm^2. The vertical struts were tested along the build direction, while horizontal struts were tested perpendicular to it. The obtained results indicated that for cross-sections smaller than 1.5 mm^2, the vertical struts had higher Yield Strength (YS) and lower elongation. In contrast, for cross-sections larger than 1.5 mm^2, the YS values were similar, and the elongation was higher compared to the horizontal struts. Additionally, the study revealed that the effect of orientation was less significant for cross-sectional areas higher than 1.5 mm^2, with orientation only being noticeable for small specimens (<1.5 mm^2), as demonstrated in Fig. 14a and b. In another study [39], researchers conducted a comparative analysis between numerical models derived from as-designed and as-built geometries. The study involved the use of L-PBF technology and Ti6Al4V lattice struts. Findings indicated that the initial YS was influenced by the size and orientation of the struts. Specifically, for vertical struts, the initial YS decreased with size. On the other hand, for 45° struts, the initial YS increased with larger diameters. Bültmann et al. [103] investigated the effect of strut diameter on the mechanical properties of L-PBF 316L specimens. Based on Fig. 13d and e, which examines the variation of YS, Ultimate Tensile Strength (UTS), and uniform elongation across the diameter of multi-strut specimens, the YS and UTS remain relatively unaffected by variations of the strut diameter; however, a reduction in diameter leads to a corresponding decrease in uniform elongation.

Compressive tests have been also widely applied to explore the effect of build orientation on mechanical properties of AM metallic materials [74,82,104,122,123], as summarized in Table 2.

Wauthle et al. [104] conducted a static compressive test on L-PBF Ti6Al4V diamond-like lattice structures and reported that the poor quality of horizontal struts led to the early failure of the structures. The results indicated that if there are vertical struts to bear the load, lower-quality horizontal struts do not considerably affect the mechanical performance. However, considering the current manufacturing capabilities, it is recommended to avoid horizontally oriented struts for isotopically loaded lattice structures or situations where the direction of loading is unknown, unless the load can be sufficiently sustained by other struts. Liu et al. [74] conducted a static compressive test on L-PBF AlSi10Mg lattice consisting of regular octet and rhombicuboctahedron units manufactured with geometric defects. They developed numerical models based on two different Representative Volume Elements (RVE), corresponding to the as-designed and as-manufactured geometry, to investigate the effect of the defects on mechanical properties for different building orientations. A parametric study was performed to evaluate the effects of strut thickness variation and strut waviness on elastic modulus and compressive strength, considering that these defects depend on build orientation. It was found that increasing the amplitude of the geometric defects leads to a decrease in both elastic modulus and compressive strength, with thickness variation having a higher effect on compressive strength, while waviness has a more notable effect on elastic modulus. Moreover, analysis of the failure modes of the cellular specimens indicated that strut over/under sizing, which depends on build orientation, can influence the failure mode. This influence is observed in the transition from diagonal shear failure to horizontal crushing failure in the case of octet lattice structures. Similarly, for rhombicuboctahedron lattices, it results in the transition from local buckling failure to the crushing of the distal polyhedral parts of the cells. This was expressed as the ratio between the average radius of vertical struts and the average

radius of diagonal struts, stating that for the regular octet, when horizontal struts are 1.8 times thicker than diagonal struts, diagonal shear plane of failure transforms into horizontal crushing. While, in the case of rhombicuboctahedron design, the failure mechanism was regulated by local buckling of the vertical struts for values of the ratio smaller than 1.2, and for higher values of the ratio, by crushing of the distal polyhedral of the cells.

Additionally, Dallago et al. [82] conducted quasi-static compressive tests on cubic L-PBF Ti6Al4V lattice specimens, printed vertically (A) and horizontally (B). Numerical models were used to investigate the effect of defects on elastic modulus, which was found to be closely related to build orientation in horizontal struts. The results indicated that oversizing of struts increased the elastic moduli, while waviness and junction centre displacement (due to over-melting of horizontal struts) decreased the elastic moduli, as they introduced bending in the predominantly stretch-dominated lattice. Lu et al. [76] analysed the impact of different building orientations on 24 L-PBF Ti6Al4V Gyroid TPMS scaffolds. The results indicated reduction of compressive modulus in both the height and width directions. Specifically, the compressive modulus of the scaffolds was found to be 3267 ± 90 MPa for the height direction, which was 24 % lower than the designed value (4323 MPa), and 3691 ± 172 MPa for the width direction, 14.6 % lower than the designed value. The stress–strain curves provided in Fig. 14c, indicate slightly different compression mechanisms when the scaffolds were compressed along the height and width directions.

More detailed regarding the failure mode under mechanical loading, Murchio et al. [41] also performed static tensile test on L-PBF Ti6Al4V single struts produced by four different orientations (90°, 45°, 15°, and 0°). The failure mechanism of the tested struts with 90° and 45° build orientations was associated with the significant porosity. Conversely, in the case of specimens fabricated at 15° and 0° orientations, the failure mechanism was attributed to the higher geometrical inaccuracies, which were found to increase the strain intensification. Guo et al. [123] analysed the plateau stress of an EB-PBF dodecahedron porous tantalum scaffold. The results demonstrated a positive correlation between the plateau stress of the scaffold and the strut angle, with an increase in the strut angle from 35.3° to 43° resulting in an elevation in the plateau stress. The average plateau stress improved from 28.4 MPa to 37.3 MPa as the strut angle increased from 35.3° to 43°. Moreover, under identical loading, the deformation of the scaffold decreased as the build angle increased.

Sombatmai et al. [39] used three different FE models to study single struts, including the reconstructed model from μCT, the model with the mean equivalent diameter from μCT, and the as-designed geometry. Tensile tests were performed on L-PBF Ti6Al4V struts with diameters of 0.3, 0.5, 1, and 2 mm, considering 90° and 45° building orientations. Referring to Fig. 15a and b, which depict the force–displacement responses of distinct specimens, the μCT model was concluded to give the most accurate evaluation of the mechanical properties. All specimens showed a trend where the difference between the predicted and actual forces increased as displacement increased in the elastic range. However, after yielding, the difference in predicted forces mainly remained constant. Moreover, based on the data presented in Fig. 15c and d, the mechanical behaviour of the specimens was significantly influenced by their size. Specifically, a notable reduction in the strain at failure was evident as the specimen size decreased. Furthermore, specimens with a 90° build angle exhibited higher failure strain than those with a 45° build angle. These findings were consistent with the presence of external defects in the specimens, which tended to be more pronounced in smaller specimens, particularly those with a 45° build angle.

Table 1
Studies on the influence of build orientation on tensile response of PBF specimens.

Ref	AM technology and material	Yield Strength (YS)	Ultimate tensile strength (UTS)	Young's modulus (E)	Elongation
Hartunian et al. [127]	L-PBF Ti6Al4V	Highest at X orientation vs. Y and Z orientations	Highest at X orientation vs. Y and Z orientations	–	–
Murchio et al. [41]	L-PBF Ti6Al4V	Lowest at 45° vs. 90°, 15°, and 0° (see Fig. 14d)	Lowest at 45° vs 90°, 15°, and 0° (see Fig. 14d)	–	–
Dong et al. [33]	L-PBF AlSi10Mg	Highest at 90° vs. 60°, 45°, and 35.5° (see Fig. 13a- c)	Highest at 90° vs. 60°, 45°, and 35.5° (see Fig. 13- c)	Highest at 90° vs. 60°, 45°, and 35.5° (see Fig. 13a-c)	Highest at 90° vs. 60°, 45°, and 35.5° (see Fig. 13a-c)
Hossain et al. [84]	L-PBF Ti6Al4V-ELI	No correlation with build orientations	Highest at 90°, and weakest at 20°	–	–
Wu et al. [40]	EB-PBF Ti6Al4V	Highest at 90° vs. to 75°,60°,45°,30°, 15°, and 0°	–	Highest at 90° vs. to 75°,60°,45°,30°, 15°, and 0°	–
Bültmann et al. [103]	L-PBF 316L	Highest at 45° vs. to 60°, 75°, and 90° (see Fig. 13f)	Highest at 45° vs. to 60°, 75°, and 90° (see Fig. 13f)	–	Highest at 45° vs. to 60°, 75°, and 90° (see Fig. 13f)
Hossain et al. [84]	L-PBF SS316L	No correlation with build orientations	No correlation with build orientations	No correlation with build orientations	–
Liu et al. [129]	L-PBF Inconel 718	Lowest at 90° vs. 45°, and 0° (see Fig. 12c and d)	Lowest at 90° vs. 45°, and 0° (see Fig. 12c and d)	–	–
Sun et al. [130]	EB-PBF Inconel 718	Highest at 55° vs. to 90°, 45°, and 0° (see Fig. 12e)	Highest at 55° vs. to 90°, 45°, and 0° (see Fig. 12e)	–	Highest at 55° vs. to 90°, 45°, and 0°
Awd et al. [109]	L-PBF AlSi10Mg	Highest at 0° vs. to 90°, and 45° (see Fig. 12f)	Highest at 0° vs. to 90°, and 45° (see Fig. 12f)	–	–
Barba et al. [34]	L-PBF Ti6Al4V	–	Highest at 0° vs. to 90°, (see Fig. 12a and b)	–	

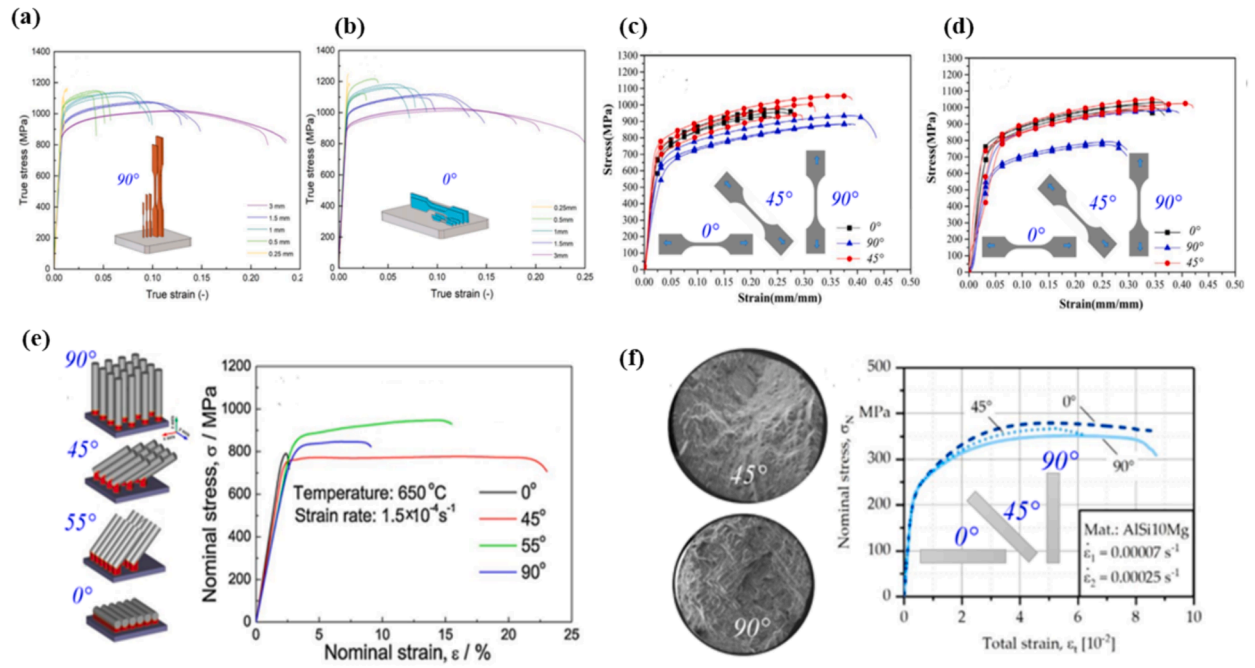

Fig. 12. (a, b) stress–strain data for L-PBF Ti6Al4V specimens, with a focus on the 0° and 90° build orientations [34]. (c, d) stress–strain curves of the L-PBF Inconel 718 specimens fabricated with varying orientations and energy densities [129]. (e) The stress–strain behaviour of EB-PBF Inconel 718 specimens with orientations of 0°, 45°, 55°, and 90° investigated under a strain rate of 1.5×10^{-4} s^{-1} at the temperature of 650 °C [130]. (f) Average results of tensile tests on L-PBF AlSi10Mg specimens with build orientations of 0°, 45°, and 90° [109].

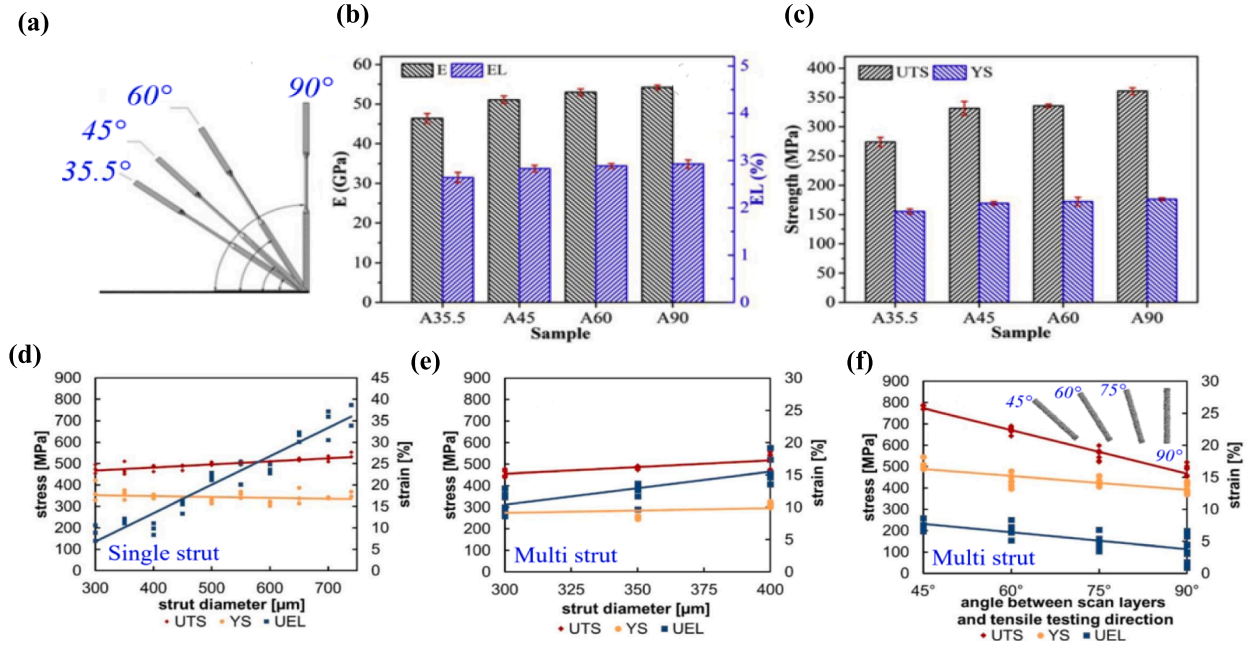

Fig. 13. The impact of build orientation on the tensile characteristics of L-PBF AlSi10Mg specimens (a) showing the build orientation (b) elastic modulus and elongation (c) UTS and YS [33]. The L-PBF 316L specimens were evaluated for their YS, UTS, and elongation in relation to (d) single struts, (e) multi-struts, (f) angle between the scan layers and the tensile testing direction of the multistrut specimens [103].

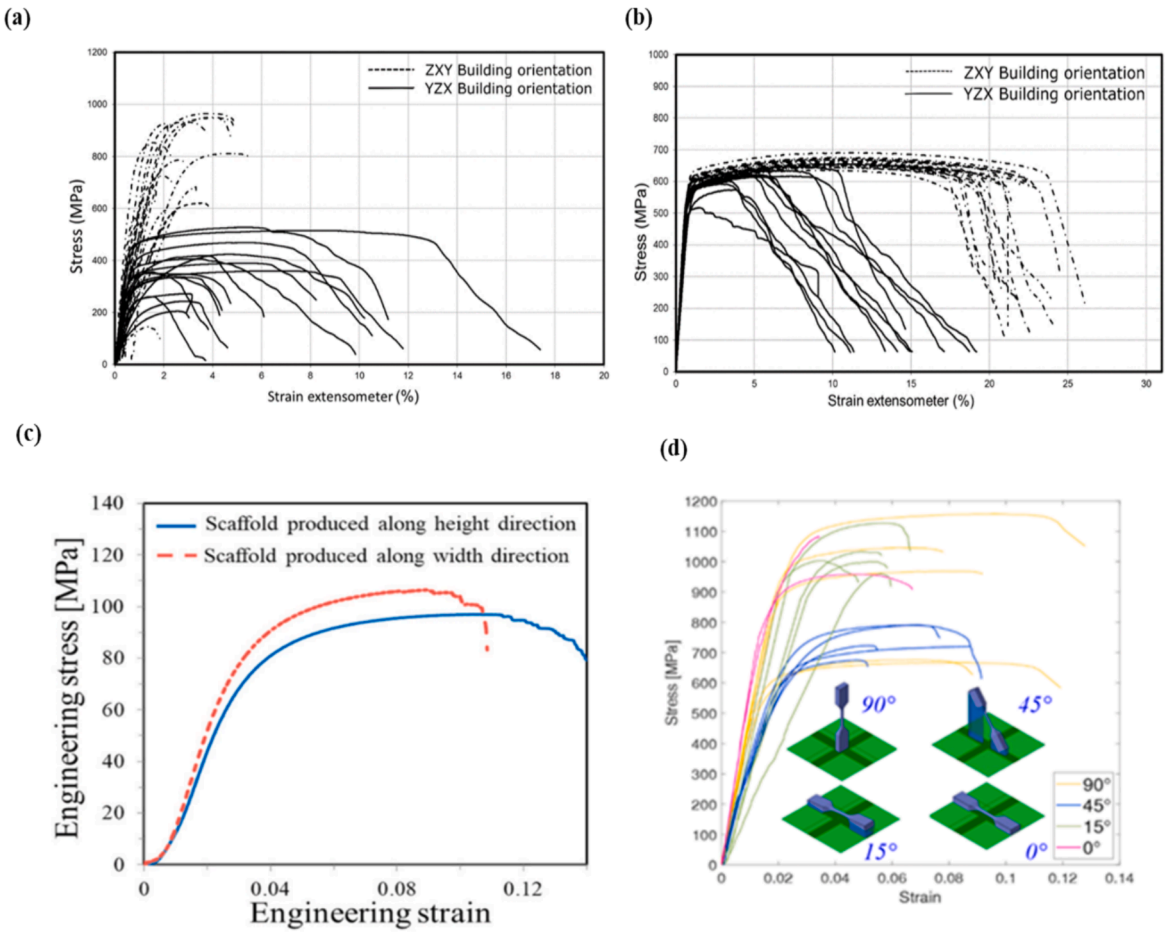

Fig. 14. (a) Engineering stress–strain curves for the L-PBF CP-Ti Grade 2 specimen having a diameter smaller than 1.5 mm^2, both in the vertical build orientation (ZXY) and the horizontal build orientation (YZX) [131] (b) Engineering stress–strain curves for L-PBF CP-Ti Grade 2 specimens with diameter larger than 1.5 mm^2 made in the vertical orientation (ZXY) and the horizontal build orientation (YZX) [131] (c) Engineering stress and strain curves produced for both height and width directions for L-PBF Ti6Al4V [76]. (d) Stress–strain data for four different L-PBF Ti6Al4V strut categories, which are distinguished by distinct colours in the accompanying legend [41].

Table 2
Studies on the influence of build orientation on compressive response of PBF specimens.

Ref.	AM technology and material	Yield Strength (YS)	Compressive strength	0.2 % offset stress	Elastic modulus (E)	peak stress
Guo et al. [123]	EB-PBF Tantalum	increased from 35.3° to 43°	–	–	increased from 35.3° to 43°	–
Wauthle et al. [104]	L-PBF Ti6Al4V	Lowest at 45° vs. vertical and horizontal	Lowest at 45° vs. vertical and horizontal	–	–	–
Dallago et al. [82]	L-PBF Ti6Al4V	–	–	Highest at 90° vs. 0°.	Highest at 90° vs. 0°.	Highest at 90° vs. 0°.
Weißmann et al. [122]	L-PBF Ti6Al4V	Highest at 0° vs. 45° and 90°.	–	–	Highest at 0° vs. 45° and 90°.	–

To conclude, considering different build orientations, many studies indicate higher UTS, YS, young modulus, strain at failure, compressive strength, and elongation, etc. either at 90° or 0° [33,39,40,82,84]. Contrarily, others conclude that the abovementioned static properties were higher at 45° build orientation [39,103]. Yet, YS and UTS have been even reported to be independent from the building orientation [84].

6.3. Fatigue strength

Understanding the fatigue performance of AM components is crucial to provide reliable load-bearing components in applications that involve cyclic loading, like aerospace, railway, and automotive industries. It is now well established that fatigue strength of AM parts, both bulk and lattice structures, is considerably influenced by their build orientation [41,73,82,87,108,132–140]. This is mainly due to the differences that appear during manufacturing in terms of geometrical inaccuracy, defects (porosity, staircase effect, etc.), microstructural inhomogeneity, surface roughness, and residual stresses, as discussed in previous sections.

6.3.1. Defects

It is essential to emphasize that surface defects have a significant impact on the likelihood of fatigue crack initiation in as-built specimens. A surface with more irregularities will increase the probability of premature crack initiation due to local stress concentration, thus reducing fatigue resistance [141–143]. A similar tendency is recognized with respect to porosity, where pores located at the surface or near it can act as possible stress concentrators and consequently become suitable crack nucleation sites under cyclic loading. This was clearly exemplified in the work of Chern et al. [132] on the fatigue strength of rectangular EB-PBF Ti6Al4V specimens. They reported an anisotropic fatigue behaviour when horizontally and vertically built specimens were tested by four-point cyclic bending. Vertically built specimens exhibited a shorter fatigue life (lower initiation time and faster crack propagation rate) as a consequence of the inter-layer melt defects that acted as crack-initiation sites when they were loaded in crack opening mode I. This trend was confirmed in another study on L-PBF Ti6Al4V specimens with three different building orientations of (0°, 50°, and 90°) considered for dog-bone specimens [133]. Under axial fatigue tests, vertically built specimens (90°) overperformed the as-built series due to their smoother surface profile. In contrast, the 0° and 50° built specimens showed a much higher surface roughness, especially on the down-skin, due to the need to use support structures.

6.3.2. Residual stress

Morettini et al. [134] detected that surface roughness is not the only parameter which plays a part in the fatigue strength of AM specimens, examining DMLS Ti6Al4V dog-bone specimens subjected to axial fatigue tests. DMLS is a process similar to L-PBF during which the powders are consolidated by sintering rather than melting, resulting in lower temperatures and lower laser power. It was demonstrated that vertically built specimens had a fatigue strength 30 MPa lower than their horizontal counterparts, despite the higher surface roughness of these latter ones. They attributed this behaviour to the presence of larger compressive residual stresses in the central area of the specimens, generated during cooling. These results were in contrast with the findings by Meneghetti et al. [87] on DMLS maraging steel specimens. In this study, horizontal specimens demonstrated the lowest axial fatigue strength, even after an age hardening heat treatment.

6.3.3. Lattice structures

Variables that determine the fatigue behaviour of lattice structures are more complex due to the intricacy of the structure itself. According to several studies, the effect that various build orientations have on the generation of surface defects and porosity remains significant and can be highly detrimental in these structures as well [41,73,82,86,108]. The presence of nodes with sharp fillet radii

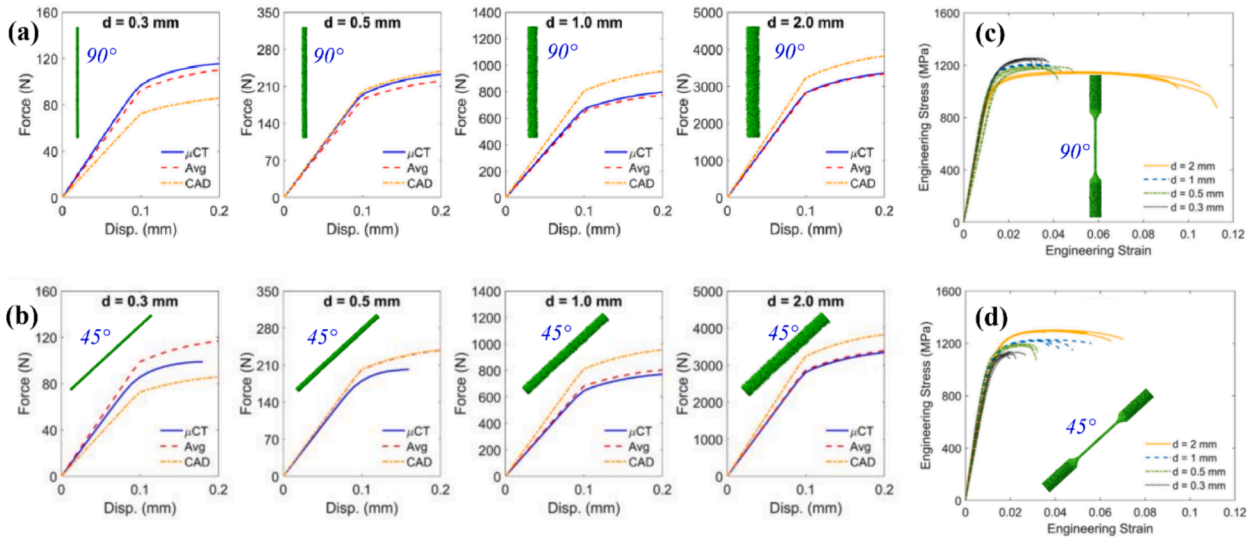

Fig. 15. The mechanical responses of L-PBF Ti6Al4V single struts, assessed numerically using 3 different μCT, μCT-Avg, and CAD models. Comparison was conducted separately for two distinct specimen types with build orientations of (a) 90° and (b) 45° [39]. Stress–strain curves on L-PBF Ti6Al4V single strut specimens with (c) 90° and (d) 45° build angles [39].

may also affect the fatigue resistance of lattice specimens [73,82]. Overall, in lattice structures, the impact of miniaturization caused by the small size of the struts is more pronounced, resulting in a higher density of flaws as compared to bulk specimens [41].

An insightful case study was provided by Persenot et al. [108], who studied EB-PBF Ti6Al4V thin (2 mm) specimens with 3 different orientations (90°, 45°, 0°). The vertically built specimens exhibited the lowest uni-axial fatigue life. Fig. 16a shows radial μCT slices of the specimens built at different orientations. The authors identified two main types of surface defects: unmelted powders and irregularities in layer stacking, commonly known as the staircase effect. Notches were predominantly found in the 90° and 45° specimens, which were orthogonally oriented to the building direction, as shown in Fig. 16b. On the other hand, they were almost absent in the horizontal struts. Comparing radial slices of the specimens obtained before and after fatigue failure and by observation of the fracture surfaces, it was found that cracks mainly initiated from the superficial notch-like defects (see Fig. 16c and d) and that the fatigue strength was strictly linked with the build orientation since it influenced the shape, size and number of notch-like defects on the sericulture's surface. The 0° specimens showed the highest fatigue life, despite higher roughness. This highlights that surface roughness cannot be the only important parameter when assessing fatigue strength in as-built AM specimens.

Using a similar approach, Murchio et al. [41] conducted a series of tests on L-PBF Ti6Al4V struts manufactured at four different inclinations. The results highlighted a strong effect of build orientation, but contrary to the previous studies, lower building angles led to lower fatigue strength, as demonstrated by the S-N curves illustrated in Fig. 16e and f. In this case, 0° specimens demonstrated the lowest fatigue strength while the 45° ones exhibited the highest. Failure of the struts was attributed to the miniaturization effect, which heightened their sensitivity to surface defects. Low-angle struts were found to have higher geometrical inaccuracy and surface roughness, as described in subsections 3.1 and 4.1, which made them more prone to crack nucleation from surface micro-notches. This was confirmed by SEM analysis of the fracture surfaces (see Fig. 16g). Comparatively, in another study carried out by the same authors [73], the effect of adding a node along the struts was examined on fatigue strength. Similar to their previous findings [41], the 45° oriented struts showed the highest fatigue strength; however, the horizontal struts were less affected in terms of their fatigue life, thanks to the presence of the node (shorter unsupported length). The analysis of the fracture surfaces indicated that in vertical and 45° specimens, which had better geometrical accuracy, the failure occurred mainly at the node junction, where the fillet radius was smaller, and therefore it became a critical stress concentration point. Reasonably, in 15° and 0° struts, the fracture started along the gauge length, mainly triggered by the geometrical inaccuracy and the higher surface roughness, especially at the down-skin region. These results were similar to those reported by Dallago et al. [82] who analysed the fatigue behaviour of L-PBF Ti6Al4V cubic lattice specimens. In vertically built struts, crack initiation occurred at the sharper and more irregular node fillet radius located at the down-skin. However, when load-bearing struts were printed horizontally, the critical point was the strut itself, particularly in the centre, due to its geometrical inaccuracy. This resulted in a reduced fatigue performance compared to the vertical ones, regardless of the fillet radius. Furthermore, it was reported that in the specimens in which the main load-bearing struts were built vertically, cracks nucleated close to the nodes and then propagated to the neighbouring struts. On the contrary, in lattices where the main load-bearing struts were those printed parallel to the printing plane (horizontally), cracks nucleated in several struts at the same time and far from the nodes, causing diffused damage in the structure.

6.3.4. Additional case studies

Solberg et al. [135] provided a detailed insight into the effect of build orientation on fatigue strength, specifically exploring the impact of down-skin and up-skin surface. Uni-axial fatigue behaviour of L-PBF maraging steel grade 300 specimens was assessed in a wide range of orientations. Evaluating similar studies, they concluded that although the obtained fatigue performance was lower than that for conventional manufacturing methods, the data reported in the literature concerning directional fatigue behaviour within AM-produced specimens on the same material were contradicting (see Fig. 16h). These results were attributed to a combination of effects of different as-built features such as defect orientation, microstructural anisotropy, and surface roughness. To individualize the effect of various parameters depending on the build orientation, all the faces of the specimen were machined except one, thus creating a set where the critical surface varied from 0° up-skin to 135° down-skin. The results showed that specimens built near the 90° orientation had longer fatigue life when compared to those built closer to the 0° orientation (see Fig. 16i). Furthermore, the specimens with as-built up-skin surfaces (closer to 0°) presented higher fatigue life than the ones with down-skin surfaces (closer to 135°) due to the 4-fold lower surface roughness. Fig. 16j compares the fracture surfaces of the 0° and 135°specimens. In both cases, failure originated from the as-built surface, but from different zones: in the centre for 0° and from the corner for 135°.

The effect of build orientation on the fatigue strength of 5 different Al alloys fabricated by L-PBF was evaluated by Nezhadfar et al. [136]. Fig. 16k-m summarize the main results obtained in this study. The evidence authors presented supports the idea that volumetric defects play a crucial role in fatigue crack initiation and, consequently on fatigue performance. Scalmalloy and AD1 specimens excelled AlSi10Mg, QuesTek Al, and AlF357 specimens regardless of the build orientation, mainly due to their lower defect density. In fact, a comparison of the AlSi10Mg and AD1 specimens' fracture surfaces in Fig. 16n demonstrates that in the first case, cracks initiated from the volumetric defects close to or on the surface, while in the second case, they mainly originated from the surface itself. However, not only the density of defects determines the fatigue behaviour of the specimens, but also their type (i.e., pores, lack-of-fusion (LoF)) and size are important. This was made evident in the case of AlF357 and QuesTek Al alloy, which showed anisotropy. Vertical AlF357 specimens overperformed the horizontal ones because cracks initiated from tiny pores instead of the large LoF defects (see Fig. 16n). On the other hand, vertical QuesTek Al specimens demonstrated shorter fatigue life than horizontal ones due to their larger projected area of LoF defects on the loading plane.

Another study on L-PBF AlSi10Mg alloy [137] investigated the effect of the as-built condition on 3-point bending fatigue behaviour. To assess the effect of build orientation and take into account also the influence of as-built surface characteristics, 5 different series of specimens built at different angles were tested (see Fig. 16o). The specimens were especially designed to develop maximum stress at

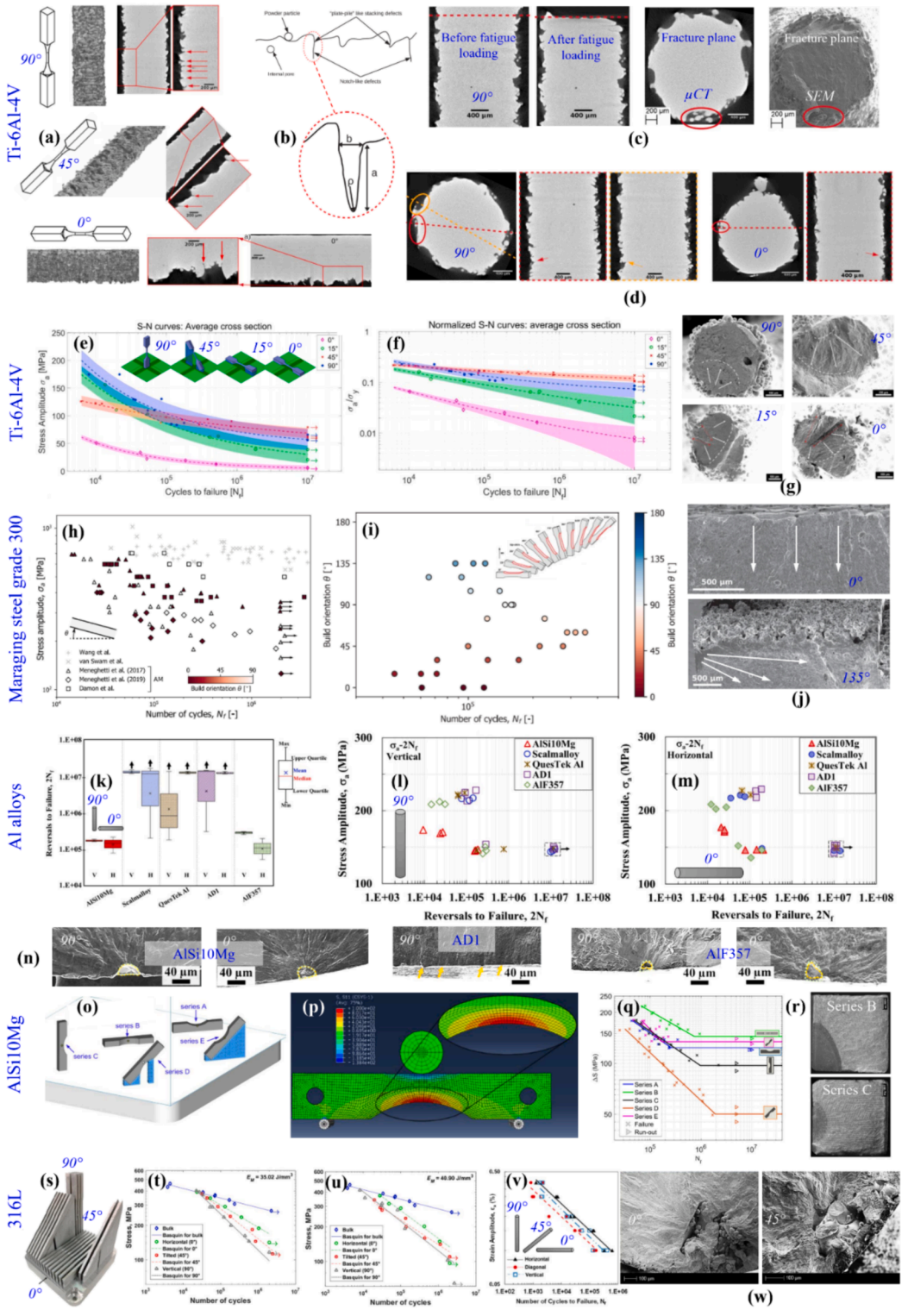

(caption on next page)

Fig. 16. (a) Effect of build orientation on the surface profile of as-built thin EB-PBF Ti6Al4V specimens, with magnification around the defects. (b) Schematic illustration of different types of surface/near-surface defects that can be found in EB-PBF as-built specimens along with the shape of the notch-like defects. (c) Comparison between topographical radial slices of the specimens taken before and after fatigue failure. Identification and observation of the critical cross-section led to the recognition of the defect that led to failure. (d) Examples of surface notch-like defects responsible for the failure of 90° and 0° specimens identified by μCT [108]. (e) S-N semi-logarithmic plots of the fatigue behaviour of strut-like L-PBF Ti6Al4V specimens built at different orientations. (f) S-N double-logarithmic plots normalized by the yield strength in each orientation. (g) Fracture surface images obtained by SEM; fatigue crack initiation and propagation paths are shown by white arrows and dotted curved lines [41]. (h) Comparison of S-N fatigue curves for maraging steel grade 300 specimens reported by several authors. (i) Uni-axial fatigue life (expressed in number of cycles to failure, Nf, at 500 MPa load) of L-PBF maraging steel grade 300 specimens according to the building orientation. (j) SEM fracture surfaces of 0° and 135° specimens; white arrows indicate the initiation and propagation of the fatigue cracks from the as-built surface [135]. (k) Cycles to failure of vertical and horizontal L-PBF Al specimens, tested at 0.002 mm/mm strain amplitude, shown in box and whisker plots; arrows indicate runout. Comparison between S-N plots of: (l) vertical specimens and (m) horizontal specimens. (n) SEM fracture surfaces of some of the specimens tested [136]. (o) Different series of 3-point bending fatigue L-PBF AlSi10Mg specimens; blue areas indicate the position of the supports used for the diagonal series. (p) FE model showing stress distribution along fatigue specimens; maximum stresses are developed close to the notched face. (q) Comparison of different S-N plots obtained for each series of specimens. (r) SEM fracture surfaces of series B and C specimens [137]. (s) L-PBF SS 316L specimens built at different orientations. (t, u) Double-logarithmic S-N plots for the tested specimens via reverse bending fatigue employing two different energy density inputs [138]. (v) Strain-life curves obtained by uniaxial strain-controlled fully reversed loading tests on L-PBF SS 316L specimens built at 3 different orientations. (w) Details of the fracture surfaces of 0° and 45° specimens. In the first one, the defect responsible for crack initiation is an inclusion resulting from LoF and unmelted powder, while in the second one, the killer defect is an inclusion of partially melted powder [139]. (For interpretation of the references to color in this figure legend, the reader is referred to the web version of this article.)

the notched face (see Fig. 13p). As shown in the S-N plots in Fig. 16q, horizontal specimens (series B) demonstrated the highest fatigue strength with respect to the vertical (series C) and diagonal specimens. Among inclined specimens, those with the notch on the up-skin (series E) overperformed the ones with a down-skin notched face (series D). These results indicated a correlation between roughness and fatigue performance as well as the size of surface defects. Fig. 16r illustrates the fracture surfaces of series B and C; in series B that had smoother surfaces and smaller features, the crack began from the corner of the specimen. Whereas, in C series, the crack started at the centre of the notched face and then propagated between the two adjoining layers. Additionally, it was mentioned that residual stresses played an important role and were responsible for the low fatigue limits of the C and D series with respect to the others.

Ponticelli et al. [138] studied the fatigue strength of L-PBF 316L specimens subjected to reverse bending loading. To evaluate the effect of building orientation and volumetric energy density input, they produced specimens in 3 different inclinations (see Fig. 16s) employing two diverse combinations of process parameters (resulting in 2 dissimilar energy density inputs). The resulting S-N points interpolated by Basquin Law are shown in Fig. 16t and u. It was concluded that the low-cycle fatigue limit of L-PBF specimens was similar to that of the bulk material, whereas at the high-cycle fatigue regime, building orientation and porosity strongly affected the L-PBF specimens' performance. Horizontally built specimens demonstrated the highest fatigue resistance, while vertical ones had the lowest. These results are similar to those reported in other studies on this material employing uniaxial strain-controlled fatigue tests [139] (see Fig. 16v). Researchers attributed this behaviour to the orientation of the deposited layers with respect to the loading direction; that is in the horizontal specimens the deposited layers were preferentially disposed perpendicularly to the stress induced by bending, generating a more tortuous path for crack propagation. In addition, the use of higher volumetric energy densities resulted in lower fatigue limits. This was explained by the fact that a higher energy density is associated with a higher layer thickness, producing a less efficient consolidation and, therefore a higher density of volumetric defects from which cracks can initiate [138]. In this sense, Shrestha et al. [139] recognized 3 types of defects present in these specimens: i) voids formed due to the LoF between the subsequent layers, ii) inclusions formed due to partially melted powder particles, and iii) un-melted powder particles clustered near a void; with the first group being more detrimental when they were preferentially orientated with respect to the loading direction. Some examples of these defects are shown in Fig. 16w. In addition, to study the R-ratio dependency of fatigue defect sensitivity, Murchio *et al.* [144] conducted a comprehensive investigation into the fatigue properties of L-PBF Ti6Al4V miniaturized strut-like specimens, fabricated at four distinct build orientations of 0°, 15°, 45°, and 90°. The specimens were subjected to four different stress ratios of R=0.1, R= − 1, R= − 4, and R=10. The results revealed that the dependency on mean stress decreases as the build angle increases, which is attributed to progressively lower surface roughness that primarily drives failure at R=0.1 and R= − 1. In contrast, vertical specimens at R= − 4 exhibit a pronounced susceptibility to sub-surface defects, significantly affecting their fatigue strength.

6.3.5. Future prospective

Having gone through the reported results, the consensus among the researchers indicates that the building orientation significantly affects fatigue performance due to factors such as surface and internal defects, residual stresses, and microstructural inhomogeneity. In the case of thin struts, it was indicated that notch-like defects have been found to particularly impact fatigue performance, especially when loaded in specific directions. However, it was demonstrated that surface roughness, as a primary factor influencing the fatigue life of the samples, is not always the determining parameter and characteristics like residual stresses can be influential as well. In most reported cases, vertically built specimens exhibit the lowest fatigue strength. Additionally, down-skin surfaces, especially in L-PBF, have a more detrimental effect compared to up-skin surfaces due to their lower accuracy and higher roughness, serving as local micro-notches and sometimes masking the significance of geometrical notches.

Moreover, the development of efficient optimization frameworks for enhancing the fatigue behavior of PBF materials within fatigue optimization algorithms has garnered significant attention recently [145]. These frameworks aim to systematically improve the fatigue life of PBF components by optimizing various parameters such as build orientation, process settings, and post-treatment methods. By

integrating these optimization strategies into fatigue algorithms, researchers can better predict and enhance the performance of PBF materials under cyclic loading conditions.

The potential for future studies in this area is substantial, as ongoing advancements could lead to more robust and reliable L-PBF components in critical applications. Future research could explore the integration of machine learning and artificial intelligence to further refine these optimization frameworks, allowing for real-time adjustments and improvements. Additionally, investigating the interplay between different factors such as thermal history, microstructural evolution, and residual stresses could provide deeper insights into the mechanisms governing fatigue behavior in L-PBF materials. By addressing these challenges, future studies can contribute to the broader adoption and success of L-PBF technologies in various industries, particularly those requiring high-performance and fatigue-resistant components.

6.4. Fracture toughness

Undoubtedly, toughness is considered as one of the most essential and indispensable material attributes for achieving the highest structural performance. The currently widely acknowledged technique for evaluating fracture toughness in ductile materials, such as metals, is based on the Elasto-Plastic Fracture Mechanics (EPFM) theory. In the case of AM materials, it is essential to determine the influence that defect size and defect type have on toughness besides bulk material properties. The fracture toughness characterization of PBF parts has become increasingly important within the AM scientific community. This is due to the anisotropy and variety of defects that can be encountered in such parts. In particular, the influence of building orientation on defects such as porosity, second phases, LoF, and more interestingly, the presence of inherent melt pool boundaries, which can act as crack initiators or influence crack growth and propagation, is being investigated.

Oliveira de Menezes et al. [146] investigated the fracture toughness of L-PBF A357 alloy compact tension C(T) specimens, obtained in 3 different orientations, according to ASTM E1820-18 standard. Fig. 17a schematically illustrates the 3 differently oriented groups of specimens examined, noting that H, L and T stand for height, longitude and thickness directions, respectively. This study showed that the material fracture toughness, as measured by the J_{IC} integral, was significantly affected by the build orientation and the direction of loading. The lowest value of fracture toughness was observed in the as-built condition for the specimens loaded in the building direction (H), with the notch placed along the build plate (T-L) and oriented with respect to L direction (H-L specimens). Upon analysing micrographs obtained perpendicularly to the crack planes, it was observed that the crack in H-L specimens grew along the melt pool boundaries, which were conveniently aligned with the crack plane. On the other hand, the crack propagation path was more convoluted and less specific for T-L and H-T specimens, resulting in higher fracture toughness (see Fig. 17b). These results were confirmed in a subsequent work [147], in which the effect of different heat treatments was assessed. In this case, an artificial aging cycle (T6) induced microstructural coarsening and consequently, led to the elimination of the anisotropy caused by the presence of the melt pool boundaries, although it reduced the overall fracture toughness for T-L and H-T specimens. This behaviour was attributed to a change in the crack propagation mechanism, in which the existence of small uniformly distributed Si particles and porosity were considered as the main causes for the low resistance to crack propagation rather than the presence of the melt pool boundaries existing in the as-built condition. A similar approach was carried out by Araújo et al. [148] who investigated the fracture toughness of 3-point bending L-PBF AlSi10Mg specimens in 3 different processes and subjected them to different heat treatments. The obtained fracture characteristics expressed in terms of J_{IC} and crack-tip opening displacement (δ-CTOD) are summarized in Fig. 17c. Th horizontal as-built specimens (0°) showed the highest fracture toughness values, whereas vertically-built specimens (90°) had the lowest, observing the same crack propagation mechanism through melt pool boundaries that was reported in previous studies [146,147] (see Fig. 17d and e). More interestingly, a change was identified in the mechanism according to the resulting microstructure obtained after different heat treatments. In particular, the differences in type, size, distribution, and amount of porosity played an important role, recognizing that non-spheroidal LoF defects were more detrimental than rounded pores generated by the entrapment of gases.

The effect of building orientation on the fracture toughness of specimens produced by PBF techniques was also inspected in other materials such as Ti6Al4V [149], low-alloy steels [150] and stainless steels [151]. These cases provide further evidence that the lowest fracture toughness occurs when the material in its as-built condition is subjected to loading along the building direction. Toughness values in those conditions could be even 30–40 % lower than in the case of the same material in the wrought condition (i.e., produced by a non-AM process) [151]. These studies also support the idea that this anisotropic behavior can be partially mitigated through the application of proper post-processing methods, that should be studied case-by-case. For instance, stress relief and Hot Isostatic Pressing (HIP) have proven effective for materials like Ti6Al4V [149], helping to reduce residual stresses and improve the uniformity of mechanical properties. HIP, in particular, applies high pressure and temperature to close internal pores and enhance the material's overall density and structural integrity. Similarly, quenching and tempering treatments for 4130 steel were employed to refine the microstructure, enhance toughness, and reduce anisotropy [150]. These treatments involve heating the material to a high temperature followed by rapid cooling (quenching) and then reheating to a lower temperature (tempering) to achieve the desired balance of hardness and ductility. By carefully selecting and applying these post-processing techniques, considering the chemical, microstructural and physical aspects of the part, the inherent anisotropic behavior of AM parts can be significantly reduced, leading to improved performance and reliability across various applications.

Based on the results in the literature, it can be concluded that the fracture toughness of PBF fabricated parts is influenced by various factors, including build orientation, the shape, and the type of associated defects. Different build orientations result in anisotropic material properties due to the layer-by-layer construction, which affects the bonding quality between consequent layers and creates variations in density. This anisotropy can lead to differences in how cracks propagate through the material. The shape and type of defects, such as porosity, micro-cracks, and surface roughness, are also critical. These defects are often influenced by the build

orientation, with certain orientations being more prone to specific types of defects. Additionally, residual stresses introduced during the manufacturing process, which vary with orientation, can significantly impact fracture toughness by affecting the material's internal stress state. The microstructure, including grain size and morphology, further contributes to the material's fracture resistance and is influenced by the build direction. Therefore, optimizing build orientation, understanding how it affects pores density and distribution and minimizing defects through careful process control are essential for enhancing the fracture toughness of AM parts.

6.5. Wear resistance

Identifying wear mechanisms and wear resistance are of major interest for a wide range of applications. However, comparatively, few studies have been carried out to investigate the effect of build orientation on the wear resistance of AM products [128,152–154]. The wear properties of AM materials depend on several key factors, including the material composition, which influences hardness and toughness; the microstructure, which varies with the AM process and affects grain size and phase distribution; the surface finish, where smoother surfaces typically exhibit better wear resistance; and the build orientation, as anisotropy can lead to directional dependencies in wear resistance. Additionally, porosity and defects, particularly surface lack of fusion pores aligned with the sliding direction, can alter the actual contact area across the sliding interface and thereby reducing wear resistance [155–157].

Wear properties are known to be intrinsically dependent substantially on hardness and microstructure; in AM materials, these aspects are directly correlated with the fabrication process parameters like the cooling rate experienced by different layers, according to the selected build orientation. As a result, numerous studies have consistently reported findings that align with the main results presented in Sections 4, 5, and 6.1. These indicate that the build orientations that promote smoother, more geometrically accurate, and harder surfaces that these characteristics are expected to lead to superior wear resistance. The evidence of this relationship was clearly observed in a study that compared the wear resistance of DMLS Ti6Al4V specimens built in two different orientations [128]. Vertically built specimens showed the highest wear resistance and the highest microhardness. As it was highlighted in Section 6.1, the microstructure found in these specimens played an important role; while the horizontally built specimens exhibited a mixture of α and β phases, in the vertical specimens, harder α' martensite was also identified. Also, Bahshwan et al. [152] investigated the role of microstructure on wear mechanisms in L-PBF 316L SS disc-shaped specimens built in 3 different orientations. The vertically oriented

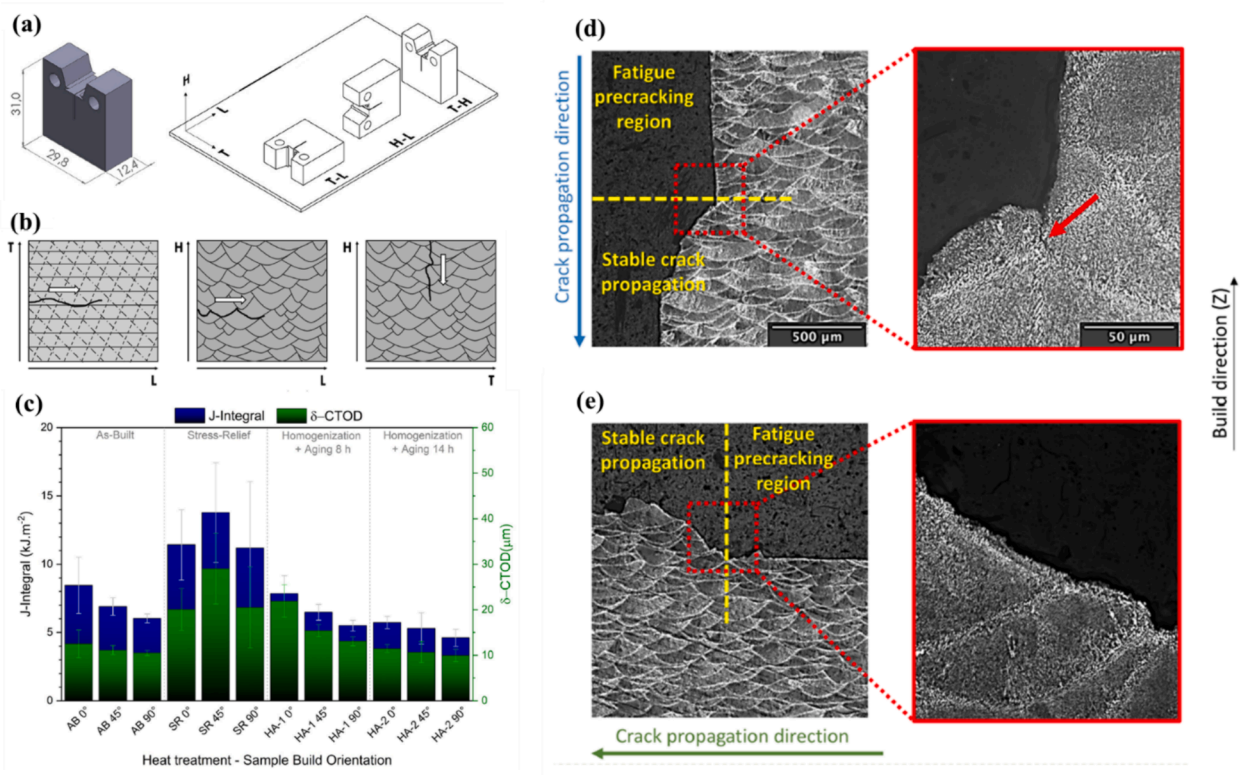

Fig. 17. (a) Scheme of the L-PBF A357 alloy CT specimens, indicating the building direction (H) and the build plate (T-L). (b) Schematic representation of the crack propagation path in the 3 analysed directions. The arrows indicate the crack propagation direction [146]. (c) Fracture parameters in terms of J-integral and δ-CTOD for L-PBF AlSi10Mg specimens produced at different building orientations and subjected to different post-processing thermal treatments. Micrographs of the crack pathway at (d) 0°, and I 90° specimens, showing the crack propagation along melt pool boundaries; the red arrow in (d) points to a secondary crack [148]. (For interpretation of the references to color in this figure legend, the reader is referred to the web version of this article.)

disc exhibited the highest abrasive-oxidative wear, a behaviour which was attributed to two main contributions; firstly, larger columnar grains promoted by epitaxial growth were found in this plane. Therefore, it could be inferred by the Hall-Petch relation that these larger grains led to lower hardness. Secondly, the presence of LoF defects in this plane triggered surface cracking that was added to the overall material loss.

These results agree with other reports from Podgornic et al. [153] who studied the influence of the build direction on the wear resistance of L-PBF maraging steel specimens. Among the 3 build orientations of 0°, 45°, and 90°, the best combination of abrasive and adhesive wear resistance was reported for the specimens built horizontally (0°). On the other hand, the worst wear resistance was found in the vertical specimens (90°) when the sliding took place across the layers, similarly to what was described by Bahshwan et al [152].

An alternative to overcome the anisotropic behaviour in terms of wear resistance was presented by Yang et al. [154], who investigated the effect of 3 scanning strategies to promote the rotation of grains and consequently enhance the wear resistance of L-PBF 316L SS specimens. It was demonstrated that the best strategy was to follow a zigzag scanning with a rotation of 90° between subsequent layers. This contributed to the remelting and change in the orientation of the grains, from columnar, epitaxial grains grown along the build direction to grains aligned in the horizontal direction (see Fig. 18a, b). This configuration showed a higher resistance to slip and, therefore a higher resistance to wear mechanisms. It was suggested that wear resistance can be enhanced by controlling the heat flow during L-PBF to rotate grains away from the "soft" orientation, where the grains have low resistance to slip due to variation of

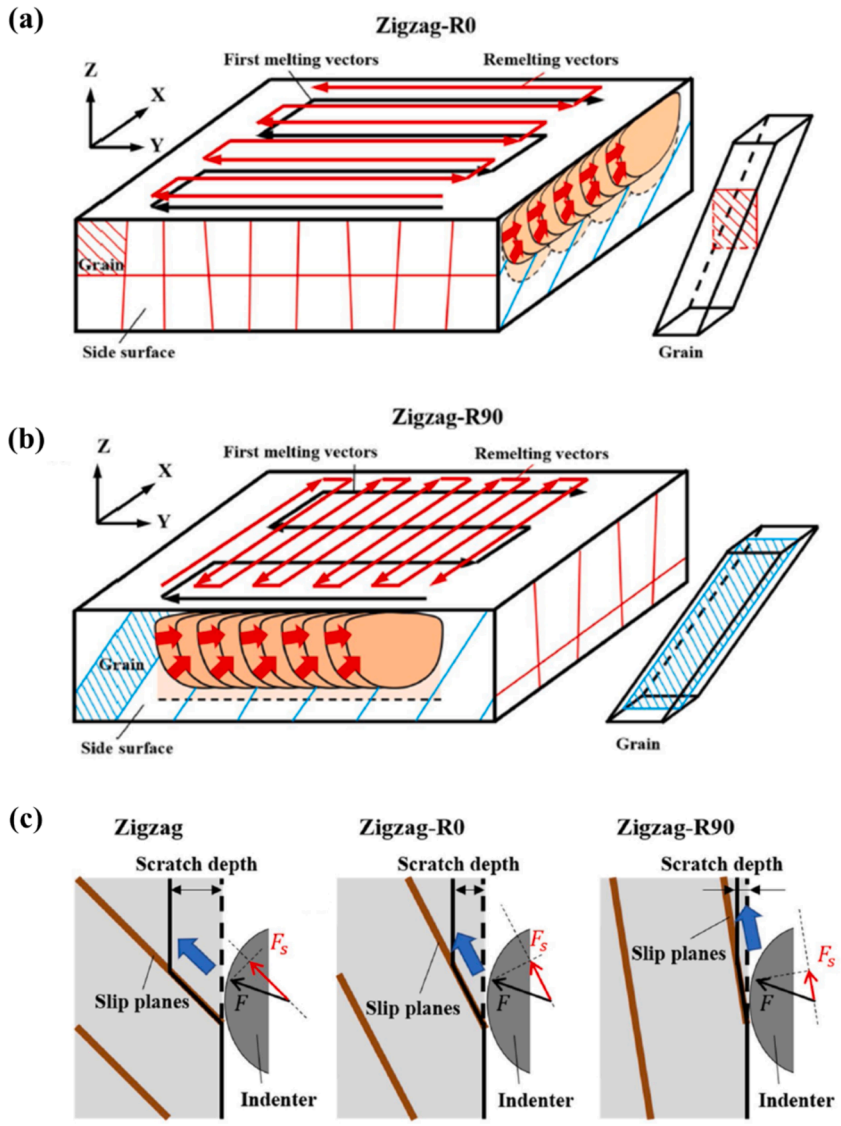

Fig. 18. Effect of zigzag scanning strategy on L-PBF 316L SS specimens regarding grain growth direction and final texture due to the remelting process. (a) R0 strategy (b) R90 strategy (c) Schematic demonstration of the effect of grain rotation on wear resistance [154].

the angle between the slip and wear planes (see Fig. 18c).

6.6. Corrosion resistance

Some metallic materials employed within AM field are prone to passivate under usual environmental conditions. Ti alloys, Al alloys, and stainless steels all develop a passive layer (TiO_2, Al_2O_3, and Cr_2O_3, respectively) on their surfaces. However, several authors report that the corrosion resistance of parts produced by AM is usually lower than their counterparts of the same material obtained by conventional manufacturing processes [158–162]. Moreover, the build orientation of the parts plays an important role in the development of the microstructure and a certain crystalline texture, as described in Section 5. Numerous studies have reported that the variation of microstructure induced by different build orientations within the same component affected the corrosion resistance [158–160,163–165]. For instance, Romero-Resendiz et al. [160] investigated the electrochemical behaviour of EB-PBF Ti6Al4V specimens. The AM specimens showed higher corrosion rates in 1 M NaCl solution compared to the wrought counterpart obtained by forging. The results were explained by the presence of a preferred grain orientation in the case of the EB-PBF specimens that could increase the surface energy and therefore promote the corrosion process. Pazhanivel et al. [163] studied the effect of microstructure and heat treatment on the corrosion resistance of L-PBF Ti6Al4V specimens. In a 3.5 % NaCl solution, the as-built specimens showed the highest corrosion rates. As a result of the heat treatment, the consequent microstructural alteration, and significant grain refinement, the corrosion resistance was enhanced.

Interestingly, a different trend was reported for the corrosion resistance of L-PBF 316L SS specimens in a 0.6 M NaCl solution [164]. The potentiodynamic curves were compared between specimens obtained along 3 building orientations: 0°, 45°, and 90°, and the wrought material. Unexpectedly, the L-PBF specimens presented superior resistance to pitting and greater passivation window than their respective wrought counterpart. Among the AM specimens, the horizontally built ones showed the highest resistance. Experimental evidence suggested that in the case of AM specimens, a more stable protective oxide layer was formed. However, the rationale behind this trend was not clarified.

Du et al. [165] investigated the influence of build orientation on the corrosion behaviour of L-PBF Inconel 718 specimens in a 3.5 % wt NaCl solution. Their results indicated improved corrosion resistance with increasing the build angle. This observation was justified by the grain boundary density that increased at higher building angles, which enhanced the corrosion resistance.

7. Post-treatments effects on inclined features

Despite the great promise, AM technologies suffer from some limitations that necessitate the adoption of post-processing strategies to improve the quality and performance of the as-built part and aim to equalize the targets set by traditional manufacturing processes [166].

There are some unavoidable defects in the printed parts, which can only be partially mitigated by proper tuning of the process parameters [167]. As an example, the staircase effect associated with the presence of “stairs” that lead to an irregular surface topography also as a consequence of excessive layer thickness, is not fully eliminable through parametric optimization, but can be reduced through post-processing strategies [168]. Depending on the part geometry, the adoption of a build direction will affect the “surface complexity” and the geometrical accuracy (i.e., staircase effect and non-uniform shrinkage). The build orientation also influences the extent of the supports needed to sustain eventual overhangs, which also need to be removed from the specimens after processing. Moreover, depending on the adopted scan strategy, voids/pores may be induced within the layer or between successive layers, potentially generating cracks and promoting their propagation [167]. Thus, post-processing can be significantly helpful in addressing various inherent defects and imperfections.

The post-treatments specifically used to address the adverse characteristics induced by build orientation are presented in the following section, considering the two major groups of bulk treatments and surface treatments, with the former basically including heat treatments. The surface treatments are presented [154] categorizing them into subtractive, mechanical, coatings, and hybrid treatments. Lastly, the repercussions of post-treatments as the build orientation changes are investigated in separate subsections with respect to microstructure, surface, mechanical properties, and fatigue behaviour. For more detailed information on general post-treatments used for AM materials, regardless the orientation, please refer to [169].

7.1. Bulk post-treatments

The application of heat treatments is aimed at releasing the residual tensile stresses generated by the concentrated heat input and the continuous and fast heating/cooling cycles in the material during the thermal- based AM processes. Heat treatments can also be applied to mitigate the phenomena of segregation and non-equilibrium phase formation, to modify the microstructure, and thus to modulate the mechanical properties like ductility/strength (e.g., causing allotropic phase modifications) [170].

Cerri et al. [171] analysed the effects of two heating cycles on prismatic L-PBF Ti6AL4V-ELI specimens produced in Z (vertical), 45°, XY (horizontal with the base on the narrower side), and XZ (horizontal with the base on the wider side) directions. The standard heat treatment was performed at 704 °C for 120 min, while the non-standard one took place at 740 °C for 130 min, both inducing the formation of the same amount of bimodal phase in the material. On the macroscale, neither α nor β columns exhibited any dependence on the crystallographic orientation, for all building orientations. Tensile tests indicated that, regardless of the orientation, both YS and UTS decreased while elongation slightly increased, even after the heat treatment was applied. Specifically, vertical and horizontal UTS values were about 40 MPa higher than the other build orientations (Z and 45°).

HIP treatment implies the simultaneous application of thermal annealing (T>0.7 T_m) and pressure (~100 MPa) in an inert atmosphere, with variable results according to the temperature, pressure, and permanence time. It can be particularly employed to resolve cracks and pores in AM parts. Furthermore, similar to simple thermal processes, HIP homogenizes the microstructure, promotes allotropic variations, and relieves residual stresses. Despite its efficiency in enhancing bulk material properties, since HIP does not affect surface properties, it is typically paired with surface post-treatments to further enhance the mechanical performance of AM materials [170].

The effects of SR and HIP (1000 °C, 100 MPa, 2 h) were investigated on Ti6Al4V L-PBF lattice structure specimens realized in 3 orientations (0°, 45°, 90°) and 4 different locations around the build plate (corners and the centre) [172]. SR treatment (650 °C, 3 h) enhanced the material strength by promoting homogeneity and preserving grain orientation. The SR specimens oriented at 45° were more prone to have brittle failures due to the maximum orientation of shear stresses. Overcoming the β-transus temperature (980 °C), the HIPed specimens showed a bimodal α/β microstructure (i.e., specifically Widmanstätten pattern), resulting in higher strength and fracture strain. In addition, the columnar, anisotropic structures were mainly deleted after HIP. Overall, HIP treatment eliminated the effect of build orientation and location on the build plate, while the SR series evidenced higher strength for the 45° builds compared to the other two orientations.

7.2. Surface post-treatments

Surface post-treatments can play a crucial role in addressing the issues caused by the presence of inclined geometric features in PBF fabricated parts. These inclined features often lead to surface roughness, residual stresses, and microstructural irregularities, which can negatively impact the mechanical properties and overall performance of the parts. By applying appropriate surface post-treatments, these challenges can be mitigated, resulting in enhanced surface finish, improved dimensional accuracy, and reduced stress concentrations. Fig. 19 represents schematic illustrations of some of the mostly applied surface post-treatments on PBF parts including subtractive and non-subtractive treatments.

By strategically selecting and applying these post-treatments, manufacturers can effectively address the specific challenges posed by inclined geometric features in PBF-fabricated parts. This not only improves the performance and longevity of the components but also broadens the scope of PBF technology in producing complex and high-precision parts for various industrial applications. Future research in this area could focus on optimizing these post-treatment processes and developing new methods to further enhance the quality and performance of PBF fabricated parts with complex geometries.

7.2.1. Subtractive surface post-treatments

These processes consist of removing the external layers of the AM part, where the majority of orientation-induced defects (e.g., porosities, partially melted powders, spatters, etc.) exist. This will result in considerably reduced surface roughness without interfering with the inner material, and offers a substantial performance improvement, especially in load-bearing parts subjected to cyclic loading [174,175].

Machining is one of the most common mechanical finishing processes used in the AM field. However, its application is limited to simple geometries and cannot be easily adapted to particularly complex shapes due to surface inaccessibility [175]. Serjouei et al. [176] developed a predictive model for S-N fatigue curves, considering the effect of build orientation and various heat treatments, mean stress ratio, location and size of the pores in stainless steel 316L specimens built with different laser-based AM technologies (i.e., L-PBF, DMLS). The experimental tests generally indicated enhanced fatigue resistance for the machined specimens compared to the as-built condition. The vertically built specimens showed the poorest performance compared to the horizontally built ones for both machined and non-machined conditions.

Wood et al. [177] studied the influence of building orientation and various post-treatments, including machining and shot peening on the fatigue performance of L-PBF stainless steel 316L specimens produced in vertical or horizontal directions. Interestingly, for all build directions, the machined and shot peened specimens showed comparable fatigue resistance despite different surface roughness (0.7 μm for machined and 4 μm for the shot peened series, in terms of Ra), thanks to the compressive residual stresses induced by the shot peening treatment. When compared to the as-built counterparts, the machined specimens showed the highest fatigue strength. However, the fatigue strength was found to be inferior in vertically built specimens due to lack of fusion issues, as the specimens were built parallel to the loading axis.

Polishing is another common post-treatment for AM products, which can be performed in many ways, including mechanical polishing, chemical polishing, electrochemical polishing, laser polishing, magnetically driven abrasive polishing, hydrodynamic cavitation abrasive finishing and ultrasonic cavitation abrasive finishing [170]; in all mentioned cases, the objective is to obtain a smooth, mirror quality surface. Several treatments specifically utilized for the post-processing of AM specimens constructed at different angles are mentioned here.

The corrosion resistance of DMLS Al10SiMg specimens produced along horizontal and vertical build directions and subsequently either mechanically polished by emery paper and alumina or shot peened by ceramic microspheres, were investigated by Cabrini et al. [88]. The post-treatments were found to be crucial in enhancing corrosion resistance since pores or residual unmelted powders on the as-built surface served as initiation sites of corrosion. The density of porosities in the as-built specimens showed variation based on their building orientation. Specifically, the horizontal specimens displayed lower average pitting potentials in comparison to the vertical series. This implied a lower probability of forming corrosion pits on horizontally built specimens. During the AM process, laser scanning led to the formation of an oxide layer that offers little protection since it is discontinuous and more exposed to corrosion attacks between the laser tracks. To fix this issue, post-treatments can be applied to remove this inefficient layer. Polishing was found

more efficient than shot peening in this regard. The polished specimens showed better corrosive resistance in terms of pitting potential in both building directions. However, reaching the same surface finishing after polishing, the horizontally built specimens evidenced better corrosion behaviour than the vertically built ones. One disadvantage of employing polishing to improve the mechanical and electrochemical performance of AM materials is the failure to close the pores, while shot peening can lead to some extent of pore closure. Consequently, the effectiveness of the formed protective oxide film is dependent on the number and dimension of residual/exposed pores.

Chemical etching and polishing have been widely used in the post-processing of AM materials thanks to their geometrical flexibility. These treatments do not require mechanical tools, making them ideal for dealing with surface flaws on complicated structures with restricted access (e.g., lattice structures) [178,179]. The part is submerged in an acid solution, which erodes it with or without the help of an electric current. Lhuissier et al. [14] applied chemical etching with variable etching times for EB-PBF Ti6Al4V lattice structures. The authors reported the effects of etching on both vertical and horizontal struts with two major defect types of partially melted powder particles and plate-pile like stacking irregularities observed in the specimens. Notably, the global etching rate of differently oriented struts was reported to be similar.

7.2.2. Non-subtractive surface post-treatments

Sand blasting is a mechanical surface treatment in which sand or ceramic beads are accelerated at a defined pressure to impact the target surface. It is commonly used in various industries for scale removal and surface cleaning; however, depending on the size of the beads and the compressed air used for bead acceleration, it can also induce slight surface plastic deformation and modify surface roughness [180].

The work of Cerri et al. [171] (subsection 7.2) investigated the effects of sand blasting on Ti6Al4V L-PBF specimens. Sand blasting reduced the surface roughness (Ra) reduction from around 20 μm up to 15 μm by removing the partially melted particles that were not well adhered to the surface. The procedure did not considerably modify the microstructure; even though the grains were not plastically deformed, sand blasting led to compressive residual stresses at the most superficial layer (~6 μm). Although the mechanical properties were not considerably affected, the reduction of roughness and the removal of the attached particles can be favourable in biomedical applications.

As a mechanical surface treatment, shot peening is quite similar to sandblasting in concept; however, it requires more precise control over the process parameters such as bead type (e.g., steels, ceramics), bead size, bead morphology, impact velocity, and stand-off distance between the nozzle and the target surface. This treatment is widely used in various industries for inducing compressive

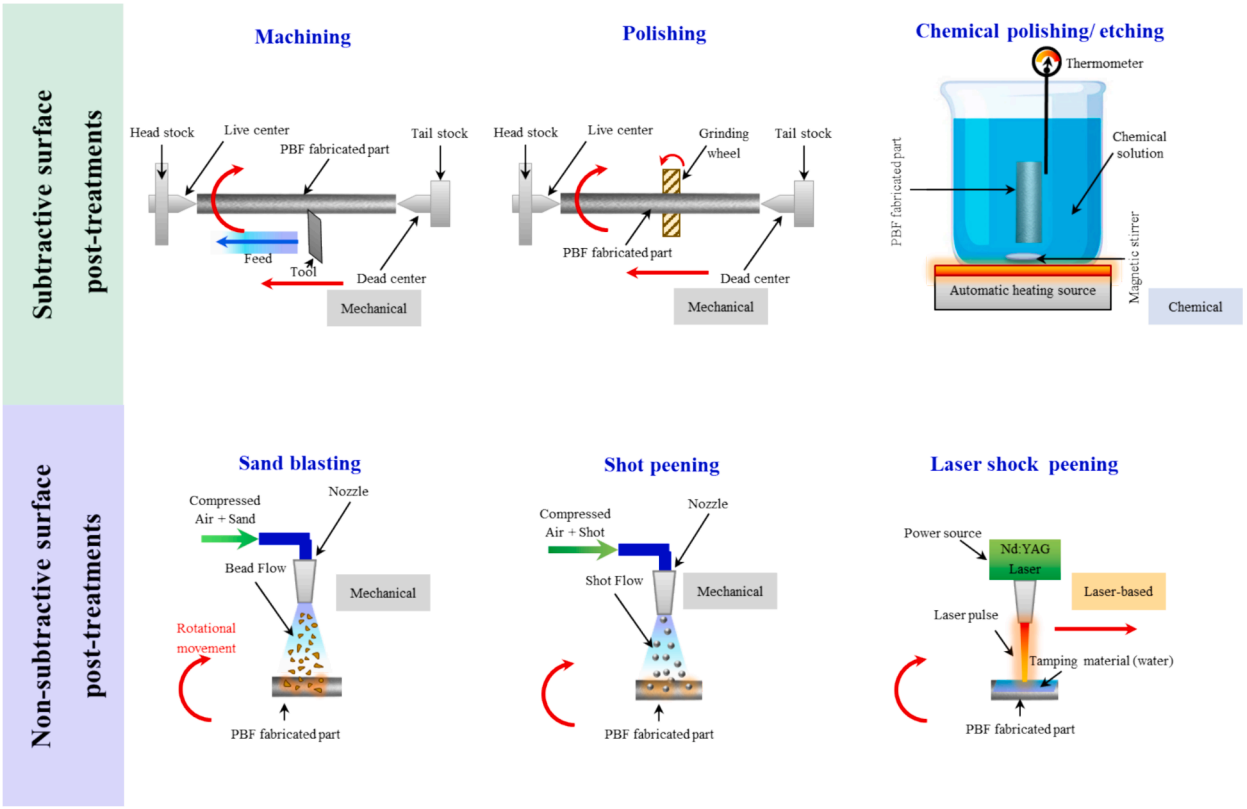

Fig. 19. Schematic illustration of several subtractive and non-subtractive surface post-treatments. Adopted from Maleki and Shamsaei [173] with some modifications.

residual stresses, surface work-hardening, surface grain refinement, and mainly to enhance the cyclic performance of metallic components [181–183]. The process has also been widely used for the post-processing of AM materials to address the typical shortcomings in terms of surface quality as well as limited fatigue performance in the as-built condition [170,180,184]. Two main shot peening parameters are Almen intensity, which is a measure of the kinetic energy of the impacting beads, and the coverage area treated [25].

Laser shock peening is another non-subtractive surface treatment that is based on inducing plastic deformation on the surface layer through pulsed laser exposure. The high controllability of this process makes it particularly suitable for AM parts with quite complex shapes. Similar to shot peening, laser shock peening can also lead to grain refinement and compressive residual stresses on the surface layer, thus improving fatigue resistance properties [185].Moreover, the surface roughness of laser shock peened specimens is generally lower than that of shot peened ones. The effect of laser shock peening (using 10 ns pulsed Nd: YAG laser) was investigated on L-PBF 316L stainless steel dog bone specimens with 0°,45°, and 90° build orientations. It was observed that the specimens oriented at 45° exhibited improved UTS and YS, due to grain refinement and compressive residual stresses. After laser shock peening, the extent of fibre texture oriented along ⟨1 1 0⟩ parallel to the build direction decreased, mostly in 90° oriented specimen, leading to a reduction in anisotropy. Overall, the treatment resulted in improved strength but reduced ductility in 0° and 45° specimens, while the 90° specimen showed a good combination of strength and ductility [186].

7.2.3. Coatings

Coating deposition consists of various techniques adopted to cover the surface of a part with a film of a material (e.g., metal, ceramic, polymer) different from the base material, mainly to enhance mechanical/electrochemical properties or induce specific surface functionalities. Coating deposition can be used to preserve the surface from a corrosive environment, reduce surface roughness, mask surface defects and pores, and in some cases, improve the biological response of the component [169].

Coating represents a valid option to overcome the difficulties derived from excessive surface roughness or eventual porosity that may affect AM components-performance. Indeed, coating represents a feasible strategy to fill the superficial open pores regardless of the parts' build direction [187].

7.2.4. Hybrid treatments

Hybrid post-treatment solutions are used to unite the benefits derived from various existing processes. They are mainly composed of a heat treatment, which is a standard approach in AM (aimed at microstructural homogenization, inducing anisotropy and releasing undesired residual stresses) paired with a surface treatment mainly to target the surface roughness issues in AM materials.

Jamshidi et al. [188] investigated the combination of the HIP and three surface treatments, i.e., sand blasting (SB), polishing (PL) and chemical etching (CE) on L-PBF Ti6Al4V specimens made along vertical and horizontal orientations. HIP eliminated the internal LoF porosities and thus increased the specimen's density and the partially melted particles attached to the specimen's periphery were eliminated after all the applied surface treatments. In the as-built condition, the vertically built specimen demonstrated higher UTS and YS compared to the horizontally built one, due to the preferential grain orientation along the direction of the applied load in the tensile test. HIP reportedly improved ductility and porosity in both build directions. Regarding fatigue performance, the HIP + CE treatment led to the highest fatigue performance improvement due to the high roughness reduction (Sa from 12.2 to 6.6 μm), leading to a fatigue limit around eight times higher than the as-built conditions. Nonetheless, also the other treatments enhanced significantly the printed parts: HIP P + PL and HIP improved the fatigue limit of six and four times, respectively. Moreover, cell culture tests indicated that the CE treatment enhanced cellular affinity, leading to significant improvement in bone integration.

7.3. Effects of post-treatments on microstructure of inclined features

The post-treatments, which mainly impact microstructure are those targeting the bulk. Thus, as-built condition, HT, and HIP treatment outcomes on various materials will be comparatively examined in this section.

L-PBF Ti6Al4V specimens produced in 0°, 30°, 45°, 60° and 90° directions, were explored by Ren et al. [189]. Some of the specimens were left as-built while the others underwent the following treatments: heat treatment in an argon atmosphere Below ß-Transus (BT) (800 °C, 2 h), HIP (920 °C, 100 MPa, 2 h) and heat treatment above ß-Transus (AT) (1050 °C, 2 h). In Fig. 20a-h, clear differences existed between the specimens, but no significant distinction was observed between the building directions. The SEM observations in the as-built case (Fig. 20a, e) indicated long columnar grains oriented along the build direction. In the BT case (Fig. 20b, f), V atoms precipitated from the α' phase, and the β phase formed along the grain boundaries. In the HIP specimens (Fig. 20c, g), at the boundary of columnar grains, a visible α phase grain boundary existed while an α + β phase was formed inside the columnar grains. The results indicated that the α phase partially underwent a spheroidization process. For the AT treatment (Fig. 20d, h), the temperatures above β-transus enhanced the growth of the grains, which made them equiaxed or semi-equiaxed. The EBSD analysis of the as-built specimens confirmed the preferential orientation of the texture. This texture remained unchanged after BT and HIP treatments, while AT led to very high pole intensity values. The pole values of intermediate orientations (i.e., 30°, 45°, 60°) were similar to those at 0° and 90°.

The effects of heat treatment and its combination with HIP were analysed by Ghorbanpour et al. [124] on L-PBF IN718 specimens with regular and functionally graded structures built along both horizontal and vertical directions. Within the same structure, two portions built with different process parameters and beam shapes coexisted; particular emphasis is given to the study of the microstructure at their interface. Some specimens underwent a heat treatment, which was a combination of homogenization (1065 °C, 1 h) and a double ageing process (760 °C, 10 h – 650 °C, 8 h), while the other specimens were also subjected to an additional HIP treatment (1180 °C, 150 MPa, 3 h). The interface microstructure changed sharply in the as-built specimens, while it became smoother for the HT

and HT P + HIP ones. From a microstructural point of view, the as-built condition revealed a preferential orientation of the grains (Fig. 20i, l). The heat treatment reduced the grain size but did not affect their orientation; residual porosities/defects were still present, especially in the vertically built specimens (Fig. 20j, m). HT P + HIP (Fig. 20k, n), instead, reduced the microstructural anisotropy and sensibly reduced the number of defects detected.

Kuo et al. [190] used DMLS to produce IN718 vertical and horizontal specimens to study the effect of heat treatments on specimens of different orientations. The specimens included as-built, subjected to solution treatment (980 °C, 1 h), and two-step ageing treatment (718 °C, 8 h – 621 °C, 10 h) (STA) or direct ageing treatment (718 °C, 8 h – 621 °C, 10 h) (DA). δ phases in the grains were noticed to grow along the building direction. The manufacturing laser process generated high thermal rates, producing a high density of dislocations, as shown in Fig. 20o. The dislocations persisted even after the STA treatment, as the subgrains can also be observed in Fig. 20p. Both in STA and DA cases, the formation of γ' and γ'' phases were identified throughout the whole microstructure (Fig. 20q).

Sangid et al. [191] investigated the influence of heat treatment on L-PBF Inconel 718 specimens produced in vertical and horizontal directions. The as-built specimens' microstructure was strongly anisotropic along the direction of hatching, as shown in Fig. 20r, s. The stress relief treatment was applied to all specimens (1065 °C, 1.5 h) before the removal from the build plate; the specimens which underwent exclusively stress relieving were considered as-built. In another set, referred to as heat treated, stress relief was followed by three distinct steps of homogenizing (1177 °C, 1 h), solution treating (982 °C, 1 h) and aging (718 °C, 8 h – 621 °C, 18 h). After the heat treatment, the microstructural anisotropy was reduced, and the structure became homogeneous both in the vertical and horizontal series with no visible scan tracks in the material. The microstructure dislocations were also regularized, and the strain pattern appeared similar between vertical and horizontal series both at 45° bands.

In another study, the microstructural consequences of annealing (300 °C, 2 h) or solution treatment (530 °C, 6 h) in air, followed by water quenching were analysed on L-PBF AlSi10Mg lattice structures [192]. From the optical micrographs in Fig. 20t-v, it is noted that the microstructures were composed of several melt pools both in the as-built condition and after annealing, while they were not present after the solution treatment. The structure of the as-built specimens exhibited a primary α-Al phase accompanied by α-Al/Si eutectic microstructure. Upon analysing the inverse polar figures of the strut portions in their as-built condition, a gradient in the microstructure was observed since the portions at the bottom of the struts and nodes became more equiaxial. This gradient persisted after annealing, with enlarged grains and Si precipitation in α-Al. The structure appeared homogeneous after the solution treatment, in which the microstructural gradient was not visible; further coarsening of Si particles and formation of an intermetallic phase (β-AlFeSi) were also observed.

The interplay between the building orientation and heat treatment of L-PBF AlSi10Mg struts produced in vertical and inclined (35.5° from horizontal plane) orientations was investigated by Delroisse et al. [102]. The treatments included T6 heat treatment (i.e., annealed 525 °C, 5 h), water quenched and artificially aged (165 °C, 7 h). Two distinct zones were identified in the as-built condition in inclined struts (Fig. 20w). Zone A is in the top part of the strut, and it is featured by a finer microstructure, with small cells of primary Al in the Si eutectic phase. Zone B is at the bottom of the struts and is characterized by inter-eutectic cells 2.5–3 times bigger than those in zone A. The differences between the two zones were attributed to more efficient heat conduction in zone A, considering that the faster heat flux hinders the coarsening. The vertical struts were more homogeneous in microstructure and had reduced porosities due to gas entrapment, whereas in zone B, porosities were more pronounced because of pore growth caused by longer exposure to high temperatures. After heat treatment, the struts exhibited a uniform microstructure without visible melt pools and with Si growth and spheroidization (Fig. 20x).

7.4. Effects of post-treatments on surface topography of inclined features

One of the most significant drawbacks of AM processes is the poor surface finish quality, which is in turn affected by building orientation. This section will present a discussion on the interrelationships between building orientation and various post-treatments that have been applied to address its effect on surface topography and roughness including shot blasting, shot peening, anodization, etching, and polishing.

The effects of shot blasting on L-PBF 316L stainless steel specimens were investigated by Krishna et al. [193]. To evaluate surface roughness, 38 up-skin surfaces of two complex-shaped specimens were analysed at inclinations ranging from 0° to 90°. Fig. 21a shows the surface topographies in the as-built and post-processed conditions. The as-built specimens show a raster pattern and staircase effect, with randomly attached partially melted particles, the density of which increases with the inclination. However, after shot blasting, the removal of the attached particles reduced the surface roughness Sa but at the same time created fine features caused by the impact of the beads. The surface roughness of the post-processed specimen analysed vs. build inclination, followed the same trend as the as-built case, with a reduction in the surface anomalies height (Fig. 21b). It should be noted that sand blasting significantly reduced the surface roughness values for all conditions with different build orientations compared to the as-built state, except for the 40° orientation. This exception indicates that the effectiveness of sand blasting in smoothening the as-built AM surfaces can vary depending on the specific build orientation and the starting roughness. While sand blasting generally improves the surface finish by removing asperities and creating a more uniform texture, the 40° orientation might present unique challenges, such as complex geometric features that are less responsive to this post-treatment method.

The developed interfacial area ratio (Sdr) represents the additional surface given by the roughening with respect to the datum plane. Sdr is a standard surface roughness parameter that quantifies the ratio of the actual surface area (including the microscopic peaks and valleys) to the projected (flat) surface area. It is expressed as a percentage and provides an indication of the complexity and topography of a surface. A higher Sdr value signifies a rougher surface with more pronounced topographic features, while a lower Sdr value indicates a smoother surface. From Fig. 21c, it is evident that Sdr increased with build inclination in the as-built case, while there

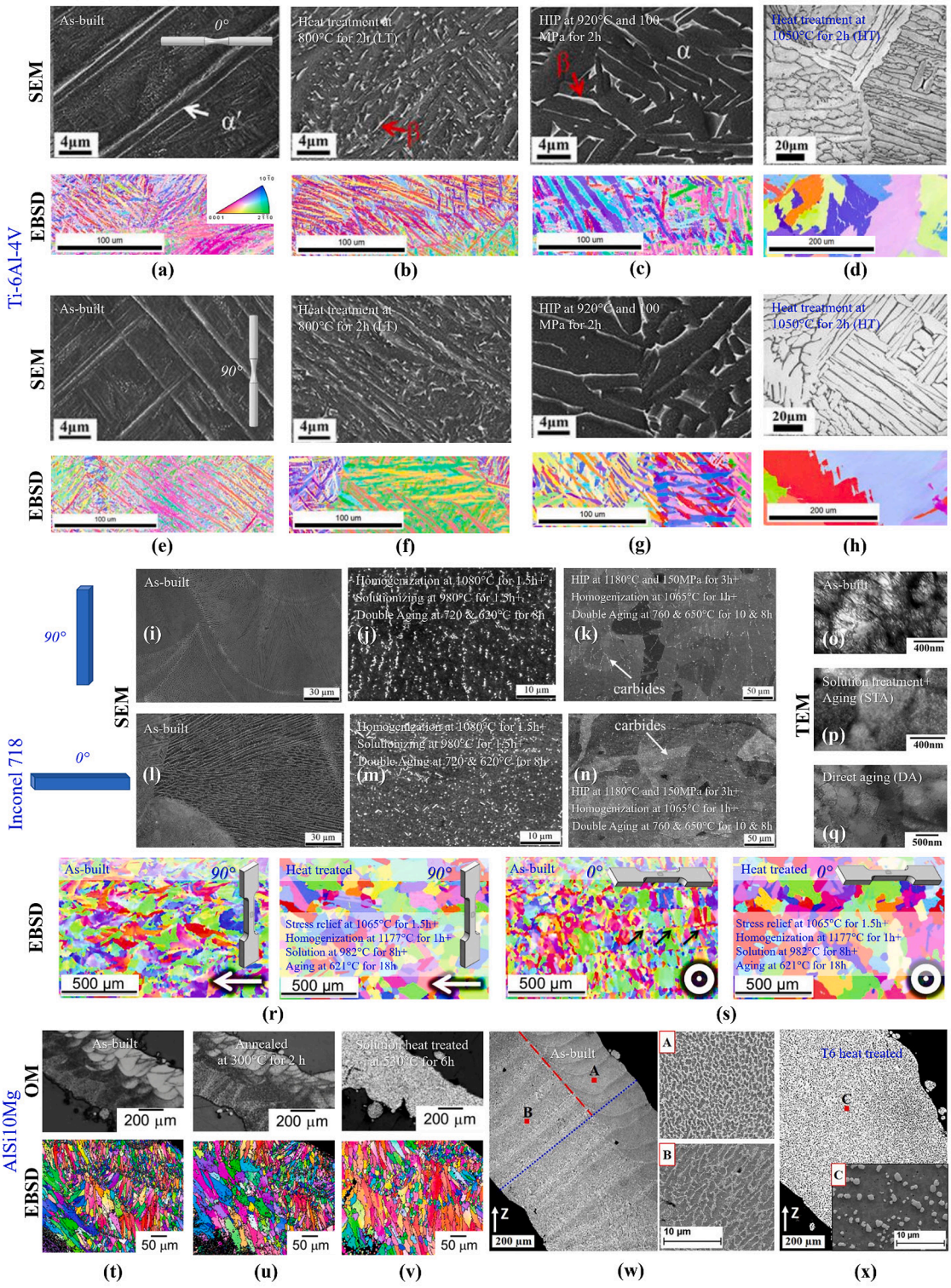

Fig. 20. Microstructure of the longitudinal section of L-PBF Ti6Al4V specimens, oriented at 0° (a-d) and 90°(e-h), in different states of as-built (a,e), LT (b, f), HIP (c,g), HT (d, h) [189]. Optical micrographs of longitudinal cross-sections of IN718 specimens produced by L-PBF, oriented at 90° (i-k) and 0° (l-n); in different states of as-built (i, l), HT (j, m), HT + HIP (k, n) [124]. Transmission Electron Microscope images of DLMS IN718 specimens produced at 0° and 90°, in different conditions of as-built (o), solution treated and aged (p) or directly aged (q) [190]. Inverse Polar figures for the microstructure of L-PBF IN718 specimens before and after HT: vertical (r) horizontal (s) (white arrows in the bottom right corner indicate the building direction; black arrows evidence the fine microstructure formed due to rapid solidification) [191]. Optical micrographs and IPF of struts in

L-PBF AlSi10Mg lattice structures in various conditions of as-manufactured (t), annealed (u), and solution heat treated (v) [192]. L-PBF AlSi10Mg struts in the as-built condition, a finer microstructure is present in zone A, whereas a coarsened one is in zone B (w). The strut, after T6 heat treatment, is featured by homogeneous microstructure (x) [102].

is a significant reduction of Sdr in the blasted specimens. However, the overall effect of the blasting treatment was independent form the building orientation.

L-PBF AlSi10Mg notched specimens shot peened using two distinct sets of parameters i.e., SP1 using cast steel spheres of 0.43 mm diameter, 10 Almen intensity and SP2 using ceramic spheres of 0.1–0.15 mm diameter at 5 Almen intensity, both at 100 % coverage, were analysed by Maleki et al. [25]. In the as-built state, the typical irregular surface topographies mainly partially melted and unmelted particles were found on all up-skin, down-skin and smooth surface of the notch, with higher density and extent in the down-skin regions. The as-built condition exhibited $S_a = 60$ μm on the smooth surface of the notch, with 480 % and 290 % increase on the down-skin and up-skin surfaces, respectively. Both SP1 and SP2 treatments led to substantial morphologic modification of the surfaces by removing the irregularities (Fig. 21d). SP2 was more effective in modifying the surface and making it more homogeneous. However, the process slightly increased the roughness on smooth notched surfaces due to the formation of dimples in the regions where the high-energy shots impacted. Shot peening, overall, was beneficial for the inclined surfaces in terms of roughness reduction (Fig. 21e). Compared to the as-built condition, the up-skins S_a exhibited a decrease of 36 % after both SP1 and SP2; the down-skins S_a decreased by 44 % after SP1 while after SP2 was still comparable to the as-built case.

Rovetta et al. [194] examined the effects of anodization and etching on the surface topography of L-PBF AlSi10Mg specimens manufactured in 0° and 45° orientations. The anodization procedure was conducted at a constant voltage of 60 V for 20 min while the etching was performed in Kroll reagent for 10 min at room temperature. The SEM observations (see Fig. 21f) in the as-built condition evidenced a homogeneous distribution of partially melted particles in the 0° orientation, while the 45° specimens presented inhomogeneities caused by particle clusters. Surface modification induced by anodization was not noticeable at 0°, while it produced cracks on the particles and increased the clusters in number and size at 45°. The etching treatment, instead, led to the detachment of particles and clusters, disregarding the building orientation. The outcomes regarding roughness values for 0° and 45° orientations are recalled in Fig. 21g and Fig. 21h, respectively. Consequently, the results indicate the significance of the post-treatment choice rather than the inclination of the specimen.

Finally, magnetic abrasive finishing was utilized as a polishing technique on L-PBF 316L stainless steel specimens. These specimens were inclined at seven different angles ranging from vertical (90°) to horizontal (0°) [195]. G50 steel grit was used as the abrasive, and the finishing process was carried out using vibrations at a frequency of 28.8 Hz and an amplitude of 20 mm. In the as-built condition, there were higher percentages of balling and unmolten particles in vertically oriented parts. These defects could be mostly removed after a 75 min treatment, although the effects varied based on the specific building orientation; in 30°, 45°, and 60° specimens, that is, in some cases, few particles were left in the valleys (Fig. 21i). In terms of the surface profile, the peaks were levelled, while the valleys remained in the 15° and 75° specimens. Fig. 21j shows the variations in roughness according to the inclinations at 15-minute intervals during the polishing process. The surface roughness Ra increased with the angle until 60° and then decreased due to a reduction in unmolten particles. For all the building orientations, the progressive removal of the surface imperfections gradually reduced roughness. Despite the material removal rate being independent of time, surface roughness improvement decreased progressively and plateaued after 60 min of polishing. The specimens showed an average Ra decrease of 56 %, with vertically built specimens experiencing a maximum decrease of about 76 % due to the presence of easily detachable particles.

7.5. Effects of post-treatments on hardness and tensile behaviour of inclined features

Microstructural modification may induce significant variations in the part's mechanical properties. Hence, the following section examines how various post-treatments affect the tensile and hardness of the material.

In the experiment by Ren et al.[189], also detailed in Section 7.3, the effects of LT, HIP, and HT treatments were investigated on the tensile behaviour of Ti6Al4V L-PBF specimens. Fig. 22a-c shows the obtained trends for tensile and static strength and the elongation in the as-built and in the three post-treated conditions analysed. In the as-built specimen, these parameters are highly dependent on the inclination since it varies the entity of residual stresses and the internal porosities. The tensile and static strength in as-built conditions reach a maximum at 45°, then decrease, reaching its minimum at 90°. As-built sample made at 90° (AB-90°) was the most critical condition because of the higher residual stresses and numerous sensitive areas for crack initiations. As the angle increased from 0° to 45°, the elongation decreased, exhibiting the lowest range at 45°. However, as the angle continued to increase from 45° to 90°, the elongation started to increase again. This trend can be attributed to the variations in density; the inclined specimens present higher porosity, which results in lower elongation. In the LT specimens, building orientation has a less but still significant impact on the results compared to the as-built specimen. As the temperature during heat treatments increases, a coarser microstructure is formed, which leads to improved elongation, but decreased strength. Notably, in the cases of HIP and HT, the mechanical properties remain unaffected by the building orientation. The results indicate that in the HIP specimens, pore closure had a positive impact on the elongation, which was the highest among all the studied conditions.

The two heat treatments of stress relief (SR) (ASTM F2924 class 1) and HIP (ASTM F2924 class 2) were also applied to a series of L-PBF diamond cell-like lattice Ti6Al4V structures considering 5 different orientations of the unit cell [104]. This design strategy resulted in different strut orientations, influencing ductility and density, that were reported to be most critical in the case of horizontal struts having the highest level of porosity. The effect of heat treatments was found to be independent of the build orientation. SR resulted in

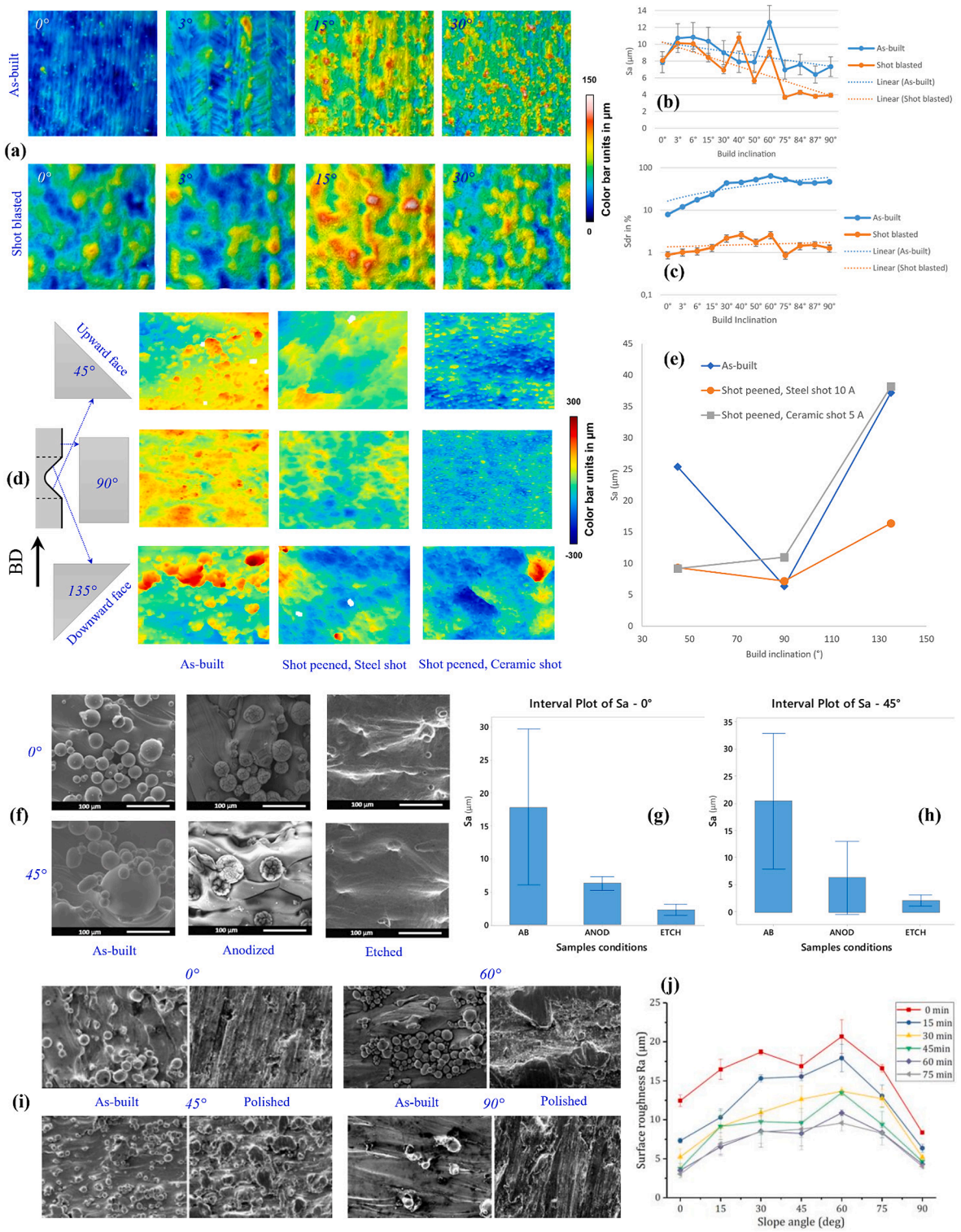

Fig. 21. (a) Surface topography measurements of L-PBF 316L stainless steel specimens in as-built and shot blasted conditions, in 0°, 3°, 15°, and 30° inclinations with the extracted area measuring 0.5 × 0.5 mm^2; (b) S_a and Sdr measurements in as-built and shot blasted conditions in various building inclinations [193]. (d) Surface topography of L-PBF AlSi10Mg notched specimens on the up-skin, smooth, and down-skin surfaces of the notch, in as-built, and shot peened (SP1 and SP2) conditions; (e) Surface roughness trends in as-built, SP1, and SP2 conditions as a function of build inclination [25]. (f) SEM micrographs of L-PBF AlSi10Mg specimens' surface inclined at 0° and 45°, in as-built, anodized, and chemically etched conditions; (g) Comparison of surface roughness in the as-built, anodized, and chemically etched condition in 0° inclined specimens; (h) Comparison

of surface roughness in the as-built, anodized and chemically etched condition in 45° inclined specimens [194]. (i) SEM images of L-PBF stainless steel 316L specimens built at various building inclinations, in as-built and polished with magnetic abrasive finishing conditions; (j) Ra measured as a function of the building inclination to monitor magnetic abrasive finishing effects at 15 min intervals [195].

stronger structures, while HIP enhanced the formation of lamellar α + β microstructure, leading to a reduction in strength and an increase in ductility (contrary to the trends reported in [172]). The SR specimens were slightly stronger, yet more brittle (Fig. 22d-f). By properly orienting the cell and building direction avoiding the horizontal struts, reducing porosity, and choosing post-processing techniques, a positive impact can be made on the complex lattice structure.

L-PBF was used to fabricate AlSi10Mg specimens with 7 different inclinations (ranging from horizontal 0° to vertical 90° with a 15° increasing angle from the horizontal configuration) by Hovig et al. [196]. Several conditions were considered: as-built, SR (300 °C, 2 h) and air-cooled, and T6 heat-treated. During the processing phase, a set was pre-heated at 200 °C. Upon comparison of the as-built specimens fabricated at room temperature and with pre-heated plate, a 40 % reduction in residual stresses was observed due to a decrease in thermal gradient in the pre-heated case. Additionally, the tensile behaviour of the as-built, pre-heated, and SR specimens did not differ significantly. Therefore, the SR phase can be considered unnecessary when pre-heating is performed. Elastic modulus was not affected by the building orientation in the studied conditions, although the data were scattered (Fig. 22g). Reportedly, YS and UTS did not seem to be affected by the building angle; T6 treated specimen's Ys and UTS exhibited a decrease at 15° followed by an increase, with the maximum value reached at 75° (Fig. 22h, j). The elongation increased from 0° to 90°, both in as-built and SR conditions, whereas, the average elongation doubled after T6 treatment; however, the ductility improvement that was derived from the recrystallization of the microstructure, was accompanied by a 10 % reduction in YS and UTS (Fig. 22i). Hovig et al. [197] also adopted the same building orientations as [196] and analysed the mechanical properties for L-PBF 18Ni300 maraging steel specimens. The specimens were machined to eliminate the contribution of surface roughness derived from the building process, and then solution treated (815 °C, 1 h) followed by aging (500 °C, 5 h), denoted as SA P + A, and direct aging (500 °C, 5 h), denoted as DA. Fig. 22k-n depicts the trends of the mechanical properties for the two different post-treatments, compared with the forged bar aged at 482 °C standards (Metallic Materials Properties Development and Standardization (MMPDS-11)), shown in dashed lines. The average values for elastic modulus were slightly below the reference, and only the DA specimen was found affected by the building orientation. The specimen at a 60° angle had the highest stiffness, with an 8 % increase in elastic modulus compared to the lowest at a 90° angle. The values of YS and UTS were coherent with the literature findings and independent of the build angle. Finally, the elongation at fracture reached its minimum value at 15° and 90° orientations in SA.

On the other hand, the variations of tensile properties investigated by Sangid et al. [191], as detailed in Section 7.5, highlighted the existence of anisotropy, especially in the as-built condition. The tensile test, performed by monotonic loading of the specimens at 2.3 % strain followed by unloading to zero, evidenced a decrease of 37 % in YS from horizontal to vertical orientation. After the heat treatment (homogenizing, solution treating and aging), the anisotropy was reportedly reduced, and the specimens were considerably strain-hardened (Fig. 22o). EBSD analysis of heat treated specimens in Fig. 22p showed a preferential slip in the maximum shear stress direction (45°) and a more localized strain in vertical rather than horizontally oriented specimens.

Zhang et al. [195] investigated L-PBF Cr-Cu-Zr specimens produced in the horizontal and vertical orientations. The ageing treatments were performed at different temperatures (350 °C, 400 °C, 450 °C, 500 °C) and soaking times (0, 5, 15, 30, 45, 60, 90, 120, 240, 360, 480, and 600 min). The aged specimens exhibited higher strength than the as-built series with anisotropic mechanical properties. Also, the vertical specimens were shown to have a better performance. The optimal ageing temperature and time to enhance the tensile properties and hardness were found to be 500 °C and 30 min (Fig. 22q, r). Besides, it was noticed that increasing the duration of the treatment would lower the hardness. It can be noticed in Fig. 22u, v that the vertically built part had higher penetration resistance than the horizontal one.

Vickers hardness trends for horizontally and vertically oriented heat-treated specimens were also measured in the study by Ghorbanpour et al. [124] (also detailed in Section 7.3) IN718 L-PBF specimens were built in horizontal and vertical direction and a set was also functionally graded in terms of process parameters; specifically the hardness comparison considers mainly the sides processed with different power levels (i.e., P = 250 W and P = 950 W). In the horizontal configuration, the 250 W side was in contact with the baseplate, so it was subjected to more thermal cycles, featuring a higher hardness with respect to the 950 W, although the hardness decreased along the height of the part. Accordingly, the transition from 250 W to 950 W, which in vertical parts occurred orthogonal to the build direction, implied that the two sides were subjected to the same number of thermal cycles. As a result, they exhibited similar hardness. In both the functionally graded and non-graded parts, the hardness was comparable within the heat-treated specimens but higher than in the as-built case (Fig. 22s, t).

7.6. Effects of post-treatments on fatigue behaviour of inclined features

Fatigue behaviour is known to be affected by the synergic effects of several parameters related to the bulk and superficial state of the part produced; these can be in turn modulated through suitable post-processing techniques. This section briefly reviews the data available on the effect of post-treatments that have been applied to inclined AM specimens.

Fatigue properties of EBM Ti6Al4V specimens produced at 0°, 45°, and 90° orientations were analysed and compared with the data from their respective machined counterparts [108]. Then, HIP treatment (920 °C, 100 MPa, 2 h) was performed on the 90° specimen. The results indicated fatigue strength improvement (see Fig. 23a) after machining compared to the as-built series. Additionally, the building orientation was found to have an impact only on the microstructure, with better outcomes observed in the horizontal

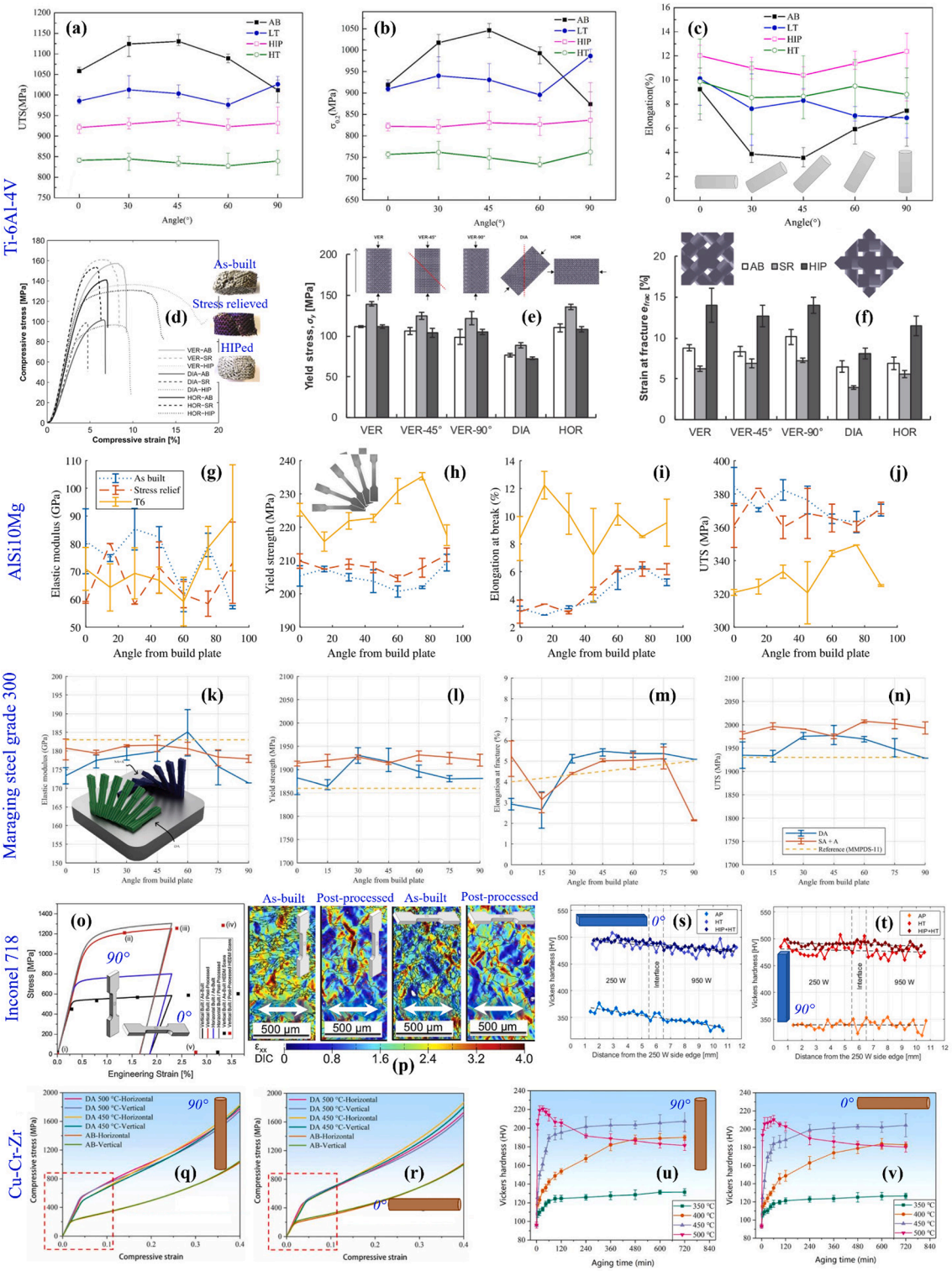

Fig. 22. (a) Tensile strength, (b) static strength, and (c) elongation of L-PBF Ti6Al4V specimens, oriented at 0°, 30°, 45°,60° and 90°, in different states of as-built, LT, HIP, and HT (d, h) [189]. (d) Stress–strain curves, with images of the specimens after compression test (e) yield stress, and (f) strain at fracture of L-PBF diamond cell-like lattice Ti6Al4V structures fabricated at 5 different orientations of the unit cell, in as-built, SR-ed or HIP-ed conditions [104]. Mechanical properties of L-PBF AlSi10Mg specimens produced with different orientations ranging from 0° to 90° with 15° intervals, in as-built, SR and T6 conditions: (g) Elastic modulus, (h) YS, (i) Elongation at break, (j) UTS [196]. Mechanical properties of L-PBF 18Ni300 maraging steel specimens produced with different orientations ranging from 0° to 90° with 15° intervals, in SA + A, and DA condition,

compared with forged bar as the reference counterpart: (k) Elastic modulus, (l) YS, (m) elongation at break, and (n) UTS [197]. (o) Stress–strain curves and (p) EBSD strain maps of L-PBF IN718 specimens manufactured in vertical and horizontal orientation, in as-built and heat treated (homogenizing, solution treated and aging) conditions. The white arrows indicate the loading direction [191]. Vickers hardness of L-PBF IN718 specimens with functionally graded structures in as-built, HT, HT + HIP conditions, built along (s) vertical, and (t) horizontal direction [124]. Compressive stresses (q, r) and Vickers hardness (u, v) of L-PBF Cr-Cu-Zr specimens produced in vertical and horizontal directions, respectively [195].

configuration. To evidence the major role of surface condition rather than the internal defects, it was confirmed that the HIP treatment, which eliminated internal porosities, did not affect the specimen's fatigue life.

Fatigue analysis of inclined Ti6Al4V L-PBF specimens after LT, HIP, and HT treatments was experimented by Ren et al. [189] (Section 7.5). In Fig. 23b, the variation of the fatigue cycles according to the building orientation in the as-built and LT cases can be observed, while no effect was noticed in the HIP and HT cases. The trends correspond to those of the static strength described in Section 7.5. It was reported that the fatigue behaviour was mainly affected by the size and location of pores and the extent of residual stresses, while in the near pore-free HIP and HT cases, the crack initiation was linked to plastic slip (Fig. 23c).

Afkhami et al. [198] obtained comparable fatigue behaviour for L-PBF 316L specimens and the conventional specimens when

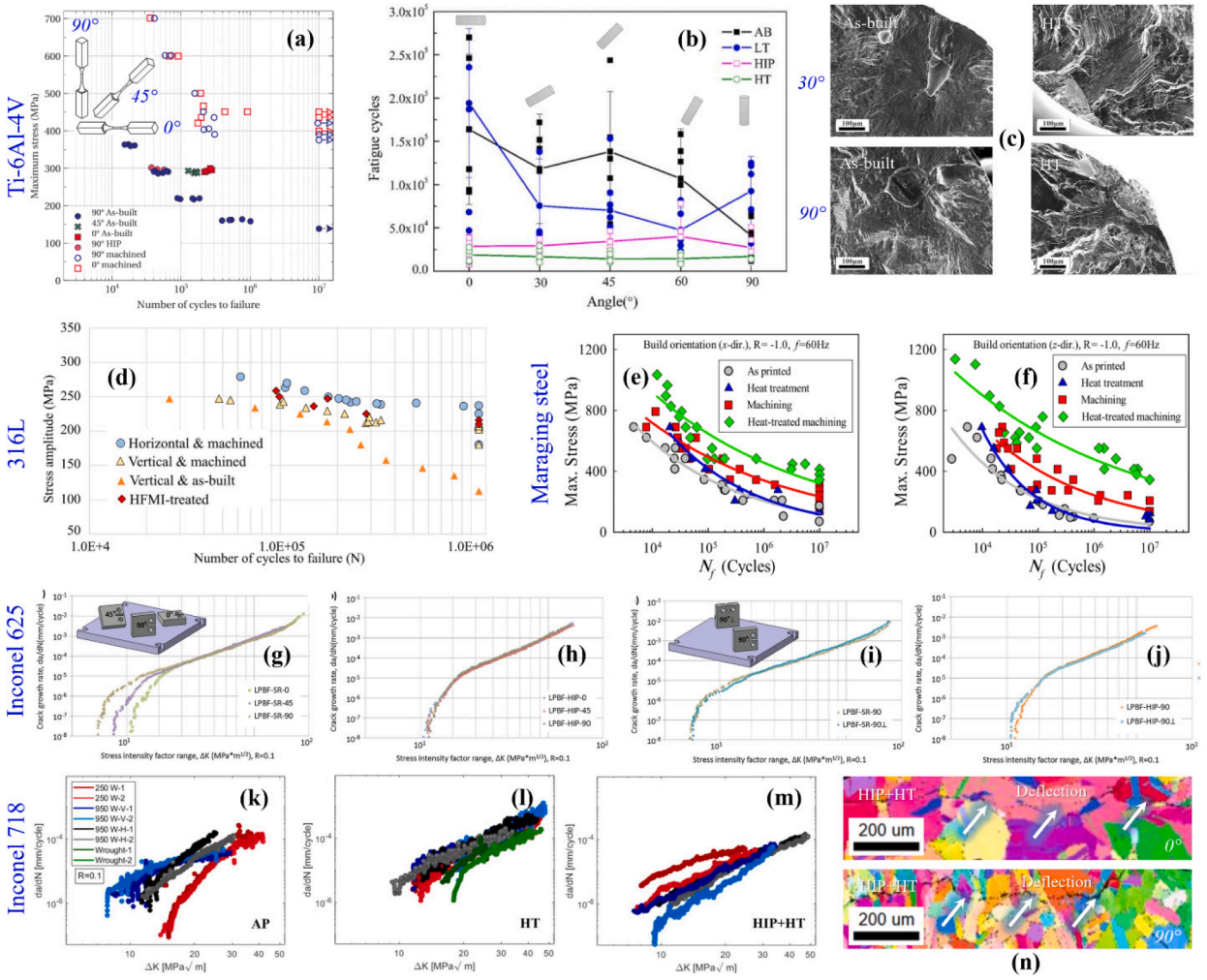

Fig. 23. (a) Number of cycles to failure for EBM Ti6Al4V specimens, produced in 0°, 45° and 90° as-built, 0° and 90° machined and 90° HIP conditions [108]. (b) The fatigue life of L-PBF Ti6Al4V specimens oriented at 0°, 30°, 45°,60°, and 90° in different states of as-built, LT, HIP, HT. (c) Crack initiation sites in as-built and HT specimens for 30° and 90° orientations [189]. (d) Number of cycles to failure for L-PBF 316L specimens in horizontal orientation (machined), and in vertical orientation (as-built, machined, and HFMI treated states) [198]. The fatigue life of L-PBF maraging steel specimens in as-built, heat treated, machined, and heat treated + machined conditions, in horizontal (e) and vertical (f) orientations [199]. Fatigue crack propagation diagrams of L-PBF Inconel 625 specimens produced in orthogonal and vertical directions in SR (g, i) and HIP (h, j) conditions when the crack propagates parallel or orthogonal to the building plate, respectively [174]. Fatigue crack growth curves in L-PBF Inconel718 specimens in (k) as-built, (l) HT, (m) HIP + HT conditions, and (n) IPF maps in HIP + HT condition [124].

proper post-processing was applied. The specimens were produced in horizontal orientations followed by machining, with the vertical orientation specimens being categorized into as-built, machined, and high-frequency mechanical impact treated (HFMI) (Fig. 23d). Reducing surface roughness improved fatigue strength by removing major stress concentration sites. In the vertical orientation, the machined specimens showed 85 % increase in fatigue limit, while the HFMI specimens showed a 90 % increase compared to the as-built series. On the other hand, the horizontal specimens showed an improvement of 15 % compared to the vertical orientation. The dependency on the build orientation and the applied post-treatment were more evident in the low-stress amplitude, in which the notch effect was predominant.

In another work, the fatigue behaviour of L-PBF maraging steel specimens fabricated in vertical and horizontal orientations was examined in as-built, heat-treated (aging, 490 °C, 6 h), machined, or heat treated + machined conditions [199]. All three post-processes improved the fatigue life compared to the as-built condition, with the greatest increase observed for the vertical specimens. Interestingly, the effect of orientation was not significant in the parts subjected to both post-processing techniques (Fig. 23e, f).

Also, Poulin et al. [174] studied the effect of build orientation on L-PBF Inconel 625 notched specimens built with 4 different orientations: horizontal, inclined at 45°, vertical with the notch parallel to the building orientation, and vertical with the notch orthogonal to the building orientation. Half of the specimens were post-treated with stress-relieving heat treatment (870 °C, 1 h), with the other half undergoing HIP treatment (1120 °C, 100 MPa, 4 h).

On the inclined surfaces, staircase effects were noticeable, and a high density of partially melted powder particles was observed, particularly on the downward-facing surfaces. The high anisotropy derived from the build orientation could not be reduced in the SR specimens, whereas HIP eliminated the anisotropy for all series and led to a significant pore closure. The fatigue crack propagation diagrams in all three building directions, with c parallel to the build plane, are compared in SR and HIP conditions in Fig. 23g and h, respectively. It was reported that only SR treatment showed a dependency on the building orientation in the near-threshold region, although, in the Paris regime, the orientation was not significant in both SR and HIP specimens. In Fig. 23i,j when comparing the diagrams of crack propagating parallel to the building plate versus orthogonal direction, it was found that L-PBF parts showed results similar to those of wrought alloy. However, in the case of HIP series, the results were slightly lower for the cracks propagating orthogonally to the building plate as compared to the vertically propagating cracks. Additionally, crack propagation is investigated in another study on IN718 L-PBF parts in which a set of specimens was functionally graded, i.e., different sides of the specimens featured different process parameters, both in vertical and horizontal direction. A set was left as-built, another was heat treated (HT) (homogenisation, solution treating and double aging) and the last underwent both the HT and HIP. The crack propagation in as-built specimens (Section 7.3) (Fig. 23k), indicated higher ΔK_{th} when the power level was 250 W due to the presence of finer grains compared to the level 950 W, so more grain boundaries impeded the crack propagation [124]. The coarser grains from HT parts, however, could bear the slip damage more efficiently. It explained the higher ΔK_{th} value obtained for HT parts compared with the as-built state, along with the precipitation of strengthening phases.

In Fig. 23l it is evident that the wrought material still performed better, thanks to its equiaxed fine grains. In HT P + HIP, the grain size and the number of precipitates increased, while the porosities were reduced, with all cases experiencing an increase in ΔK_{th} (Fig. 23m); the maximum value was reported for the 950 W horizontal specimen. The microstructure in HIP P + HT is shown in Fig. 23n, where the upper image refers to the 250 W side, in which random, fine grains were distinguished, while the bottom image refers to the 950 W side, having coarser grains and moderate $\langle 0\,0\,1 \rangle$ orientation, consistent with the wrought material. It is reported that the cracks in the L-PBF parts propagated from right to left primarily through trans-granular paths, while in wrought parts they propagated through a combination of intergranular and trans-granular cracking. This study evidenced that the proper post-processing may enhance the fatigue behaviour of L-PBF parts to a level higher than the wrought specimens.

8. Summary and future perspectives

Metal AM is an emerging technology which is diffusing in multiple sectors such as automotive, aerospace, and biomedical applications. It comprises a wide variety of techniques and among them, this review focuses mainly on PBF technologies, resorting to the selective melting of a powder bed to create an object in a layer-by-layer process. The quality and properties of a PBF metal parts depend on numerous factors, from powder properties, geometrical design, manufacturing technology and process parameters to post-treatments. Among these parameters, build orientation holds a crucial role in defining the superficial and mechanical properties of the produced parts.

Build orientation is found to be strictly linked with the thermal history of the AM part, affecting, in turn, a wide range of its physical, microstructural and mechanical attributes. The effect of build orientation on various properties has been experimentally investigated on several metal alloys using different AM techniques, where the same specimen is produced at different build orientations and characterized in detail. Although there has been an increasing interest towards this topic, there are no available guidelines for design for AM on the choice of build orientation with respect to the desired performance of the object. Thus, the present work provides a comprehensive review of the effects of build orientation on all the major properties of AM metal parts. Here we critically discuss the significant influence of build orientation on all major characteristics like manufacturability, geometrical accuracy, surface roughness and morphology, porosity, microstructure, static and fatigue strength, fracture toughness, wear and corrosion behaviour, and its interplay with various post-treatments.

Regarding the manufacturability of metal parts, the focus has been mostly on L-PBF and EB-PBF techniques that have essentially different requisites for support structures during manufacturing. This topic has been mainly explored for thin structures such as lattice struts to evaluate the feasibility of realizing specimens at low build orientation without the need for support. A possible output of these investigations can be the creation of “manufacturability maps” to describe the quality of the printed parts. This surely needs a

collective effort but can be of great impact on boosting the design and manufacturing freedom provided by AM.

Remaining on the topic of design freedom, a cherished attribute of AM technologies, is highly restricted by the effect of build orientation on geometrical fidelity. The part geometry has proved to be significantly affected by build orientation. Many studies highlight that a lower build angle corresponds to a decrease in size accuracy and variation with respect to the nominal shape. This is mainly attributed to the fact that the down-skin areas with a low build angle are supported by powder with lower thermal conductivity compared to the bulk material, which leads to lower heat dissipation and, consequently, a larger melt pool that eventually can compromise geometrical accuracy. This observation has been confirmed for various specimen types including bulk and lattice geometries. L-PBF specimens demonstrated a higher dimensional accuracy compared to the EB-PBF ones, which is coherent with the use of powders with lower particle size distribution for L-PBF. The apparent effect of orientation on geometrical accuracy can be a crucial matter to be mindful of, especially when discussing structural applications of AM materials.

From design for AM and post-processing point of view, the need for material removal and the associated limitations define the boundaries for achieving the desired surface quality without sacrificing part functionality. This paper indicates that researchers might explore alternative post-treatment methods or developing design strategies that minimize the need for extensive support, their removal and post-treatment altogether.

From this review, it also emerged that build orientation plays a major role in determining the surface roughness of the specimens. As a general trend in L-PBF, it is verified that roughness increases with the inclination angle and typically the down-skin surfaces show a higher roughness and more defects compared to the up-skin. It is worth noting that an opposite trend is reported in the case of EB-PBF specimens: the higher the inclination the lower the roughness. Many studies also showed the influence of feature sizes with a focus on strut size in lattice structures; the results indicated that the feature size tends to increase the up-skin roughness, while it does not affect the down-skin surface quality. Such dependency of roughness on build orientation implies considerable inhomogeneity of surface quality in parts of intricate geometries, where the individual part can be an integration of several surfaces with varying inclinations with respect to the build direction, letting alone the need for supports during manufacturing the removal of which will further deteriorate the surface quality.

Interestingly, regarding the effect of building orientation on porosity, the available results are largely contradicting, and the degree of porosity also appears to be significantly influenced by the material used, showing a notable material dependency in certain instances. Some studies report higher porosity in inclined specimens, while in others, vertical specimens show the highest porosity. Enigmatically, the complex thermal history is indicated as the cause of both the opposite trends. On inclined surfaces, particularly those featuring complex geometries such as notched geometries where the building orientation undergoes sudden changes, it may be challenging to ensure uniform heat distribution and some regions of the inclined surface may receive insufficient thermal energy. In most instances, AM parts with inclined surfaces commonly exhibit elevated porosity under the inclination due to several factors related to thermal history differences. These include issues like overheating and underheating, heat accumulation and residual stresses, melt pool instability, and inadequate energy density. Inconsistencies in the thermal history, driven by changes in geometry and building orientation, can lead to regions of the material being either overheated or underheated. Overheating may result in excessive evaporation of volatile elements, creating volumetric defects specifically in the up-ward faces, while underheating may also cause insufficient material melting and deposition. In the context of inclined surfaces, heat accumulation becomes a notable concern. The cumulative heat from the laser or electron beam can impact the lower layers, coupled with rapid cooling or uneven heating, resulting in heightened thermal stresses. These stresses may induce warping, cracking, or incomplete fusion between layers, ultimately contributing to increased porosity. The melt pool dynamics on inclined surfaces can be less stable as well. Inconsistent thermal histories affect the stability of the melt pool during layer deposition. Factors such as energy reflection, heat dissipation, and temperature fluctuations can lead to irregular melt pool shapes, impacting the uniformity of material deposition and promoting porosity. In addition, insufficient energy density in the inclined regions may also lead to incomplete melting and fusion of powder particles, giving rise to the formation of pores in the final AM part. Overall, addressing these thermal history-related challenges is crucial for minimizing porosity and enhancing the quality of AM components.

Although in many cases the overall porosity is very low, the link between build orientation, thermal history, and porosity is highly relevant, and its interplay with other process parameters should be further investigated.

Microstructure as a key property of a metal part that highly affects its mechanical properties, is extremely dependent on the manufacturing process. In PBF technologies, grains tend to be elongated along the build direction due to the development of thermal gradients. Moreover, grains tend to be coarser on the down-skin areas, which stay at a higher temperature for longer times, while finer grains are observed on the up-skin. This also brings notable anisotropy in the microstructural features that in turn will affect the performance of the part in various in-service conditions.

In the case of mechanical properties, the building orientation is reported to significantly impact the resulting static and fatigue strength. However, also in this case, the existing research yield conflicting results. While certain studies posit higher static strength in vertical building orientation compared to and horizontally built specimens, others suggest highest strength obtained at an inclination of 45°, or, alternatively, report no noticeable correlation between building orientation and static strength. Notably, the number of studies that have investigated the impact of building orientation on failure mechanism, plateau stress, and reaction forces is limited and restricted to specific materials and processing parameters.

On the other hand, a consensus exists regarding the effect of building orientation on fatigue performance mainly but not limited to its interplay with the presence of surface and internal defects, undesired tensile residual stresses, and microstructural inhomogeneity. Remarkably, the variety of surface features affect the fatigue performance in different ways. It is demonstrated that defects with a notch-like geometry are especially detrimental to fatigue performance mainly when loaded in a particular direction. These defects are essentially caused due to the inherent nature of the process, such as the staircase effect that can generate preferentially aligned lack of

fusion defects. It could be the reason why, for the majority of the cases reported in the literature, vertically built specimens exhibit the lowest fatigue strength. Additionally, it is proven that down-skin surfaces are more harmful than up-skin surfaces due to their lower geometrical accuracy and higher surface roughness, especially in L-PBF, where supporting structures are frequently needed. The surface irregularities on down-skin surfaces have been proved to act as local micro-notches and, in some cases, even mask the criticality of geometrical notches, in a way that fracture planes are displaced in correspondence of the local micro-notches rather than occurring at the geometrical notch root.

Fracture toughness is also demonstrated to be intrinsically anisotropic in PBF parts. Apart from microstructural inhomogeneity, this observation is why certain orientations favour the propagation of cracks along weak zones such as melt-pool boundaries. Consequently, specimens that are loaded orthogonally to the build plane have shown the lowest toughness usually exhibiting more brittle fracture behaviour.

A limited number of studies have explored the effects of build orientation on other properties such as wear and corrosion resistance. In most cases analysed, microstructure and hardness were reported to play major roles on these properties for AM metallic materials. Since build orientation influences both microstructure and hardness, this result is expected to be also extensible to wear and corrosion behaviour. For instance, finer-grain microstructures that result in higher hardness (due to the Hall-Petch effect) are presumed to contribute to enhanced wear resistance. In this sense, some studies have reported lower wear resistance in the case of vertically built specimens due to the presence of large columnar grains. Also, regarding corrosion, finer microstructures are supposed to be more effective to grow a passive layer. yet, there is not a general agreement about the direct relation between build orientation and the resulting wear and corrosion behavior, and no clear tendency was highlighted in the literature. Nevertheless, the results support the idea that, at large, these properties are lower in AM materials with respect to their conventional counterparts.

To remedy the noticeable inhomogeneity in terms of geometrical accuracy, surface roughness and morphology, residual stress distribution and microstructural features caused by build orientation in AM parts, the literature gives large relevance to post-treatments. In this regard many new or classic (but AM-customized) post-processing techniques have been suggested in the literature. Many treatments focus on addressing surface issues, but other issues like bulk porosity, tensile residual stresses, and microstructural anisotropy may be partially remediated by the application of proper bulk treatments (like heat treatment). Indeed, oftentimes, hybrid post-treatments that bring in the opportunity to interfere with both surface and the bulk material (e.g., heat treatment followed by severe plastic deformation-based surface treatment) have exhibited significant potential to obtain desirable performance for the AM part. Considering more complex geometries, surface access and reachability is still a significant limitation. The data reported confirms that new post-treatment tools or techniques are needed to offer access to the hard-to-reach areas within intricate parts.

Even though the need for post-processing treatments to advance the performance of AM parts is already well-established, there is still a large gap to be bridged before we can have a clear roadmap of post-treatment selection for desired performance. Besides the costs, the intrinsic characteristics of the post-treatments should be compatible with the size and geometrical details as well as material properties of the AM parts to ensure optimized results.

The literature study underscores the inherent complexity when evaluating the influential parameters that impact the manifestation of build orientation's effects. The scatter of the literature data and the high extent of contradicting trends point out the significant dependency of the results on material, technology and process parameters. It is evident that variations in these parameters can substantially influence the data. This necessitates the urgent requirement for systematic studies that can effectively scrutinize the role of these defining parameters. Employing extensive Design of Experiments (DOEs) in conjunction with validated numerical studies could serve as a promising approach to comprehensively assess the interplay between different process parameters. Considering the complex physical basis, investigating the intricate process-parameter-properties linkage requires adopting a multi-fidelity approach and leveraging data-driven methods.

Although the present study focuses on the orientation during the building phase, the choice of post-treatment was also briefly addressed, as it can significantly influence the quality of the final product. Adopting the most favorable orientation, such as minimizing supports or using horizontal struts for higher geometrical precision, combined with the appropriate post-treatments, can help reduce the performance gap between traditional and AM processes. This approach has the potential to enhance the competitiveness of additive parts in the market by achieving "complexity freedom" and, when designed and implemented correctly, offering improved mechanical properties.

Despite the extensive data available in the literature, the variety of specimen types, dimensions, materials, and technologies makes it challenging to draw solid, generalizable conclusions on the actual effect of build orientation. This variability underscores the need for design guidelines specifically for AM, with particular attention to the impact of build orientation, enabling more informed decisions in the design, optimization, and fabrication phases. Incorporating the building direction into a fatigue optimization algorithm could further refine these processes. Moreover, the results highlight the defining role of defects and the interaction between surface and sub-surface defects. Future research challenges include understanding the synergistic effect of sub-surface defects and surface irregularities on the fatigue strength of AM components, particularly for those with as-built surfaces and thin cross-sections. Addressing these challenges will facilitate the successful exploitation of AM technologies across various sectors, including structural applications that demand high geometrical and performance fidelity.

The available data clearly demonstrate that the physical limitations in PBF technologies with build orientation act as the boundaries that define the frontier of what's achievable in terms of surface quality, microstructure, as-built performance. For instance, the stair-stepping effect and melt pool dynamics set a fundamental limit on how smooth a surface can be in PBF. Researchers can improve the process (finer layers, better process control and monitoring) but cannot eliminate the inherent issues. The frontier lies in better understanding the physical basis to be able to modulate it towards desired characteristics, pushing these limitations to achieve

parts with minimal need to post-treatments. On the other hand, anisotropy due to build orientation presents a trade-off. In the reported data, it is shown that researchers can optimize build orientation for desired properties in specific directions (e.g., strength), but achieving perfectly isotropic material might not be physically possible. The frontier lies in developing techniques that beside minimizing anisotropy manage to engineer it and eventually leverage it for specific functionalities based on target working condition.

The current body of knowledge available on the effect of build orientation and inclined features on various properties of metal AM material, highlights the necessity of feeding this information and trends into the AM chain to enhance the quality of the builds considering the geometrical, local and global inclinations. All phases including the DfAM, manufacturing and post-processing steps can highly benefit from these data (especially where clearly established trends are identified) to tackle the challenges associated with inhomogeneity, surface and bulk defects, etc.; even partially addressing these issues in the design and manufacturing phases, can reduce the need for post-processing and thus limited effort will be required to develop and/or customize adapt post-processing techniques to bridge the remaining performance gaps.

Based on the current information, the AM community may explore various research questions to fully address and control the effect of build orientation in AM, including (i) the primary causations and fundamental physical laws governing the significant sensitivity of AM component properties (such as roughness, porosity, hardness, and microstructure) to build orientation, (ii) the potential to leverage thermal history and cooling rate locally to gain greater control over build characteristics and correlate AM process parameters with orientation-affected material characteristics to facilitate the design process, (iii) the feasibility of adopting machine learning algorithms and detecting appropriate data extraction methods to predict and optimize build strategies, such as variable layer thickness and local scan patterns, to achieve specific microstructural and mechanical properties based on build orientation, and (iv) the potential venues to utilize the real-time process control instruments during PBF to obtain correlations between the impact of design and manufacturing parameters and features associated with build orientation. This list, which can be expanded, sheds light on urgent inquiries that significantly impact the current comprehension of how orientation defines the performance of AM parts. By answering these questions and bringing this information early enough into the AM field, we can develop a more informed manufacturing, exploiting these results towards more efficient components with enhanced performance and longer lifetimes. This information can be used also as an efficient tool for customization of the products leveraging the role of inclination in locally modulating the (microstructural, physical and mechanical) properties to better address case-by-case target applications.

CRediT authorship contribution statement

Ivan Aiza: Writing – review & editing, Writing – original draft, Visualization, Formal analysis, Data curation. **Chiara Baldi:** Writing – review & editing, Writing – original draft, Visualization, Formal analysis, Data curation. **Federico Mat ías de la Vega:** Writing – review & editing, Writing – original draft, Visualization, Formal analysis, Data curation. **Sara Sebastiani:** Writing – review & editing, Writing – original draft, Visualization, Formal analysis, Data curation. **Niccol ò Enrico Veronese:** Writing – review & editing, Writing – original draft, Visualization, Formal analysis, Data curation. **Mohammad Yousefi:** Writing – review & editing, Writing – original draft, Visualization, Formal analysis, Data curation. **Mohammad Hossein Mosallanejad:** Writing – review & editing. **Erfan Maleki:** Writing – review & editing, Visualization, Formal analysis, Data curation. **Mario Guagliano:** Supervision. **Luca Iuliano:** Supervision. **Abdollah Saboori:** Writing – review & editing, Formal analysis, Conceptualization, Supervision. **Sara Bagherifard:** Writing – review & editing, Formal analysis, Conceptualization, Supervision.

Declaration of competing interest

The authors declare that they have no known competing financial interests or personal relationships that could have appeared to influence the work reported in this paper.

Data availability

No data was used for the research described in the article.

Acknowledgement

This work has been developed within the Surfing project (Surface Post-treatments to Boost the Functionality of Additively Manufactured Parts) defined in the framework of Alta Scuola Politecnica (ASP) Program (18th cycle), supported by Politecnico di Milano and Politecnico di Torino, Italy.

References

[1] Greene JP. Additive Manufacturing in Automotive. In: Greene JP, editor.)Automotive Plastics and Composites, Elsevier, 2021: pp. 325–335. doi: 10.1016/B978-0-12-818008-2.00003-9.

[2] Blakey-Milner B, Gradl P, Snedden G, Brooks M, Pitot J, Lopez E, et al. Metal additive manufacturing in aerospace: a review. Mater Des 2021;209. https://doi.org/10.1016/j.matdes.2021.110008.

[3] Tamayo JA, Riascos M, Vargas CA, Baena LM. Additive manufacturing of Ti6Al4V alloy via electron beam melting for the development of implants for the biomedical industry. Heliyon 2021;7:e06892.

[4] Maleki E, Bagherifard S, Guagliano M. Application of artificial intelligence to optimize the process parameters effects on tensile properties of Ti-6Al-4V fabricated by laser powder-bed fusion. Int J Mech Mater Des 2022;18:199–222. https://doi.org/10.1007/s10999-021-09570-w.

[5] Armstrong M, Mehrabi H, Naveed N. An overview of modern metal additive manufacturing technology. J Manuf Process 2022;84:1001–29. https://doi.org/10.1016/j.jmapro.2022.10.060.

[6] Maleki E, Unal O, Bandini M, Guagliano M, Bagherifard S. Individual and synergistic effects of thermal and mechanical surface post-treatments on wear and corrosion behavior of laser powder bed fusion AlSi10Mg. J Mater Process Technol 2022;302:117479. https://doi.org/10.1016/j.jmatprotec.2021.117479.

[7] Dadkhah M, Mosallanejad MH, Iuliano L, Saboori A. A comprehensive overview on the latest progress in the additive manufacturing of metal matrix composites: potential, challenges, and feasible solutions. Acta Metall Sin (English Lett) 2021;34:1173–200. https://doi.org/10.1007/s40195-021-01249-7.

[8] Madhavadas V, Srivastava D, Chadha U, Aravind Raj S, Sultan MTH, Shahar FS, et al. A review on metal additive manufacturing for intricately shaped aerospace components. CIRP J Manuf Sci Technol 2022;39:18–36. https://doi.org/10.1016/j.cirpj.2022.07.005.

[9] Hutasoit N, Javed MA, Rashid RAR, Wade S, Palanisamy S. Effects of build orientation and heat treatment on microstructure, mechanical and corrosion properties of Al6061 aluminium parts built by cold spray additive manufacturing process. Int J Mech Sci 2021;204:106526. https://doi.org/10.1016/j.ijmecsci.2021.106526.

[10] Mosallanejad MH, Niroumand B, Aversa A, Saboori A. In-situ alloying in laser-based additive manufacturing processes: a critical review. J Alloys Compd 2021;872:159567. https://doi.org/10.1016/j.jallcom.2021.159567.

[11] ISO; ASTM, ISO/ASTM 52900:2015 Additive manufacturing — General principles — Terminology, (2015). https://www.iso.org/standard/69669.html.

[12] ISO; ASTM, ISO/ASTM 52911-1:2019(en) Additive manufacturing — Design — Part 1: Laser-based powder bed fusion of metals, (2019). https://www.iso.org/obp/ui/#iso:std:iso-astm:52911:-1:ed-1:v1:en.

[13] Khorasani A, Gibson I, Awan US, Ghaderi A. The effect of SLM process parameters on density, hardness, tensile strength and surface quality of Ti-6Al-4V. Addit Manuf 2019;25:176–86. https://doi.org/10.1016/j.addma.2018.09.002.

[14] Lhuissier P, de Formanoir C, Martin G, Dendievel R, Godet S. Geometrical control of lattice structures produced by EBM through chemical etching: Investigations at the scale of individual struts. Mater Des 2016;110:485–93. https://doi.org/10.1016/j.matdes.2016.08.029.

[15] Li Y, Liang X, Yu Y, Li H, Kan W, Lin F. Microstructures and mechanical properties evolution of IN939 alloy during electron beam selective melting process. J Alloys Compd 2021;883:160934. https://doi.org/10.1016/j.jallcom.2021.160934.

[16] Tian Q, Guo S, Melder E, Bian L, "Grace" Guo L. deep learning-based data fusion method for in situ porosity detection in laser-based additive manufacturing. J Manuf Sci Eng 143 2021. https://doi.org/10.1115/1.4048957.

[17] Saboori A, Aversa A, Marchese G, Biamino S, Lombardi M, Fino P. Application of directed energy deposition-based additive manufacturing in repair. Appl Sci 2019;9:3316. https://doi.org/10.3390/app9163316.

[18] Gora WS, Tian Y, Cabo AP, Ardron M, Maier RRJ, Prangnell P, et al. Enhancing surface finish of additively manufactured titanium and cobalt chrome elements using laser based finishing. Phys Proc 2016;83:258–63. https://doi.org/10.1016/j.phpro.2016.08.021.

[19] Maleki E, Bagherifard S, Unal O, Bandini M, Guagliano M. The effects of microstructural and chemical surface gradients on fatigue performance of laser powder bed fusion AlSi10Mg. Mater Sci Eng A 2022;840:142962. https://doi.org/10.1016/j.msea.2022.142962.

[20] Maleki E, Bagherifard S, Guagliano M. Correlation of residual stress, hardness and surface roughness with crack initiation and fatigue strength of surface treated additive manufactured AlSi10Mg: experimental and machine learning approaches. J Mater Res Technol 2023;24:3265–83. https://doi.org/10.1016/j.jmrt.2023.03.193.

[21] Behjat A, Shamanian M, Taherizadeh A, Lannunziata E, Bagherifard S, Gadalińska E, et al. Microstructure-electrochemical behavior relationship in post processed AISI316L stainless steel parts fabricated by laser powder bed fusion. J Mater Res Technol 2023;23:3294–311. https://doi.org/10.1016/j.jmrt.2023.01.229.

[22] Ansarian I, Taghiabadi R, Amini S, Saboori A. Enhancing the corrosion behavior of laser powder bed fusion processed CP-Ti via ultrasonic peening. Mater Lett 2024;354:135410. https://doi.org/10.1016/j.matlet.2023.135410.

[23] Calignano F. Design optimization of supports for overhanging structures in aluminum and titanium alloys by selective laser melting. Mater Des 2014;64:203–13. https://doi.org/10.1016/j.matdes.2014.07.043.

[24] Maleki E, Bagherifard S, Ahmad N, Shao S, Unal O, Guagliano M, et al. Fatigue performance of U-notched additively manufactured AlSi10Mg parts: the effects of chemical and thermal post-treatments. Add Manuf Lett 2023;7:100175. https://doi.org/10.1016/j.addlet.2023.100175.

[25] Maleki E, Bagherifard S, Razavi N, Riccio M, Bandini M, du Plessis A, et al. Fatigue behaviour of notched laser powder bed fusion AlSi10Mg after thermal and mechanical surface post-processing. Mater Sci Eng A 2022;829:142145. https://doi.org/10.1016/j.msea.2021.142145.

[26] Maleki E, Bagherifard S, Sabouri F, Bandini M, Guagliano M. Hybrid thermal, mechanical and chemical surface post-treatments for improved fatigue behavior of laser powder bed fusion AlSi10Mg notched samples. Surf Coat Technol 2022;430:127962. https://doi.org/10.1016/j.surfcoat.2021.127962.

[27] Maleki E, Bagherifard S, Unal O, Bandini M, Guagliano M. On the effects of laser shock peening on fatigue behavior of V-notched AlSi10Mg manufactured by laser powder bed fusion. Int J Fatigue 2022;163:107035. https://doi.org/10.1016/j.ijfatigue.2022.107035.

[28] Das P, Chandran R, Samant R, Anand S. Optimum part build orientation in additive manufacturing for minimizing part errors and support structures. Procedia Manuf 2015;1:343–54. https://doi.org/10.1016/j.promfg.2015.09.041.

[29] Delfs P, Tows M, Schmid H-J. Optimized build orientation of additive manufactured parts for improved surface quality and build time. Addit Manuf 2016;12:314–20. https://doi.org/10.1016/j.addma.2016.06.003.

[30] Zhang S, Lane B, Whiting J, Chou K. An investigation into metallic powder thermal conductivity in laser powder bed fusion additive manufacturing. In: 2018 International Solid Freeform Fabrication Symposium; 2018. https://doi.org/10.26153/tsw/17169.

[31] Leirmo TS, Martinsen K. Deterministic part orientation in additive manufacturing using feature recognition. Proc CIRP 2020;88:405–10. https://doi.org/10.1016/j.procir.2020.05.070.

[32] Baghi AD, Nafisi S, Hashemi R, Ebendorff-Heidepriem H, Ghomashchi R. Experimental realisation of build orientation effects on the mechanical properties of truly as-built Ti-6Al-4V SLM parts. J Manuf Process 2021;64:140–52. https://doi.org/10.1016/j.jmapro.2021.01.027.

[33] Dong Z, Liu Y, Li W, Liang J. Orientation dependency for microstructure, geometric accuracy and mechanical properties of selective laser melting AlSi10Mg lattices. J Alloys Compd 2019;791:490–500. https://doi.org/10.1016/j.jallcom.2019.03.344.

[34] Barba D, Alabort C, Tang YT, Viscasillas MJ, Reed RC, Alabort E. On the size and orientation effect in additive manufactured Ti-6Al-4V. Mater Des 2020;186:108235. https://doi.org/10.1016/j.matdes.2019.108235.

[35] Zhang B, Han X, Chen C, Zhang W, Liao H, Chen B. Effect of the strut size and tilt angle on the geometric characteristics of selective laser melting AlSi10Mg. Rapid Prototyp J 2021;27:879–89. https://doi.org/10.1108/RPJ-08-2020-0187.

[36] Beard W, Lancaster R, Barnard N, Jones T, Adams J. The influence of surface finish and build orientation on the low cycle fatigue behaviour of laser powder bed fused stainless steel 316L. Mater Sci Eng A 2023;864:144593. https://doi.org/10.1016/j.msea.2023.144593.

[37] de Luca DM, Hamilton AR, Reed PAS. Influence of build orientation on high temperature fatigue crack growth mechanisms in Inconel 718 fabricated by laser powder bed fusion: Effects of temperature and hold time. Int J Fatigue 2023;170:107484. https://doi.org/10.1016/j.ijfatigue.2022.107484.

[38] Meyer G, Musekamp J, Göbel F, Gardian F, Mittelstedt C. Manufacturability investigation of inclined AlSi10Mg lattice struts by means of selective laser melting. Manuf Lett 2022;31:101–5. https://doi.org/10.1016/j.mfglet.2021.08.002.

[39] Sombatmai A, Uthaisangsuk V, Wongwises S, Promoppatum P. Multiscale investigation of the influence of geometrical imperfections, porosity, and size-dependent features on mechanical behavior of additively manufactured Ti-6Al-4V lattice struts. Mater Des 2021;209:109985. https://doi.org/10.1016/j.matdes.2021.109985.

[40] Wu Y, Yang L. Modeling and analysis of material anisotropy-topology effects of 3D cellular structures fabricated by powder bed fusion additive manufacturing. Int J Mech Sci 2021;197:106325. https://doi.org/10.1016/j.ijmecsci.2021.106325.

[41] Murchio S, Dallago M, Zanini F, Carmignato S, Zappini G, Berto F, et al. Additively manufactured Ti–6Al–4V thin struts via laser powder bed fusion: Effect of building orientation on geometrical accuracy and mechanical properties. J Mech Behav Biomed Mater 2021;119:104495. https://doi.org/10.1016/j.jmbbm.2021.104495.

[42] Obeidi MA. Metal additive manufacturing by laser-powder bed fusion: Guidelines for process optimisation. Results Eng 2022;15:100473. https://doi.org/10.1016/j.rineng.2022.100473.

[43] Maleki E, Bagherifard S, Unal O, Revuru M, Bandini M, Guagliano M. The efficiency of tumble finishing as a final post-treatment for fatigue enhancement of notched laser powder bed fusion AlSi10Mg. Sci Rep 2023;13:4602. https://doi.org/10.1038/s41598-023-30660-6.

[44] Hegab H, Khanna N, Monib N, Salem A. Design for sustainable additive manufacturing: a review. Sustain Mater Technol 2023;35. https://doi.org/10.1016/j.susmat.2023.e00576.

[45] Shipley H, McDonnell D, Culleton M, Coull R, Lupoi R, O'Donnell G, et al. Optimisation of process parameters to address fundamental challenges during selective laser melting of Ti-6Al-4V: A review. Int J Mach Tools Manuf 2018;128:1–20. https://doi.org/10.1016/j.ijmachtools.2018.01.003.

[46] Leutenecker-Twelsiek B, Klahn C, Meboldt M. Considering part orientation in design for additive manufacturing. Proc CIRP 2016;50:408–13. https://doi.org/10.1016/j.procir.2016.05.016.

[47] Viale V, Stavridis J, Salmi A, Bondioli F, Saboori A. Optimisation of downskin parameters to produce metallic parts via laser powder bed fusion process: an overview. Int J Adv Manuf Technol 2022;123:2159–82. https://doi.org/10.1007/s00170-022-10314-z.

[48] Leary M, Maconachie T, Sarker A, Faruque O, Brandt M. Mechanical and thermal characterisation of AlSi10Mg SLM block support structures. Mater Des 2019;183:108138. https://doi.org/10.1016/j.matdes.2019.108138.

[49] Cao Q, Bai Y, Zhang J, Shi Z, Fuh JYH, Wang H. Removability of 316L stainless steel cone and block support structures fabricated by Selective Laser Melting (SLM). Mater Des 2020;191:108691. https://doi.org/10.1016/j.matdes.2020.108691.

[50] Järvinen J-P, Matilainen V, Li X, Piili H, Salminen A, Mäkelä I, et al. Characterization of effect of support structures in laser additive manufacturing of stainless steel. Phys Proc 2014;56:72–81. https://doi.org/10.1016/j.phpro.2014.08.099.

[51] Subedi SC, Shahba A, Thevamaran M, Thoma DJ, Suresh K. Towards the optimal design of support structures for laser powder bed fusion-based metal additive manufacturing via thermal equivalent static loads. Addit Manuf 2022;57:102956. https://doi.org/10.1016/j.addma.2022.102956.

[52] Herzog D, Seyda V, Wycisk E, Emmelmann C. Additive manufacturing of metals. Acta Mater 2016;117:371–92. https://doi.org/10.1016/j.actamat.2016.07.019.

[53] Attar H, Calin M, Zhang LC, Scudino S, Eckert J. Manufacture by selective laser melting and mechanical behavior of commercially pure titanium. Mater Sci Eng A 2014;593:170–7. https://doi.org/10.1016/j.msea.2013.11.038.

[54] Mosallanejad MH, Niroumand B, Aversa A, Manfredi D, Saboori A. Laser powder bed fusion in-situ alloying of Ti-5%Cu alloy: Process-structure relationships. J Alloys Compd 2021;857:157558. https://doi.org/10.1016/j.jallcom.2020.157558.

[55] Soltani-Tehrani A, Isaac JP, Tippur HV, Silva DF, Shao S, Shamsaei N. Ti-6Al-4V powder reuse in laser powder bed fusion (L-PBF): the effect on porosity, microstructure, and mechanical behavior. Int J Fatigue 2023;167:107343. https://doi.org/10.1016/j.ijfatigue.2022.107343.

[56] Gan M, Wong CH. Practical support structures for selective laser melting. J Mater Process Technol 2016;238. https://doi.org/10.1016/j.jmatprotec.2016.08.006.

[57] Gong X, Chou K. Characterization of Sintered Ti-6Al-4V Powders in Electron Beam Additive Manufacturing. In: ASME 2013 International Manufacturing Science and Engineering Conference, ASME International, Madison, Wisconsin, USA, 2013. doi: 10.1115/MSEC2013-1131.

[58] Galati M, Defanti S, Saboori A, Rizza G, Tognoli E, Vincenzi N, et al. An investigation on the processing conditions of Ti-6Al-2Sn-4Zr-2Mo by electron beam powder bed fusion: Microstructure, defect distribution, mechanical properties and dimensional accuracy. Addit Manuf 2022;50:102564. https://doi.org/10.1016/j.addma.2021.102564.

[59] Saboori A, Abdi A, Fatemi SA, Marchese G, Biamino S, Mirzadeh H. Hot deformation behavior and flow stress modeling of Ti–6Al–4V alloy produced via electron beam melting additive manufacturing technology in single β-phase field. Mater Sci Eng A 2020;792:139822. https://doi.org/10.1016/j.msea.2020.139822.

[60] Cheng B, Chou Y. Overhang Support Structure Design for Electron Beam Additive Manufacturing. In: ASME 2017 12th International Manufacturing Science and Engineering Conference, ASME International, Los Angeles, California, USA, 2017. doi: 10.1115/MSEC2017-3018.

[61] Gong X. Anderson, Ted, Chou, Kevin, Review on powder-based electron beam additive manufacturing technology. Manuf Rev (Les Ulis) 2014;1:2. https://doi.org/10.1051/mfreview/2014001.

[62] Galati M, Rizza G, Defanti S, Denti L. Surface roughness prediction model for Electron Beam Melting (EBM) processing Ti6Al4V. Precis Eng 2021;69:19–28. https://doi.org/10.1016/j.precisioneng.2021.01.002.

[63] Ghorbani HR, Mosallanejad MH, Atapour M, Galati M, Saboori A. Hybrid additive manufacturing of an electron beam powder bed fused Ti6Al4V by transient liquid phase bonding. J Mater Res Technol 2022;20:180–94. https://doi.org/10.1016/j.jmrt.2022.07.009.

[64] Cansizoglu O, Harrysson O, Cormier D, West H, Mahale T. Properties of Ti–6Al–4V non-stochastic lattice structures fabricated via electron beam melting. Mater Sci Eng A 2008;492:468–74. https://doi.org/10.1016/j.msea.2008.04.002.

[65] Zhang XZ, Tang HP, Leary M, Song T, Jia L, Qian M. Toward Manufacturing Quality Ti-6Al-4V Lattice Struts by Selective Electron Beam Melting (SEBM) for Lattice Design. JOM 2018;70:1870–6. https://doi.org/10.1007/s11837-018-3030-x.

[66] Zhang XZ, Tang HP, Wang J, Jia L, Fan YX, Leary M, et al. Additive manufacturing of intricate lattice materials: Ensuring robust strut additive continuity to realize the design potential. Addit Manuf 2022;58:103022. https://doi.org/10.1016/j.addma.2022.103022.

[67] Cloots M, Spierings AB, Wegener K. Assessing new support minimizing strategies for the additive manufacturing technology SLM. In: 24th International SFF Symposium - An Additive Manufacturing Conference, SFF 2013, 2013: pp. 631 – 643. doi: https://doi.org/10.26153/tsw/15588.

[68] Cloots M, Zumofen L, Spierings AB, Kirchheim A, Wegener K. Approaches to minimize overhang angles of SLM parts. Rapid Prototyp J 2017;23:362–9. https://doi.org/10.1108/RPJ-05-2015-0061.

[69] Leary M, Mazur M, Elambasseril J, McMillan M, Chirent T, Sun Y, et al. Selective laser melting (SLM) of AlSi12Mg lattice structures. Mater Des 2016;98:344–57. https://doi.org/10.1016/j.matdes.2016.02.127.

[70] Brøtan V. A new method for determining and improving the accuracy of a powder bed additive manufacturing machine. Int J Adv Manuf Technol 2014;74:1187–95. https://doi.org/10.1007/s00170-014-6012-3.

[71] Shah P, Racasan R, Bills P. Comparison of different additive manufacturing methods using computed tomography. Case Stud NondestrTest Eval 2016;6:69–78. https://doi.org/10.1016/j.csndt.2016.05.008.

[72] Königshofer M, Stoiber M, Unger E, Grasl C, Moscato F. Mechanical and dimensional investigation of additive manufactured multimaterial parts. Front Phys 2021;9. https://doi.org/10.3389/fphy.2021.635736.

[73] Murchio S, Dallago M, Rigatti A, Luchin V, Berto Filippo, Maniglio D, Benedetti M. On the effect of the node and building orientation on the fatigue behavior of L-PBF Ti6Al4V lattice structure sub-unital elements. Mater Des Process Commun 2021;3. https://doi.org/10.1002/mdp2.258.

[74] Liu L, Kamm P, García-Moreno F, Banhart J, Pasini D. Elastic and failure response of imperfect three-dimensional metallic lattices: the role of geometric defects induced by Selective Laser Melting. J Mech Phys Solids 2017;107:160–84. https://doi.org/10.1016/j.jmps.2017.07.003.

[75] Bagheri ZS, Melancon D, Liu L, Johnston RB, Pasini D. Compensation strategy to reduce geometry and mechanics mismatches in porous biomaterials built with Selective Laser Melting. J Mech Behav Biomed Mater 2017;70:17–27. https://doi.org/10.1016/j.jmbbm.2016.04.041.

[76] Lu Y, Cui Z, Cheng L, Li J, Yang Z, Zhu H, et al. Quantifying the discrepancies in the geometric and mechanical properties of the theoretically designed and additively manufactured scaffolds. J Mech Behav Biomed Mater 2020;112. https://doi.org/10.1016/j.jmbbm.2020.104080.

[77] Fu J, Ding J, Qu S, Zhang L, Wang MY, Fu MW, et al. Improved light-weighting potential of SS316L triply periodic minimal surface shell lattices by micro laser powder bed fusion. Mater Des 2022;222. https://doi.org/10.1016/j.matdes.2022.111018.

[78] Suard M, Martin G, Lhuissier P, Dendievel R, Vignat F, Blandin J-J, et al. Mechanical equivalent diameter of single struts for the stiffness prediction of lattice structures produced by Electron Beam Melting. Addit Manuf 2015;8:124–31. https://doi.org/10.1016/j.addma.2015.10.002.

[79] Suard M, Barrière L, Lhuissier P, Perusin S, Filloux B, Dendievel R. Influence of manufacturing orientations on the morphology of alloy 718 single struts manufactured by selective laser melting. Mater Des Process Commun 2021;3. https://doi.org/10.1002/mdp2.140.

[80] Weißmann V, Drescher P, Bader R, Seitz H, Hansmann H, Laufer N. Comparison of single Ti6Al4V struts made using selective laser melting and electron beam melting subject to part orientation. Metals (Basel) 2017;7. https://doi.org/10.3390/met7030091.

[81] Pérez-Sánchez A, Yánez A, Cuadrado A, Martel O, Nuño N. Fatigue behaviour and equivalent diameter of single Ti-6Al-4V struts fabricated by Electron Bean Melting orientated to porous lattice structures. Mater Des 2018;155:106–15. https://doi.org/10.1016/j.matdes.2018.05.066.

[82] Dallago M, Raghavendra S, Luchin V, Zappini G, Pasini D, Benedetti M. The role of node fillet, unit-cell size and strut orientation on the fatigue strength of Ti-6Al-4V lattice materials additively manufactured via laser powder bed fusion. Int J Fatigue 2021;142:105946. https://doi.org/10.1016/j.ijfatigue.2020.105946.

[83] Dallago M, Raghavendra S, Luchin V, Zappini G, Pasini D, Benedetti M. Geometric assessment of lattice materials built via Selective Laser Melting. Mater Today Proc 2019;7:353–61. https://doi.org/10.1016/j.matpr.2018.11.096.

[84] Hossain U, Ghouse S, Nai K, Jeffers JRT. Mechanical and morphological properties of additively manufactured SS316L and Ti6Al4V micro-struts as a function of build angle. Addit Manuf 2021;46. https://doi.org/10.1016/j.addma.2021.102050.

[85] Yan C, Hao L, Yang L, Hussein AY, Young PG, Li Z, et al. Metal alloys uniform TPMS structures. In: Triply Periodic Minimal Surface Lattices Additively Manufactured by Selective Laser Melting. Elsevier; 2021. p. 39–130. https://doi.org/10.1016/b978-0-12-824438-8.00003-0.

[86] Dallago M, Winiarski B, Zanini F, Carmignato S, Benedetti M. On the effect of geometrical imperfections and defects on the fatigue strength of cellular lattice structures additively manufactured via Selective Laser Melting. Int J Fatigue 2019;124:348–60. https://doi.org/10.1016/j.ijfatigue.2019.03.019.

[87] Meneghetti G, Rigon D, Cozzi D, Waldhauser W, Dabalà M. Influence of build orientation on static and axial fatigue properties of maraging steel specimens produced by additive manufacturing. Procedia Struct Integrity 2017;7:149–57. https://doi.org/10.1016/j.prostr.2017.11.072.

[88] Schneller W, Leitner M, Pomberger S, Grün F, Leuders S, Pfeifer T, et al. Fatigue strength assessment of additively manufactured metallic structures considering bulk and surface layer characteristics. Addit Manuf 2021;40. https://doi.org/10.1016/j.addma.2021.101930.

[89] Lou S, Jiang X, Sun W, Zeng W, Pagani L, Scott PJ. Characterisation methods for powder bed fusion processed surface topography. Precis Eng 2019;57:1–15. https://doi.org/10.1016/j.precisioneng.2018.09.007.

[90] Lou S, Pagani L, Zeng W, Jiang X, Scott PJ. Watershed segmentation of topographical features on freeform surfaces and its application to additively manufactured surfaces. Precis Eng 2020;63:177–86. https://doi.org/10.1016/j.precisioneng.2020.02.005.

[91] Detwiler S, Raeymaekers B. Deriving data-driven models that relate deterministic surface topography parameters of as-built inconel 718 surfaces to laser powder bed fusion process parameters. J Tribol 2022;144. https://doi.org/10.1115/1.4055606.

[92] Detwiler S, Watring D, Spear A, Raeymaekers B. Relating the surface topography of as-built Inconel 718 surfaces to laser powder bed fusion process parameters using multivariate regression analysis. Precis Eng 2022;74:303–15. https://doi.org/10.1016/j.precisioneng.2021.12.003.

[93] Gockel J, Sheridan L, Koerper B, Whip B. The influence of additive manufacturing processing parameters on surface roughness and fatigue life. Int J Fatigue 2019;124:380–8. https://doi.org/10.1016/j.ijfatigue.2019.03.025.

[94] Watring DS, Carter KC, Crouse D, Raeymaekers B, Spear AD. Mechanisms driving high-cycle fatigue life of as-built Inconel 718 processed by laser powder bed fusion. Mater Sci Eng A 2019;761:137993. https://doi.org/10.1016/j.msea.2019.06.003.

[95] Maleki E, Bagherifard S, Razavi N, Bandini M, du Plessis A, Berto F, et al. On the efficiency of machine learning for fatigue assessment of post-processed additively manufactured AlSi10Mg. Int J Fatigue 2022;160:106841. https://doi.org/10.1016/j.ijfatigue.2022.106841.

[96] Maleki E, Bagherifard S, Unal O, Sabouri F, Bandini M, Guagliano M. Effects of different mechanical and chemical surface post-treatments on mechanical and surface properties of as-built laser powder bed fusion AlSi10Mg. Surf Coat Technol 2022;439:128391. https://doi.org/10.1016/j.surfcoat.2022.128391.

[97] Nguyen HD, Pramanik A, Basak AK, Dong Y, Prakash C, Debnath S, et al. A critical review on additive manufacturing of Ti-6Al-4V alloy: microstructure and mechanical properties. J Mater Res Technol 2022;18:4641–61. https://doi.org/10.1016/j.jmrt.2022.04.055.

[98] Hovig EW. Anisotropy in metals processed by laser powder bed fusion elastic and plastic anisotropy in static and dynamic mechanical loading. NTNU 2021. https://hdl.handle.net/11250/2833897.

[99] Alghamdi A, Downing D, McMillan M, Brandt M, Qian M, Leary M. Experimental and numerical assessment of surface roughness for Ti6Al4V lattice elements in selective laser melting. Int J Adv Manuf Technol 2019;105:1275–93. https://doi.org/10.1007/s00170-019-04092-4.

[100] Fritsch T, Farahbod-Sternahl L, Serrano-Muñoz I, Léonard F, Haberland C, Bruno G. 3D computed tomography quantifies the dependence of bulk porosity, surface roughness, and re-entrant features on build angle in additively manufactured IN625 Lattice Struts. Adv Eng Mater 2022;24:2100689. https://doi.org/10.1002/adem.202100689.

[101] Maculotti G, Piscopo G, Marchiandi G, Atzeni E, Salmi A, Iuliano L. Build orientation effect on Ti6Al4V thin-wall topography by electron beam powder bed fusion, in. Procedia CIRP, Elsevier BV 2022:222–7. https://doi.org/10.1016/j.procir.2022.03.039.

[102] Delroisse P, Jacques PJ, Maire E, Rigo O, Simar A. Effect of strut orientation on the microstructure heterogeneities in AlSi10Mg lattices processed by selective laser melting. Scr Mater 2017;141:32–5. https://doi.org/10.1016/j.scriptamat.2017.07.020.

[103] Bültmann J, Merkt S, Hammer C, Hinke C, Prahl U. Scalability of the mechanical properties of selective laser melting produced micro-struts. J Laser Appl 2015;27:S29206. https://doi.org/10.2351/1.4906392.

[104] Wauthle R, Vrancken B, Beynaerts B, Jorissen K, Schrooten J, Kruth JP, et al. Effects of build orientation and heat treatment on the microstructure and mechanical properties of selective laser melted Ti6Al4V lattice structures. Addit Manuf 2015;5:77–84. https://doi.org/10.1016/j.addma.2014.12.008.

[105] Ball S, Ghayoor M, Pasebani S, Tabei A. Statistical analysis of porosity and process parameter relationships in metal additive manufacturing. Procedia Manuf 2021;53:343–7. https://doi.org/10.1016/j.promfg.2021.06.037.

[106] Aboulkhair NT, Everitt NM, Ashcroft I, Tuck C. Reducing porosity in AlSi10Mg parts processed by selective laser melting. Addit Manuf 2014;1–4:77–86. https://doi.org/10.1016/j.addma.2014.08.001.

[107] du Plessis A. Effects of process parameters on porosity in laser powder bed fusion revealed by X-ray tomography. Addit Manuf 2019;30:100871. https://doi.org/10.1016/j.addma.2019.100871.

[108] Persenot T, Burr A, Martin G, Buffiere J-Y, Dendievel R, Maire E. Effect of build orientation on the fatigue properties of as-built Electron Beam Melted Ti-6Al-4V alloy. Int J Fatigue 2019;118:65–76. https://doi.org/10.1016/j.ijfatigue.2018.08.006.

[109] Awd M, Stern F, Kampmann A, Kotzem D, Tenkamp J, Walther F. Microstructural characterization of the anisotropy and cyclic deformation behavior of selective laser melted AlSi10Mg structures. Metals (Basel) 2018;8. https://doi.org/10.3390/met8100825.

[110] Du J, Ren Y, Zhang M, Liang L, Chen C, Zhou K, et al. Improving the microstructure and mechanical properties of laser powder bed fusion-fabricated tantalum by high laser energy density. Mater Lett 2023;333:133547. https://doi.org/10.1016/j.matlet.2022.133547.

[111] Tan C, Li S, Essa K, Jamshidi P, Zhou K, Ma W, et al. Laser Powder Bed Fusion of Ti-rich TiNi lattice structures: Process optimization, geometrical integrity, and phase transformations. Int J Mach Tools Manuf 2019;141:19–29. https://doi.org/10.1016/j.ijmachtools.2019.04.002.

[112] Ehsan Saghaian S, Nematollahi M, Toker G, Hinojos A, Shayesteh Moghaddam N, Saedi S, et al. Effect of hatch spacing and laser power on microstructure, texture, and thermomechanical properties of laser powder bed fusion (L-PBF) additively manufactured NiTi, Opt Laser Technol 149 (2022) 107680. doi: 10.1016/j.optlastec.2021.107680.

[113] Vishwakarma J, Chattopadhyay K, Santhi Srinivas NC. Effect of build orientation on microstructure and tensile behaviour of selectively laser melted M300 maraging steel. Mater Sci Eng A 2020;798. https://doi.org/10.1016/j.msea.2020.140130.

[114] Thijs L, Verhaeghe F, Craeghs T, Van Humbeeck J, Kruth J-P. A study of the microstructural evolution during selective laser melting of Ti–6Al–4V. Acta Mater 2010;58:3303–12. https://doi.org/10.1016/j.actamat.2010.02.004.

[115] Zhou Q, Hayat MD, Chen G, Cai S, Qu X, Tang H, et al. Selective electron beam melting of NiTi: Microstructure, phase transformation and mechanical properties. Mater Sci Eng A 2019;744:290–8. https://doi.org/10.1016/j.msea.2018.12.023.

[116] Kreitcberg A, Brailovski V, Turenne S. Effect of heat treatment and hot isostatic pressing on the microstructure and mechanical properties of Inconel 625 alloy processed by laser powder bed fusion. Mater Sci Eng A 2017;689:1–10. https://doi.org/10.1016/j.msea.2017.02.038.

[117] Kok Y, Tan XP, Wang P, Nai MLS, Loh NH, Liu E, et al. Anisotropy and heterogeneity of microstructure and mechanical properties in metal additive manufacturing: A critical review. Mater Des 2018;139:565–86. https://doi.org/10.1016/j.matdes.2017.11.021.
[118] Thijs L, Montero Sistiaga ML, Wauthle R, Xie Q, Kruth J-P, Van Humbeeck J. Strong morphological and crystallographic texture and resulting yield strength anisotropy in selective laser melted tantalum. Acta Mater 2013;61:4657–68. https://doi.org/10.1016/j.actamat.2013.04.036.
[119] Mukherjee M. Effect of build geometry and orientation on microstructure and properties of additively manufactured 316L stainless steel by laser metal deposition. Materialia (Oxf) 2019;7:100359. https://doi.org/10.1016/j.mtla.2019.100359.
[120] Isaac JP, Lee S, Thompson S, Saharan A, Shamsaei N, Tippur HV. Role of build orientation on quasi-static and dynamic fracture responses of additively manufactured AlF357 and AlSi10Mg alloys. Addit Manuf 2022;59:103080. https://doi.org/10.1016/j.addma.2022.103080.
[121] Watring DS, Benzing JT, Hrabe N, Spear AD. Effects of laser-energy density and build orientation on the structure–property relationships in as-built Inconel 718 manufactured by laser powder bed fusion. Addit Manuf 2020;36. https://doi.org/10.1016/j.addma.2020.101425.
[122] Weißmann V, Bader R, Hansmann H, Laufer N. Influence of the structural orientation on the mechanical properties of selective laser melted Ti6Al4V open-porous scaffolds. Mater Des 2016;95:188–97. https://doi.org/10.1016/j.matdes.2016.01.095.
[123] Guo Y, Chen C, Tan L, Wang Q, Pan Y, Zhu H, et al. The role of pore structures on the fatigue properties of additively manufactured porous tantalum scaffolds produced by electron beam powder bed fusion. J Mater Res Technol 2022;19:3461–73. https://doi.org/10.1016/j.jmrt.2022.06.096.
[124] Ghorbanpour S, Deshmukh K, Sahu S, Riemslag T, Reinton E, Borisov E, et al. Additive manufacturing of functionally graded Inconel 718: Effect of heat treatment and building orientation on microstructure and fatigue behaviour. J Mater Process Technol 2022;306. https://doi.org/10.1016/j.jmatprotec.2022.117573.
[125] Zhao Y, Li K, Gargani M, Xiong W. A comparative analysis of Inconel 718 made by additive manufacturing and suction casting: Microstructure evolution in homogenization. Addit Manuf 2020;36:101404. https://doi.org/10.1016/j.addma.2020.101404.
[126] Leicht A, Klement U, Hryha E. Effect of build geometry on the microstructural development of 316L parts produced by additive manufacturing. Mater Charact 2018;143:137–43. https://doi.org/10.1016/j.matchar.2018.04.040.
[127] Hartunian P, Eshraghi M. Effect of build orientation on the microstructure and mechanical properties of selective laser-melted Ti-6Al-4V alloy. J Manuf Mater Process 2018;2. https://doi.org/10.3390/jmmp2040069.
[128] C. Palanisamy, S. Bhero, B.A. Obadele, P.A. Olubambi, Effect of build direction on the microhardness and dry sliding wear behaviour of laser additive manufactured Ti-6Al-4V, 2018. https://www.sciencedirect.com/science/article/pii/S2214785317323350 (accessed February 24, 2023).
[129] Liu SY, Li HQ, Qin CX, Zong R, Fang XY. The effect of energy density on texture and mechanical anisotropy in selective laser melted Inconel 718. Mater Des 2020;191:108642. https://doi.org/10.1016/J.MATDES.2020.108642.
[130] Sun SH, Koizumi Y, Saito T, Yamanaka K, Li YP, Cui Y, et al. Electron beam additive manufacturing of Inconel 718 alloy rods: Impact of build direction on microstructure and high-temperature tensile properties. Addit Manuf 2018;23:457–70. https://doi.org/10.1016/J.ADDMA.2018.08.017.
[131] Pehlivan E, Roudnicka M, Dzugan J, Koukolikova M, Králík V, Seifi M, et al. Effects of build orientation and sample geometry on the mechanical response of miniature CP-Ti Grade 2 strut samples manufactured by laser powder bed fusion. Addit Manuf 2020;35. https://doi.org/10.1016/j.addma.2020.101403.
[132] Chern AH, Nandwana P, McDaniels R, Dehoff RR, Liaw PK, Tryon R, et al. Build orientation, surface roughness, and scan path influence on the microstructure, mechanical properties, and flexural fatigue behavior of Ti–6Al–4V fabricated by electron beam melting. Mater Sci Eng A 2020;772. https://doi.org/10.1016/j.msea.2019.138740.
[133] Cutolo A, Elangeswaran C, Muralidharan GK, Van Hooreweder B. On the role of building orientation and surface post-processes on the fatigue life of Ti-6Al-4V coupons manufactured by laser powder bed fusion. Mater Sci Eng A 2022;840. https://doi.org/10.1016/j.msea.2022.142747.
[134] Morettini G, Razavi N, Zucca G. Effects of build orientation on fatigue behavior of Ti-6Al-4V as-built specimens produced by direct metal laser sintering. Proc Struct Integrity 2019;24:349–59. https://doi.org/10.1016/j.prostr.2020.02.032.
[135] Solberg K, Hovig EW, Sørby K, Berto F. Directional fatigue behaviour of maraging steel grade 300 produced by laser powder bed fusion. Int J Fatigue 2021;149. https://doi.org/10.1016/j.ijfatigue.2021.106229.
[136] Nezhadfar PD, Thompson S, Saharan A, Phan N, Shamsaei N. Structural integrity of additively manufactured aluminum alloys: Effects of build orientation on microstructure, porosity, and fatigue behavior. Addit Manuf 2021;47. https://doi.org/10.1016/j.addma.2021.102292.
[137] Beretta S, Gargourimotlagh M, Foletti S, du Plessis A, Riccio M. Fatigue strength assessment of "as built" AlSi10Mg manufactured by SLM with different build orientations. Int J Fatigue 2020;139. https://doi.org/10.1016/j.ijfatigue.2020.105737.
[138] Ponticelli GS, Panciroli R, Venettacci S, Tagliaferri F, Guarino S. Experimental investigation on the fatigue behavior of laser powder bed fused 316L stainless steel. CIRP J Manuf Sci Technol 2022;38:787–800. https://doi.org/10.1016/j.cirpj.2022.07.007.
[139] R. Shrestha, J. Simsiriwong, N. Shamsaei, S.M. Thompson, L. Bian, Effect of build orientation on the fatigue behavior of stainless steel 316L manufactured via a laser-powder bed fusion process, in: International Solid Freeform Fabrication Symposium, 2016. https://utw10945.utweb.utexas.edu/sites/default/files/2016/046-Shrestha.pdf.
[140] Maleki E, Bagherifard S, Sabouri F, Guagliano M. Effects of hybrid post-treatments on fatigue behaviour of notched LPBF AlSi10Mg: experimental and deep learning approaches. Proc Struct Integrity 2021;34:141–53. https://doi.org/10.1016/j.prostr.2021.12.021.
[141] Maleki E, Bagherifard S, Heydari Astaraee A, Sgarbazzini S, Bandini M, Guagliano M. Application of gradient severe shot peening as a novel mechanical surface treatment on fatigue behavior of additively manufactured AlSi10Mg. Mater Sci Eng: A 2023;881:145397. https://doi.org/10.1016/j.msea.2023.145397.
[142] Maleki E, Unal O, Guagliano M, Bagherifard S. The effects of shot peening, laser shock peening and ultrasonic nanocrystal surface modification on the fatigue strength of Inconel 718. Mater Sci Eng A 2021;810:141029. https://doi.org/10.1016/j.msea.2021.141029.
[143] Maleki E, Unal O, Guagliano M, Bagherifard S. Analysing the fatigue behaviour and residual stress relaxation of gradient nano-structured 316L steel subjected to the shot peening via deep learning approach. Met Mater Int 2022;28:112–31. https://doi.org/10.1007/s12540-021-00995-8.
[144] Murchio S, Du Plessis A, Luchin V, Maniglio D, Benedetti M. Influence of mean stress and building orientation on the fatigue properties of sub-unital thin-strut miniaturized Ti6Al4V specimens additively manufactured via Laser-Powder Bed Fusion. Int J Fatigue 2024;180:108102. https://doi.org/10.1016/j.ijfatigue.2023.108102.
[145] De Biasi R, Murchio S, Sbettega E, Carmignato S, Luchin V, Benedetti M. Efficient optimization framework for L-PBF fatigue enhanced Ti6Al4V lattice component. Mater Des 2023;230:111975. https://doi.org/10.1016/j.matdes.2023.111975.
[146] Oliveira de Menezes JT, Castrodeza EM, Casati R. Effect of build orientation on fracture and tensile behavior of A357 Al alloy processed by selective laser melting. Mater Sci Eng A 2019;766. https://doi.org/10.1016/j.msea.2019.138392.
[147] Oliveira de Menezes JTO, Castrodeza EM, Patriarca L, Casati R. Effect of heat treatments and loading orientation on the tensile properties and fracture toughness of AlSi7Mg alloy produced by Laser Powder Bed Fusion. Int J Fract 2022;235:145–57. https://doi.org/10.1007/s10704-022-00631-5.
[148] Araújo LC, Gabriel AHG, da Fonseca EB, Avila JA, Jardini AL, Seno Junior R, et al. Effects of build orientation and heat treatments on the tensile and fracture toughness properties of additively manufactured AlSi10Mg. Int J Mech Sci 213 2022. https://doi.org/10.1016/j.ijmecsci.2021.106868.
[149] Dzugan J, Seifi M, Rzepa S, Rund M, Koukolikova M, Viehrig HW, et al. The effects of post-processing on the local fracture toughness properties of electron beam powder bed fusion Ti-6Al-4V alloy. Eng Fract Mech 2022;273. https://doi.org/10.1016/j.engfracmech.2022.108697.
[150] Abdelwahed M, Bengtsson S, Boniardi M, Casaroli A, Casati R, Vedani M. An investigation on the plane-strain fracture toughness of a water atomized 4130 low-alloy steel processed by laser powder bed fusion. Mater Sci Eng A 2022;855. https://doi.org/10.1016/j.msea.2022.143941.
[151] Ramadas H, Nath AK, Sarkar S, Ganesh P, Kaul R, Majumdar JD. Fatigue crack growth rate and fracture toughness evaluation of 15–5 precipitation hardening stainless steel fabricated by laser powder bed fusion process. Mater Sci Eng A 2022;861. https://doi.org/10.1016/j.msea.2022.144356.
[152] Bahshwan M, Myant CW, Reddyhoff T, Pham MS. The role of microstructure on wear mechanisms and anisotropy of additively manufactured 316L stainless steel in dry sliding. Mater Des 2020;196. https://doi.org/10.1016/j.matdes.2020.109076.
[153] Podgornik B, Šinko M, Godec M. Dependence of the wear resistance of additive-manufactured maraging steel on the build direction and heat treatment. Addit Manuf 2021;46. https://doi.org/10.1016/j.addma.2021.102123.

[154] Yang Y, Li X, Khonsari MM, Zhu Y, Yang H. On enhancing surface wear resistance via rotating grains during selective laser melting. Addit Manuf 2020;36. https://doi.org/10.1016/j.addma.2020.101583.
[155] Bahshwan M, Myant CW, Reddyhoff T, Pham M-S. The role of microstructure on wear mechanisms and anisotropy of additively manufactured 316L stainless steel in dry sliding. Mater Des 2020;196:109076. https://doi.org/10.1016/j.matdes.2020.109076.
[156] Kan WH, Chiu LNS, Lim CVS, Zhu Y, Tian Y, Jiang D, et al. A critical review on the effects of process-induced porosity on the mechanical properties of alloys fabricated by laser powder bed fusion. J Mater Sci 2022;57:9818–65. https://doi.org/10.1007/s10853-022-06990-7.
[157] Kan WH, Huang S, Man Z, Yang L, Huang A, Chang L, et al. Effect of T6 treatment on additively-manufactured AlSi10Mg sliding against ceramic and steel. Wear 2021;482–483:203961. https://doi.org/10.1016/j.wear.2021.203961.
[158] Zhou X, Xu D, Geng S, Fan Y, Yang C, Wang Q, et al. Microstructural evolution and corrosion behavior of Ti–6Al–4V alloy fabricated by laser metal deposition for dental applications. J Mater Res Technol 2021;14:1459–72. https://doi.org/10.1016/j.jmrt.2021.07.006.
[159] Zhou X, Xu D, Geng S, Fan Y, Liu M, Wang Q, et al. Mechanical properties, corrosion behavior and cytotoxicity of Ti-6Al-4V alloy fabricated by laser metal deposition. Mater Charact 2021;179. https://doi.org/10.1016/j.matchar.2021.111302.
[160] Romero-Resendiz L, Rossi MC, Álvarez A, García-García A, Milián L, Tormo-Más M, et al. Microstructural, mechanical, electrochemical, and biological studies of an electron beam melted Ti-6Al-4V alloy. Mater Today Commun 2022;31. https://doi.org/10.1016/j.mtcomm.2022.103337.
[161] Wu B, Pan Z, Li S, Cuiuri D, Ding D, Li H. The anisotropic corrosion behaviour of wire arc additive manufactured Ti-6Al-4V alloy in 3.5% NaCl solution. Corros Sci 2018;137:176–83. https://doi.org/10.1016/j.corsci.2018.03.047.
[162] Maleki E, Unal O, Shao S, Shamsaei N. Effects of laser shock peening on corrosion resistance of additive manufactured AlSi10Mg. Coatings 2023;13. https://doi.org/10.3390/coatings13050874.
[163] Pazhanivel B, Sathiya P, Sozhan G. Ultra-fine bimodal (α + β) microstructure induced mechanical strength and corrosion resistance of Ti-6Al-4V alloy produced via laser powder bed fusion process. Opt Laser Technol 2020;125. https://doi.org/10.1016/j.optlastec.2019.106017.
[164] Sander G, Babu AP, Gao X, Jiang D, Birbilis N. On the effect of build orientation and residual stress on the corrosion of 316L stainless steel prepared by selective laser melting. Corros Sci 2021;179. https://doi.org/10.1016/j.corsci.2020.109149.
[165] Du D, Dong A, Shu D, Zhu G, Sun B, Li X, et al. Influence of build orientation on microstructure, mechanical and corrosion behavior of Inconel 718 processed by selective laser melting. Mater Sci Eng A 2019;760:469–80. https://doi.org/10.1016/j.msea.2019.05.013.
[166] Peng X, Kong L, Fuh JYH, Wang H. A review of post-processing technologies in additive manufacturing. J Manuf Mater Process 2021;5. https://doi.org/10.3390/jmmp5020038.
[167] Taufik M, Jain PK. Role of build orientation in layered manufacturing: A review. Int J Manuf Technol Manag 2013;27:47–73. https://doi.org/10.1504/IJMTM.2013.058637.
[168] Kumbhar NN, Mulay Av. Post processing methods used to improve surface finish of products which are manufactured by additive manufacturing technologies: a review. J Inst Eng (India): Series C 2018;99:481–7. https://doi.org/10.1007/s40032-016-0340-z.
[169] Maleki E, Bagherifard S, Bandini M, Guagliano M. Surface post-treatments for metal additive manufacturing: Progress, challenges, and opportunities. Addit Manuf 2021;37. https://doi.org/10.1016/j.addma.2020.101619.
[170] Ye C, Zhang C, Zhao J, Dong Y. Effects of post-processing on the surface finish, porosity, residual stresses, and fatigue performance of additive manufactured metals: a review. J Mater Eng Perform 2021;30:6407–25. https://doi.org/10.1007/s11665-021-06021-7.
[171] Cerri E, Ghio E, Bolelli G. Effect of surface roughness and industrial heat treatments on the microstructure and mechanical properties of Ti6Al4V alloy manufactured by laser powder bed fusion in different built orientations. Mater Sci Eng A 2022;851. https://doi.org/10.1016/j.msea.2022.143635.
[172] Gangireddy S, Faierson EJ, Mishra RS. Influences of post-processing, location, orientation, and induced porosity on the dynamic compression behavior of Ti–6Al–4V alloy built through additive manufacturing. J Dynam Behav Mater 2018;4:441–51. https://doi.org/10.1007/s40870-018-0157-3.
[173] Maleki E, Shamsaei N. A comprehensive study on the effects of surface post-processing on fatigue performance of additively manufactured AlSi10Mg: an augmented machine learning perspective on experimental observations. Addit Manuf 2024;86:104179. https://doi.org/10.1016/j.addma.2024.104179.
[174] Poulin JR, Brailovski V, Terriault P. Long fatigue crack propagation behavior of Inconel 625 processed by laser powder bed fusion: influence of build orientation and post-processing conditions. Int J Fatigue 2018;116:634–47. https://doi.org/10.1016/j.ijfatigue.2018.07.008.
[175] Rauch M, Hascoet J-Y. Improving additive manufactured surfaces properties with post processing techniques, (2021). https://www.euspen.eu/knowledge-base/AM21112.pdf (accessed November 15, 2023).
[176] Serjouei A, Afazov S. Predictive model to design for high cycle fatigue of stainless steels produced by metal additive manufacturing, n.d. https://ssrn.com/abstract=4103898.
[177] Wood P, Libura T, Kowalewski ZL, Williams G, Serjouei A. Influences of horizontal and vertical build orientations and post-fabrication processes on the fatigue behavior of stainless steel 316l produced by selective laser melting. Materials 2019;12:4203. https://doi.org/10.3390/ma12244203.
[178] Vanderesse N, Bocher P, Nuño N, Yánez A, Hof LA. On the characterization of roughness and geometrical irregularities of additively manufactured single titanium-alloy struts. Addit Manuf 2022;54:102731. https://doi.org/10.1016/j.addma.2022.102731.
[179] Pyka G, Burakowski A, Kerckhofs G, Moesen M, Van Bael S, Schrooten J, et al. Surface modification of Ti6Al4V open porous structures produced by additive manufacturing. Adv Eng Mater 2012;14:363–70. https://doi.org/10.1002/adem.201100344.
[180] Bagherifard S, Beretta N, Monti S, Riccio M, Bandini M, Guagliano M. On the fatigue strength enhancement of additive manufactured AlSi10Mg parts by mechanical and thermal post-processing. Mater Des 2018;145:28–41. https://doi.org/10.1016/j.matdes.2018.02.055.
[181] Bagherifard S. Enhancing the structural performance of lightweight metals by shot peening. Adv Eng Mater 2019;21. https://doi.org/10.1002/adem.201801140.
[182] Maleki E, Unal O, Reza Kashyzadeh K, Bagherifard S, Guagliano M. A systematic study on the effects of shot peening on a mild carbon steel: microstructure, mechanical properties, and axial fatigue strength of smooth and notched specimens. Appl Surface Sci Adv 2021;4:100071. https://doi.org/10.1016/j.apsadv.2021.100071.
[183] Maleki E, Maleki N, Fattahi A, Unal O, Guagliano M, Bagherifard S. Mechanical characterization and interfacial enzymatic activity of AISI 316L stainless steel after surface nanocrystallization. Surf Coat Technol 2021;405:126729. https://doi.org/10.1016/j.surfcoat.2020.126729.
[184] Bagherifard S, Slawik S, Fernández-Pariente I, Pauly C, Mücklich F, Guagliano M. Nanoscale surface modification of AISI 316L stainless steel by severe shot peening. Mater Des 2016;102:68–77. https://doi.org/10.1016/j.matdes.2016.03.162.
[185] Bikdeloo R, Farrahi GH, Mehmanparast A, Mahdavi SM. Multiple laser shock peening effects on residual stress distribution and fatigue crack growth behaviour of 316L stainless steel. Theor Appl Fract Mech 2020;105. https://doi.org/10.1016/j.tafmec.2019.102429.
[186] Deng WW, Lu HF, Xing YH, Luo KY, Lu JZ. Effect of laser shock peening on tensile properties and microstructure of selective laser melted 316L stainless steel with different build directions. Mater Sci Eng A 2022;850. https://doi.org/10.1016/j.msea.2022.143567.
[187] Tillmann W, Lopes Dias NF, Stangier D, Schaak C, Höges S. Coatability of diamond-like carbon on 316L stainless steel printed by binder jetting. Addit Manuf 2021;44. https://doi.org/10.1016/j.addma.2021.102064.
[188] Jamshidi P, Aristizabal M, Kong W, Villapun V, Cox SC, Grover LM, et al. Selective laser melting of Ti-6Al-4V: The impact of post-processing on the tensile, fatigue and biological properties for medical implant applications. Materials 2020;13:1–16. https://doi.org/10.3390/ma13122813.
[189] Ren S, Chen Y, Liu T, Qu X. Effect of build orientation on mechanical properties and microstructure of Ti-6Al-4V manufactured by selective laser melting. Metall Mater Trans A Phys Metall Mater Sci 2019;50:4388–409. https://doi.org/10.1007/s11661-019-05322-w.
[190] Kuo YL, Horikawa S, Kakehi K. The effect of interdendritic δ phase on the mechanical properties of Alloy 718 built up by additive manufacturing. Mater Des 2017;116:411–8. https://doi.org/10.1016/j.matdes.2016.12.026.
[191] Sangid MD, Book TA, Naragani D, Rotella J, Ravi P, Finch A, et al. Role of heat treatment and build orientation in the microstructure sensitive deformation characteristics of IN718 produced via SLM additive manufacturing. Addit Manuf 2018;22:479–96. https://doi.org/10.1016/j.addma.2018.04.032.
[192] Liu M, Takata N, Suzuki A, Kobashi M. Effect of heat treatment on gradient microstructure of AlSi10Mg lattice structure manufactured by laser powder bed fusion. Materials 2020;13. https://doi.org/10.3390/ma13112487.

[193] Krishna AV, Flys O, Reddy VV, Berglund J, Rosen BG. Areal surface topography representation of as-built and post-processed samples produced by powder bed fusion using laser beam melting. Surf Topogr 2020;8. https://doi.org/10.1088/2051-672X/ab9b73.
[194] Rovetta R, Ginestra P, Ferraro RM, Zohar-Hauber K, Giliani S, Ceretti E. Building orientation and post processing of Ti6Al4V produced by laser powder bed fusion process. J Manuf Mater Process 2023;7. https://doi.org/10.3390/jmmp7010043.
[195] Zhang J, Chaudhari A, Wang H. Surface quality and material removal in magnetic abrasive finishing of selective laser melted 316L stainless steel. J Manuf Process 2019;45:710–9. https://doi.org/10.1016/j.jmapro.2019.07.044.
[196] Hovig EW, Azar AS, Mhamdi M, Sørby K. Mechanical properties of AlSi10Mg processed by laser powder bed fusion at elevated temperature. In: Minerals, Metals and Materials Series, Springer, 2020: pp. 395–404. doi: 10.1007/978-3-030-36296-6_37.
[197] Hovig EW, Azar AS, Solberg K, Sørby K. An investigation of the anisotropic properties of heat-treated maraging steel grade 300 processed by laser powder bed fusion. Int J Adv Manuf Technol 2021;114:1359–72. https://doi.org/10.1007/s00170-021-06938-2/Published.
[198] Afkhami S, Dabiri M, Piili H, Björk T. Effects of manufacturing parameters and mechanical post-processing on stainless steel 316L processed by laser powder bed fusion. Mater Sci Eng A 2021;802. https://doi.org/10.1016/j.msea.2020.140660.
[199] Doh J, Raju N, Raghavan N, Rosen DW, Kim S. Bayesian inference-based decision of fatigue life model for metal additive manufacturing considering effects of build orientation and post-processing. Int J Fatigue 2022;155. https://doi.org/10.1016/j.ijfatigue.2021.106535.